Effect of Ti group addition on the magnetic properties of Mn-Zn ferrites

A thesis submitted to the
University of Manchester
for the degree of
DOCTOR OF PHILOSOPHY
in the Faculty of Science

by

Gasan S Abass Al-Abedi
B.Sc. M.Sc. (Mining Engineering), M.Sc. (Metallurgy & Materials Science)

Department of Metallurgy and Materials Science
Manchester Materials Science Centre
Manchester University and UMIST
Grosvenor Street,
Manchester M1 7HS.

1999

ProQuest LLC.
789 East Eisenhower Parkway
P.O. Box 1346
Ann Arbor, MI 48106 – 1346

(DYEWS)

Contents

Chapter 4

Chapter 5

Abstract

Citrate gel processing and the mixed oxide method have been used to produce Mn-Zn ferrites with and without the addition of TiO_2, HfO_2, CaO and/or SiO_2. It has been shown that with controlled titanium substitutions, Mn-Zn ferrite with densities higher than 99% theoretical can be made by the gel processing method, while densities higher than 97% are achievable with controlled hafnium substitution. Meanwhile, densities higher than 96% are achievable by *Hf*-substitution into Mn-Zn ferrite prepared by the mixed oxide processing method. It has been also shown that the control of sintering conditions improves the physical and magnetic properties of Mn-Zn ferrites.

This study has shown that the additions of TiO_2, HfO_2 and SiO_2 promote sintering and improve the initial permeability, while the simultaneous addition of CaO/SiO_2 or CaO on its own hampers the grain growth and reduces the initial permeability. Significant resistivity improvements and power loss reductions may be achieved by the Ti^{4+} and Hf^{4+} ion substitutions. These improvements can be attributed to the increases in grain resistivity which occur as the presence of Ti^{4+} prevents the Fe^{3+} to Fe^{2+} hopping mechanism which gives conductivity in the ferrites. Furthermore, the precipitation of HfO_2 at the grain boundaries also enhances the overall resistivity and therefore reduces the power loss of Mn-Zn ferrite. Further improvements in resistivity can be achieved by the addition of CaO or CaO/SiO_2 along with TiO_2 and HfO_2, as they interact and form a non-magnetic secondary phase at the grain boundaries and triple points. Conversely, the addition of SiO_2 alone has been shown to significantly reduce the electrical resistivity and thus increase the power loss of Mn-Zn ferrite as a result of the occurrence of grain growth.

Finally, it has been shown that the effect of high density, small grain size, homogenous microstructure and higher grain/grain boundary resistivity all result in ferrite products with much improved magnetic and electrical properties.

Declaration

I hereby declare that no portion in the work referred to in this thesis has been submitted in support of an application for another degree or qualification of this or any other university or institution of learning.

Acknowledgements

The author would like to express his sincere thanks and gratitude to his supervisor Prof. Frank R. Sale for his assiduous supervision, advise, enthusiasm, patience and encouragement that enabled this thesis to be written and will always be deeply appreciated.

Acknowledgements are also due to Prof. R. Taylor, Dr T. Daveis, Dr F. Hayes and Dr G. Sims. The author also wishes to express his thanks to Prof. R. Freer for the moral support throughout the period of his study in the centre.

Sincere thanks are also extended to Messers. Ian Brough, Joe Birchall, Neil Wardman and. Andy Wallwork for their technical assistance.

I also would like to express my thanks to EPSRC and Philips Components UK, Southport for their support throughout this study.

Lastly, but most importantly of all I thank my family for their love and continuos encouragement, especially my wife Mevlija and sons Ensar and Ismar for thier love and support during my studies.

Chapter 1

1. Introduction

The use of naturally occurring magnetite, Fe_3O_4, occurred five thousand years ago by the Chinese for direction finding on long over-land journeys. Since the 19th century magnetic materials have seen extraordinary developments in all classes. In the middle of the third decade in this century the magnetic ceramics, referred to a ferrites, were discovered by Japanese scientists. Conceivably the most important progression in recent years came with ferrites being accepted over steel and alloy magnets due to their unique low coercivity and the highest stored energy for unit cost of any materials. Since then, with the rapid development of the electronic market, the ferrite industry has grown considerably[1,2,3].

Billions of soft ferrites are used in every imaginable electronic device as new applications are being developed constantly. The manufacture of spinel ferrites is an old technology that is always under continuing pressure to produce products which have less variation in properties as well as improved properties. One of the main applications for Mn-Zn ferrites is for deflection yokes for television sets and personal computers. In this application the designers want to increase the number of lines per picture to obtain a higher resolution (high definition television HDTV), which means that the deflection unit will operate at higher frequencies. To reduce heat generation, this consequently requires a yoke ring made of a ferrite with low power losses and high permeability at higher frequencies and adequately high resistivity.

To improve the electrical and magnetic properties of manganese zinc ferrites, small amounts of cationic substitutions are widely used. The relevant elements used as substitutes can be classified into three groups. The first group contains additions that promote sintering by introducing a liquid phase, such as borates and alkali fluorides.

The second group includes additions that appear at grain boundaries as a second phase having very high resistivity, which increases the bulk resistivity of the ferrite and therefore reduces the power losses. For this application very small amounts, 0.01-0.1 wt%, of CaO and SiO_2 additions are appropriate.

The third group are cations which are soluble in the host lattice and occupy the regular positions on the tetrahedral or octahedral sites. They influence the intrinsic magnetic properties including magnetisation, anisotropy and the stability of the properties with time. In principle the majority of the cations having ionic radii of 0.05 to 0.1 nm and charges between Me^{1+} and $Me^{4+}$are soluble in the Mn-Zn ferrite lattice. Practically, the most successful have been substitutions of $Ti^{4+}$and Sn^{4+}[4].

Recent work has shown that the effectiveness of additions in this third group is dependent upon the impurity level present in the ferrite, particularly the CaO and SiO_2 content, and it seems that a small level of impurities is to be desired to allow interaction to occur at grain boundaries[5,6,7].

The main objectives of this project were examine the effects of Ti^{4+} and Hf^{4+} substitutions, with and without the presence of SiO_2 and CaO impurities, on the magnetic properties of manganese zinc ferrite. The first task was to study the effect of Ti^{4+} substitutions on the initial permeability and power losses. Possible improvements have been suggested by many authors[8,9,10,11] who indicated that the magnetic properties can be controlled by small levels of substitution of Ti^{4+} for Fe^{3+} ions. Particularly, control can be obtained by keeping the Fe^{2+} ions unchanged and at the same time increasing the Mn^{2+} and Ti^{4+} content to account for Fe^{3+}. *Roess*[12] proposed the substitution of Ti^{4+} for some of the iron to move the secondary maximum permeability, and furthermore increase the resistivity and lower significantly the losses especially at higher frequencies.

Stijntjes et. al.[9] have also observed that the substitution of Ti^{4+} ions improves the magnetic and electrical properties of Mn-Zn ferrites. Recently, *Otsuka et. al.*[6] have reported a remarkable improvement in overall magnetic properties of Mn-Zn ferrite due to the additions of TiO_2 with CaO and SiO_2. Most recently many workers, *Baumgartner et. al.*[7] and *Neamtu and Barber*[13], have studied the implications of TiO_2 additions on permeability and power losses and reported that a notable improvement was achieved especially when the TiO_2 additions were accompanied with the additions of CaO and SiO_2.

It was planned to use a commercially based composition in the proposed study and this was selected as $Mn^{2+}_{0.57}\ Zn^{2+}_{0.35}\ Fe^{2+}_{0.08}\ Fe^{3+}_{2}\ O_4$, to which various amounts of Ti^{4+} substitutions were added with appropriate compensation of the *Mn* and *Fe* contents. The Ti^{4+} substitutions used were 0.2, 0.4 and 0.6 wt%. It was decided to prepare all the samples by the citrate gel processing method to ensure maximum chemical homogeneity. The impurities, 0.04 wt% CaO and 0.02 wt% SiO_2, were added individually and together to the powders.

In the second part of the study it was planned to investigate the effect of Hf^{4+} ions on the properties of Mn-Zn ferrite that were prepared by both the gel citrate and mixed oxide processing methods. This study was included to allow comparison to the effects of technically similar additions Hf^{4+} and Ti^{4+} and also allow a study to be made of the properties of samples produced using powders from two different powder routes, as indicated below. To examine the effect of interaction with the impurities 0.02 wt% SiO_2 and 0.04 wt% CaO were added together or individually to the ferrite. *Mochizuki*[5] and *Otsuka et. al.*[6] indicated that the addition HfO_2 with CaO and SiO_2 to the ferrites would increase the electrical resistivity and therefore reduce the power losses significantly.

The third purpose of this work was to study the effect of ferrite manufacturing route on the properties of Mn-Zn ferrite. Consequently gel processing and mixed oxide methods were used to determine the significance of powder preparation method on the chemical homogeneity and microstructure and therefore the properties of final product. Two conventional mixed oxides ceramic processing routes were proposed for use in addition to the gel processing method. In the first route Hf^{4+} and the impurities were added to precalcined powder during ball milling, while in the second route all the additives were introduced from the start of the preparation, i.e. at the oxide powder mixing stage. A subsequent part of the investigation was to study of the effects of sintering temperature, time and atmosphere on the final physical, electrical and magnetic properties.

To understand the importance of additive-impurity interaction, it was planned to assess the microstructures, densities, electrical and magnetic properties of different samples using optical microscopy and electron microscopy along with measurements of electrical resistivity, power losses and initial permeability.

Chapter 2

2. Literature Review

2.1. Spinel Ferrite Structure

Bragg 1915 was first to observe the spinel structure. The spinel ferrites are a very large group of oxides that possess the structure of natural spinel $Mg\ Al_2O_4$[14]. *Hill et. al.*[15] classified as spinels more than 140 oxides and 80 sulphides which have been thoroughly studied. The oldest and most important magnetic material with practical application, magnetite Fe_3O_4, is a naturally occurring oxide while many of the commercially important spinels are synthetic. The spinel ferrites have a general structure $MeFe_2O_4$, where *Me* is a divalent ion which can be Iron, Nickel, Manganese, Magnesium, Zinc, Copper, Cobalt or mixture. Iron is trivalent ion, which may be replaced by Titanium, Manganese, Cobalt, Tin or Vanadium ions.

The ideal spinel structure is formed by a cubic close-packed face centred cubic array of oxygen atoms, in which, one eighth of the tetrahedral, also called '*A*' sites, and one half of the octahedral, also called '*B*' sites, are occupied by cations. The unit cell of spinel contains eight formula units AB_2O_4, with eight '*A*' sites, sixteen '*B*' sites and thirty-two oxygen. *Smit and Wijn*[16] described the tetrahedral site as the origin of the unit cell which can be divided into eight cubes of edge '*a/2*' as is shown in *figure 2.1*.

Due to the insertion of metal ions in the tetrahedral sites the four surrounding oxygen ions are displaced outwards along the body diagonals of the octant. The oxygen ions surrounding the filled tetrahedral sites still have cubic symmetry, meanwhile the oxygen ions surrounding the octahedral sites are also displaced, losing their tetrahedral structure. Considering this distortion the spinel structure has only approximately a face centred cubic lattice.

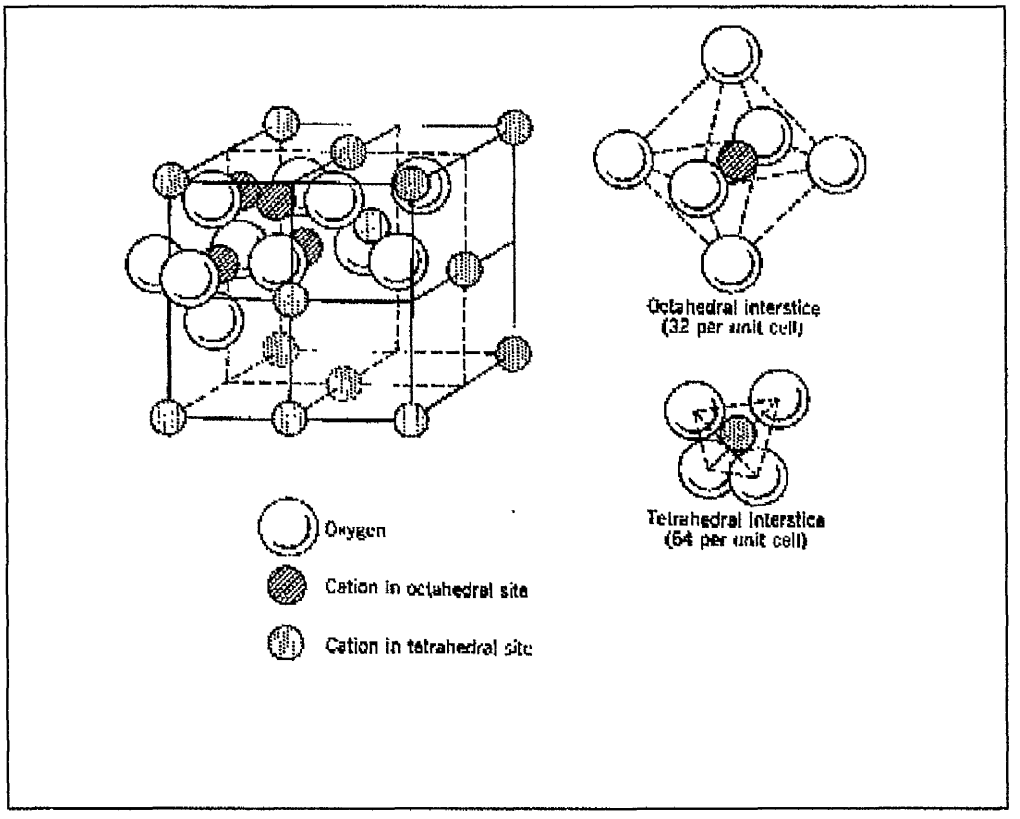

Figure 2.1. Crystal structure of cubic ferrite [16].

2.1.1. Normal and Inverse Spinel

In the spinel lattice there are two possible ideal arrangements. In the first arrangement, which is referred to as 'normal' spinel, the available eight tetrahedral sites are occupied by eight divalent ions. The sixteen octahedral sites are filled by sixteen trivalent ions. The second arrangement, which is called the 'inverse' spinel has eight divalent ions filling half of the available octahedral sites, and the rest of the bivalent and the trivalent ions are distributed randomly over the available tetrahedral and octahedral sites, as is shown in *table 2.1.*

				Occupants	
Site	***Size of site (Å)***	***Available sites***	***Occupied sites***	***Normal spinel***	***Inverse spinel***
Tetrahedral	*0.3 - 0.6*	*64*	*8*	*8 Me^{2+}*	*8 Fe^{3+}*
Octahedral	*0.6 - 1*	*32*	*16*	*16 Fe^{3+}*	*8 Fe^{3+} 8 Me^{2+}*

Table 2.1. Arrangements of metal ions in the unit cell of $MeFe_2O_4$ ferrite [17].

The ideal 'normal' ferrites spinel structure is:

$$\left(Me_{\delta}^{2+}Fe_{1-\delta}^{3+}\right)\left[Me_{1-\delta}^{2+}Fe_{1+\delta}^{3+}\right]O_4 \qquad 2.1$$

Mn-Zn ferrites have the 'normal' spinel structure, and the cation distribution of a $Zn_xMn_yFe_{3-x-y}O_{4+\gamma}$ can be given as:

$$\left(Zn_x^{2+}Mn_a^{2+}Mn_b^{3+}Fe_c^{3+}V_c^{a}\right)\left[Mn_e^{2+}Mn_d^{3+}Fe_f^{2+}Fe_g^{3+}V_c^{b}\right]O_{4+\gamma} \qquad 2.2$$

Subject to $y = a+b+c+d$, and $3-x-y = e+f+g$.

All the ferrimagnetic spinels are more or less inverse, which means that some of the trivalent 'M^{3+}' ions occupy tetrahedral '*A*' sites and an equal fraction of the trivalent ions 'M^{3+}' ions occupy octahedral '*B*' sites probably because of the tendency of the larger divalent ions to occupy the larger octahedral locations. The ionic radius effects are evident when the trivalent ions that are smaller than the divalent ions prefer the smaller tetrahedral '*A*' sites. The undistorted tetrahedral '*A*' and octahedral '*B*' sites have ionic radius of 0.052 and 0.048 (nm) respectively[18,19]. *Table 2.2* show the preferred sites for a number of ions in the Mn-Zn ferrite.

Ion/Vacancy	***Ionic Radii (nm)***	***Site***
Zn^{2+}	*0.083*	*Tetrahedral 'A'*
Mn^{2+}	*0.091*	*Tetrahedral 'A' or Octahedral 'B'*
Mn^{3+}	*0.070*	*Tetrahedral 'A' or Octahedral 'B'*
Fe^{2+}	*0.082*	*Octahedral 'B'*
Fe^{3+}	*0.067*	*Tetrahedral 'A' or Octahedral 'B'*
O^{-2}	*0.132*	-
Cation Vacancy	-	*Tetrahedral 'A' or Octahedral 'B'*

Table 2.2. Ionic radii and preferred sites of Manganese Zinc Ferrites

The electronic configuration can be explained when the (*4s*) and (*4p*) electrons of Zn^{2+} ions, which usually occupy the tetrahedral 'A' site, can form a covalent bond with electrons of the four surrounding oxygen O^{-2} ions. The preference of *Zn* ions for the tetrahedral '*A*' site was adapted to good purpose in Mn-Zn ferrites where Zinc replace some of the (Me^{2+}) magnetic ions whilst keeping the same stoichiometric amount of Fe^{3+} present. This gives a change in saturation magnetisation due to the addition of normal spinel $ZnFe_2O_4$ to various inverse spinels, as shown in *figure 2.2*. In almost all cases the addition of Zinc up to 40% to the ferrites increases the saturation magnetisation. Usually the divalent magnetic ions (Me^{2+}) occupy the tetrahedral '*A*' sites, nonetheless they prefer to move to the

octahedral '*B*' site. The nonmagnetic Zn^{2+} ions can be found only on the tetrahedral '*A*' sites. The addition of Zn^{2+} to the spinel thus improves the saturation magnetisation due to the substitution of Zn^{2+} onto tetrahedral '*A*' sites, displacing Fe^{3+} ions to the octahedral '*B*' sites where they contribute to the net moment. If the addition of Zn^{2+} continues to increase one would end up with all of the octahedral '*B*' sites Fe^{3+} ions in $ZnFe_2O_4$ in parallel alignment, and a saturation magnetisation of 10 μ_B. However further addition, above 40% *Zn* substitution, results in anti-parallel (*B-B*) interaction which diminishes the moment towards the antiferromagnetic limit of 0 μ_B.

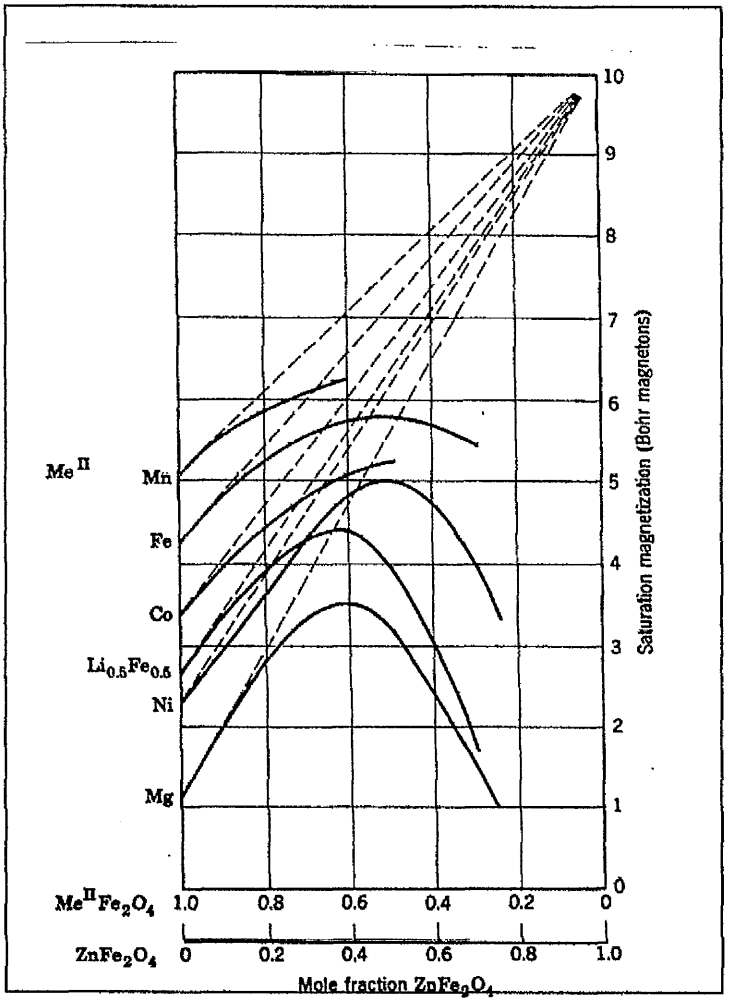

Figure 2.2 Variation of magnetic moment with increasing (Zn) substitution[20].

2.1.2. Particle Magnetism Theory

Weiss proposed the theory of molecular field and magnetic domains as the basic theory behind magnetism. The Weiss molecular field concept is shown in *figure 2.3* where a selected electron spin, shown circled, within a magnetic material experiences a field due to all the other surrounding spins, whose magnetic field enhances the magnetic influence of the chosen spin. The sources of this field are known as exchange interactions occurring between atomic moments. The magnetisation zeros at the Curie temperature are as shown. The small areas, usually referred to as Weiss domains, have a magnetic moment although there are no applied fields or overall magnetic moments. The exchange interaction in ferromagnetic materials is positive while in antiferromagnetic materials it is negative as a result of anti-parallel alignment of the spins, therefore the magnetic moment becomes zero.

The spinel structure has small domains that have a magnetic moment and the contrast with ferromagnetic materials is that these magnetic moments are the resultant of the magnetic moment of two sublattices the tetrahedral '*A*' and the octahedral '*B*' sites. The interaction between '*A*' and '*B*' sites is negative, consequently the spins of the electrons of the ions on the tetrahedral '*A*' sites are anti-parallel to the spins of the electrons of the ions on the octahedral '*B*' sites. Assuming that the total magnetic moment of the ions on the tetrahedral '*A*' sites is different from that of octahedral '*B*' sites, then it results in a net magnetic moment.

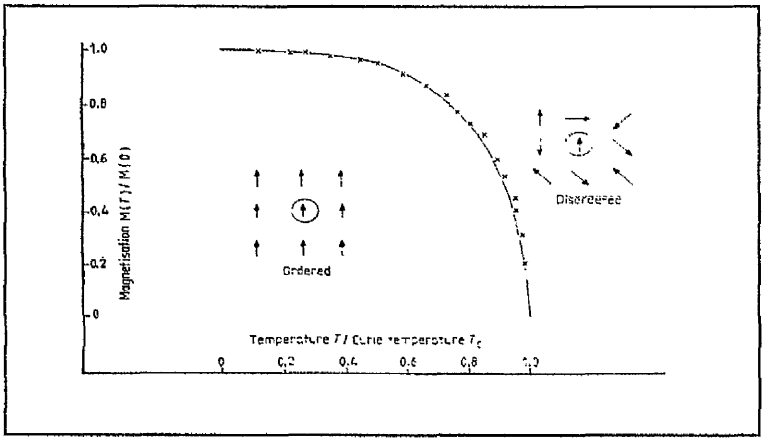

Figure 2.3. The Weiss molecular field

2.1.3 Magnetisation and Demagnetisation

Mn-Zn ferrites are usually called soft ferrites because they easily can be magnetised and demagnetised. These ferrites are characterised by high magnetic saturation with very low coercivity and narrow hystersis loops.

The hystersis loop starts when the ferrite is in a demagnetised situation, however when a small field, B<0.1 mT, is applied the domain walls bend and magnetic moments rotate in the way they want to go because of the applied field. By removing the applied field the walls and the magnetic moments return back to their initial state. Some domain walls at this stage are held by the grain boundaries, pores, inclusions and other factors. The slope of this reversible part of the loop determines the initial permeability. If the applied field is increased the domain walls start to move because they jump from one imperfection in the lattice to the other. The Weiss domains that are oriented in the direction of the applied field will grow at the expense of the Weiss domains with other directions, *figure 2.4*, and this process is irreversible.

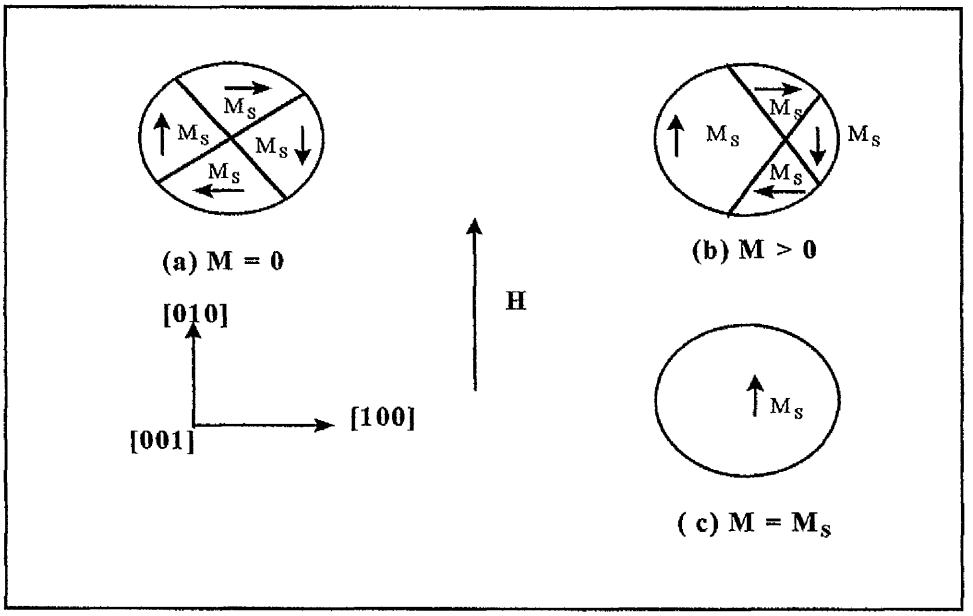

Figure 2.4. Changes in the domain structure of Fe crystals. (H) is in direction [010].

At some point the Weiss domains do not increase anymore and further increases of the applied field cause a reversible rotation of the domains in the direction of the applied field due to the Weiss domain saturation (B_{sat}). Further increase of the applied field will not result in higher magnetisation, *figure 2.5*.

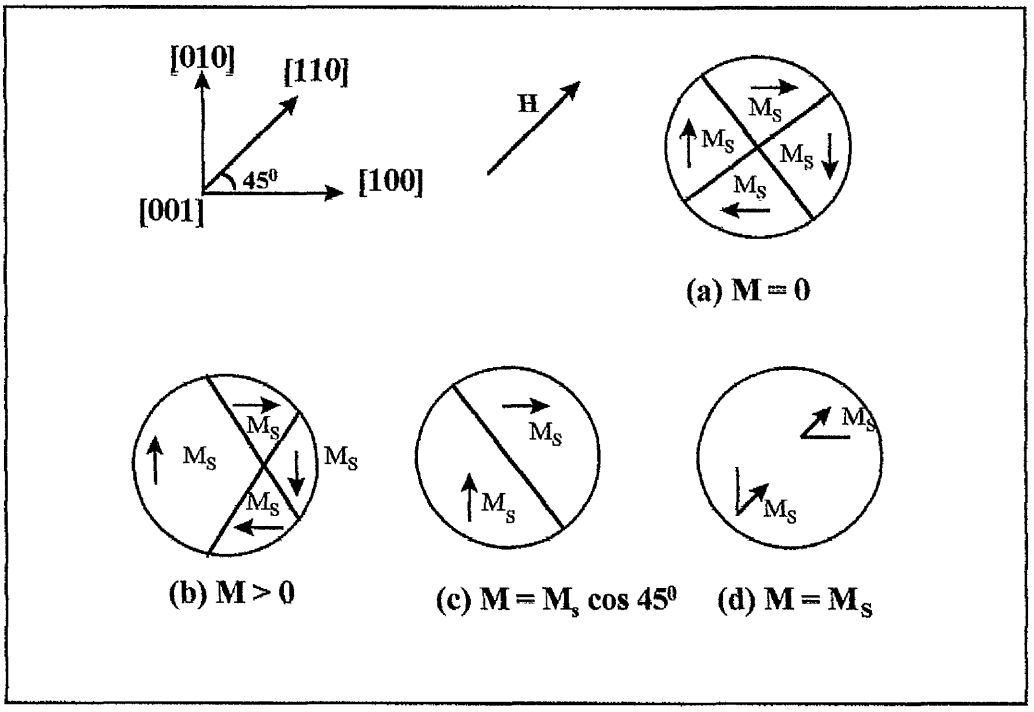

Figure 2.5. Changes in the domain structure of Fe crystal. (H) is in direction [110]

By taking away the applied field, the reversible rotation of the domain will be also removed, but the alignment of the domains will be present, and this process will result in a remanent magnetisation (B_{rem}). If a field in the opposite direction is applied then the magnetisation will decrease to zero and the value of the applied field in this process is called the coercive field (H_c). More increases of the applied field will cause magnetic saturation of the same magnitude in the opposite direction. To complete the hysteresis loop the applied field has to be reversed again.

The *B-H* loop area represents the required energy to produce changes in the magnetic domain structure. The *B-H* and the energy product symbolise the net losses in the system, generally in the form of heat. These losses are critical for the Mn-Zn ferrite yoke rings in the deflection unit applications because the ferrite is cycled around the magnetisation curve many times per second.

2.2 Effect of Additives

In addition to manganese, zinc and iron, small amounts of cationic substitutions or additions were often used in ferrites to improve the magnetic and electrical properties. As outlined in *chapter 1* there are three categories of additives[4]:

- Those, which act only indirectly by favouring, grain growth during sintering by the presence of liquid phase, such as borates and alkali fluorides.

- Additives that tend to precipitate as secondary phases on the grain boundaries which increase resistivity and reduce the power losses at high frequencies. Such additives are Ca^{2+}, Si^{4+}, Bi^{2+}, and Ba^{2+}, which are used in very small quantities, of the order of 0.01 to 01 wt%, otherwise exaggerated grain growth may occur.

- Cations which are soluble in the host lattice and occupy the regular tetrahedral '*A*' and octahedral '*B*' sites, form the third group. Their effects are to improve the electrical and magnetic properties such as magnetisation, anisotropy of the host lattice. These elements can be ones such as Ti^{4+}, V^{5+}, Sc^{3+}.

Okutani et. al.[21] and *Dreyer et. al.*[22] have made a comprehensive classification of the effect of additives/substitutes and divided them into six groups as shown in *table 2.3*.

Group	Additives/Substitutes	Effect	Comment
1	CaO and SiO_2	Increases the electrical resistivity and sintering density	Optimised amount depends on the final grain size
2	V_2O_5, Bi_2O_3, In_2O_3, SiO_2	Accelerate grain growth	For ferrites of high permeability application
3	Ta_2O_5, ZrO_2, CaO, Al_2O_3, Nb_2O_5, Cr_2O_3	Prevent grain growth	For low power loss ferrites
4	B_2O_3, P_2O_5, BaO, SrO	Causes discontinues grain growth	Optimum amount for use is less than 50 ppm
5	Na_2O, K_2O, WO_2, MoO_3	Prevent discontinuous grain growth	
6	SnO_2, TiO_2, Cr_2O_3, CoO, Al_2O_3, MgO, NiO, CuO	Dissolve in the host spinel lattice	Improving the following:, B_s-Saturation magnetis. θ_c- Curie temperature

Table 2.3. The effect of additives on the magnetic properties of ferrites[21,22].

The earliest work which studied the effect of impurities on ferrite was reported by *Guillaud*[23]. He studied the effect of alkali and alkaline earth additives on the permeability of Mn-Zn ferrite. It was shown that the solubility depended on the radius of the ions, in particular it was demonstrated that in the series Lithium, Sodium, Potassium, Rubidium, Cesium and Magnesium, Strontium, Barium the solubility decreased, while the ionic radius increases in that order.

The addition of a low level of impurity such as potassium *K*, was found to be beneficial for the initial permeability. With additions to the potassium content the

permeability continues to improve and that was explained as a result of potassium dissolving in the lattice. However the amount of potassium added to the ferrite has to be less than 0.5 wt%, otherwise the excess amount will precipitate at the grain boundaries and lead to degradation in the magnetic properties.

The various properties of ferrites not only depend on the chemical composition, preparation process, sintering temperature and atmosphere, but also depend upon the additives which are made. Major group of additives such as TiO_2[5,6,7,13,24,25], B_2O_3[26,27,28], ZrO_2[27,29], V_2O_3[30,31,32], CuO[33] and HfO_2[5, 6] have all been reported to have beneficial effects on magnetic and/or electrical properties of ferrites.

2.2.1 Effect of CaO and SiO_2 Additions

Many workers have examined the effect of CaO and/or SiO_2 individually or together in combination with the previously mentioned additives because both CaO and SiO_2 are common impurities in the raw materials often used for ferrite manufacture. *Akashi* [34] found that SiO_2, even in small quantities plays a significant role in obtaining a low electrical resistivity, due to the tendency of SiO_2 to increase the grain sizes and hence decrease the contribution of grain boundaries to the bulk resistivity. It was also found that the presence of SiO_2 would reduce the thickness of grain boundaries[34]. *Paulus and Guillaud*[35] have shown that at temperatures below the dissolution temperature, additives such SiO_2 which dissolve at 1200 ^{0}C, would segregate at the grain boundaries, forming a 'network' of almost equally distanced particles. *Giles and Westendrop*[36] have reported that SiO_2 was found to be present inside grains, especially around closed pores, of sintered Mn-Zn ferrite. *Toolenaar*[37] found that below a temperature of 1200 ^{0}C, the presence of SiO_2 had no influence on the development of a fine-grained microstructure. Conversely, *Liu et. al.*[38] have found that in samples sintered at low sintered temperature, 1170 ^{0}C, SiO_2 induces exaggerated grain growth.

Nomura and Mori [39] compared different amounts of SiO_2 additions and their effect on microstructure and power losses. In sintered ferrite containing (400 ppm) of SiO_2 large and widely distributed grains were present and the power loss was also significantly large. On the other hand, Mn-Zn ferrite, which contained 120 ppm SiO2, was composed of fine and uniform grains, and the power loss was much lower. *Kimura* [40] stated that in a Mn-Zn ferrite, exaggerated grain growth could occur with additions of SiO_2 over 200 ppm, even when there is no prolonged milling of the calcined powder. *Zenger et al.*[41] have also examined the effect of SiO_2 level in the raw materials on microstructure homogeneity. They reported that the presence of SiO_2, higher than 200 ppm, causes uncontrollable inhomogeneous grain growth, which results in high power loss.

Guillaud[23] also showed that additions of CaO to the ferrite improved the overall electrical properties, which was explained as a result of the tendency of CaO to precipitate at grain boundaries. The presence of CaO at the grain boundaries results in the creation of an electrically insulating layer between the grains which gives a reduction of eddy current loss. *Bando et. al.*[42] investigated the effect of CaO additions on the microstructures and showed that CaO added on its own hinders the grain growth.

The combined effects of small amounts of SiO_2 and CaO were reported by *Akashi*[34]. These additions were found to significantly improve the properties of Mn-Zn ferrite as a consequence of the two oxides appearing to act together through the formation of a secondary $CaSiO_3$ phase at the grain boundaries. The presence of both oxides results in much improved magnetic properties than when only CaO or SiO_2 was added.

Hamelin and Paulus[43] found that the segregation of CaO increases in the presence of SiO_2 at the grain boundaries. Combining additions of CaO with relatively small amounts of SiO_2, 200 ppm, resulted in the formation of an amorphous, $CaSiO_3$, phase film on the grain boundaries, and that reduced the power

losses significantly. *Franken and van Doveren* [44] have confirmed that additives such as CaO and SiO_2 segregate at the grain boundaries and found that where additives were present, they enriched the grain boundaries of the ferrite. *Franken and Stacy*[45] using TEM, found a secondary phase, that may be amorphous or crystalline, formed at boundaries triple point and between two or more grains. *Ishino and Narumiya*[46] showed that low-loss ferrite doped with CaO and SiO_2, also showed a similar concentration profile, with high impurity content at the grain boundaries.

Carpy and Stuijst[47] have observed that the rate of grain growth increases in the presence of a liquid phase that wets the grain boundary area. They assumed that a so-called "flux growth" process occurs, during the sintering process, for Mn-Zn ferrites with 250 ppm SiO_2 and 500 ppm CaO additions. Both additives form a liquid phase that dissolves material from the grain boundary and this material then diffuses through the liquid phase and finally precipitates. In cases where all these steps occur rapidly i.e. dissolution, diffusion and precipitation, the flux grow process will also be rapid, which allows faster grain growth than would normally occur in the solid state. In cases where one of these steps is slow, the whole growth process is delayed.

Impurity benefited gain growth could also be a result of a change in the chemical potential, that provides an additional driving force for densification and grain growth in a heterogeneous system. The kinetics of the process could be increased by the enhanced vacancy concentration, and by the change in stoichiometry due to different diffusion coefficients of the inter-diffusing species.

Roelofsma and Kools[48] have measured the solubility of SiO_2 and CaO in each other, and they found that the presence of either one reduces the amount of the other dissolved in the ferrite lattice. For low SiO_2 levels, at temperature higher than 1300 ^{0}C, the solubility of CaO in the ferrite was over 0.49%. With low CaO presence, the solubility of SiO_2 was 0.07%, whilst in the presence of 0.288% CaO additions, the SiO_2 content in the lattice was about 0.02%, even though the total amount of SiO_2 additions was 0.156%. Conversely, in case of 0.156% SiO_2 addition,

the presence of CaO in the grain was only 0.193%, whereas the total amount of CaO addition to the ferrite was 0.228%. The presence of CaO and SiO_2 at the grain boundaries may increase the grain boundary resistance and lower the eddy current losses, but grain boundary stresses may build up, that will reduce the initial permeability and increases the hysteresis losses.

Mochizuki[5] proposed a different model where he stated that during heating, Ca^{2+} ions diffuse through a liquid phase, the melting point of which was lowered by Si^{4+} ions, remaining in the glassy phase. Some of the Ca^{2+} ions take up Fe sites, and the rest remain at the grain boundaries. More recently *Yamada and Otsuki*[49] have investigated the combined effect of various amounts of CaO and SiO_2 additions on the electrical resistivity and power losses. They determined the optimum amount of both additives that improves the properties as being 0.033 wt% SiO_2 and 0.042 wt% CaO respectively. *Tung et. al.*[50] have also reported that the power losses decreased with the addition of both SiO_2 and CaO to Mn-Zn ferrite.

2.2.2 Titania and Hafnia Additions

The effect of Ti^{4+} ion substitutions on the properties of $MnFe_2O_4$ ferrite was first reported by *Smit and Wijn*[16]. The additions TiO_2 were not limited to small amounts, because TiO_2 can effectively be substituted for Fe_2O_3, as the combination of Ti^{4+} plus Fe^{2+} replaces $2Fe^{3+}$.

Many oxides of 3d and 4d elements have been used as additives to achieve changes in temperature dependence of the initial permeability and the electrical resistivity of Mn-Zn ferrites. *Stijntjes et. al.*[9] examined the effect of TiO_2, B_2O_3, and ZrO_2 on the magnetic properties of Mn-Zn ferrites. They focused on the influence of Ti^{4+} ion substitution on the secondary permeability maximum and on the electrical resistivity. The secondary permeability maximum depends on the Fe^{2+} ion content and any changes will cause a shift to higher or lower temperature because it is caused by anisotropy compensation due to the presence of Fe^{2+} ions. The Ti^{4+} ion

substitution offers a simple way to increase the Fe^{2+} content at the octahedral sites which leads to decreases of the temperature factor where the secondary permeability maximum occurs and also affects the disaccommodation factor. As a result this will increase the thermal stability of the ferrite in its operating range. To achieve such an increase in thermal stability a better control may be obtained by keeping the Fe^{2+} concentration constant and simultaneously increasing the Mn^{2+} and Ti^{4+} contents while reducing the Fe^{3+}.

Mn-Zn ferrites have a low electrical resistivity caused by the hopping effect of Fe^{2+} to Fe^{3+}. This mechanism can be prevented by additives, specially Ti^{4+}, which usually occupy the octahedral '*B*' sites next to the Fe^{2+} ions preventing the electron movements from Fe^{3+} to Fe^{2+}. The Ti^{4+} ions at the octahedral '*B*' sites form a complex with the Fe^{2+} ions in the spinel lattice. As a result of the Ti^{4+}-Fe^{2+} complex formation the electrons will be located which prevents the hopping effect and as a result the Mn-Zn ferrite resistivity improves significantly. *König*[32] reached the same conclusion by examining the effect of Ti^{4+} substitution in Mn-Zn ferrites on the compensation point (T_0) of the crystal anisotropy constants and on the shape of the permeability vs. temperature dependence curves. It was found that (T_0) was shifted to lower temperatures by Ti^{4+} substitution which was related to the Fe^{2+} content. *Yan and Johnson*[25] investigated the effect of titania on the microstructure development of Mn-Zn ferrites and observed that titania induced exaggerated grain growth without the formation of a liquid phase. They suggested two mechanisms for TiO_2-influenced exaggerated grain growth.

- Segregation of Ti^{4+} ions to the grain boundaries repels other segregates which would inhibit grain growth, or
- the creation of excess cation vacancies by Ti^{4+} ions increases the pore mobility, which, in pore loaded grain boundaries, would enhance grain growth.

Nomura and Mori[39] have concluded that the addition of TiO_2 enables the attainment of high density sintered Mn-Zn ferrite by low temperature sintering.

However *Lebourgeois et.al*[51]. reported that the Ti^{4+} substitution has only a small influence on both grain growth and the sintered density, but lowers the power losses. The reduction in power losses was explained as a result of titanium being incorporated into the spinel phase, such that magnetocrystalline anisotropy energy could be adjusted precisely.

Recently many workers have suggested that to achieve better magnetic and electrical properties in Mn-Zn ferrites, small amounts of TiO_2 or HfO_2 be used on their own or in conjunction with CaO and SiO_2. *Mochizuki*[5] and *Otsuka et.al.*[6] examined the effect of HfO_2 additions on Mn-Zn ferrites and showed that increases in the resistivity occurred and therefore the core losses were reduced.

The overall results which were been reported by *Mochizuki*[5] were that small added amounts, 0.01 wt% HfO_2 gave increases in the average grain size, and improvement in sintered density, while the overall resistivity increased, as a result of the gain in the grain boundary region. Consequently the power losses were lowered significantly. TEM analysis showed that the HfO_2 precipitated at and around the grain boundaries regions. The same conclusion was presented by *Otsuka et.al.*[6] where a remarkable increase in electrical resistivity and reduction in power losses were noticed when HfO_2 and TiO_2 were added in combination with CaO and SiO_2. They concluded that HfO_2 formed CaO-HfO_2 enriched boundary layers, which raised the electrical resistivity remarkably, and hence reduced the power loss at high frequencies due to the enhancement of the resistivity. The addition of TiO_2 with CaO and SiO_2 improves the density as well as the electrical resistivity[7]. *Neamtu and Barb*[13] and *Drofenik and* $\check{Z}nidar\check{s}i\check{c}$ [52] reported a notable improvement in the overall magnetic properties as a result of the addition of TiO_2 to Mn-Zn ferrite.

2.3 Ferrites Preparation and Processing

2.3.1 Powder Preparation Methods of Ferrites

Almost all the existing techniques of solid state chemistry can be used in the preparation of ferrites which leads to a very wide variety of forms: polycrystalline aggregates, thin and thick films, and single crystals. Some of these methods have been perfected to prepare ferrites with specific applications. The overall properties of ferrites are governed by a combination of intrinsic and extrinsic properties[53, 54]. An intrinsic property, such as saturation magnetisation depends on the material composition, while an extrinsic property, such as magnetic coercivity, is to a large extent, dependent on the microstructure which is in turn influenced strongly by the processing procedures. The ideal characteristics that ferrite powders should have; are small particle size, dispersed particles, narrow distribution in particle size, high purity, spherical particle shape and homogeneous composition.

There are many methods of preparing ferrites currently in use due to the wide variety, quantities, and formulations. Preparation methods are dependent on the required rate of throughput, equipment and availability of raw materials. The ferrite microstructures are closely dependent on the manufacturing process. Significant improvements have been made in the materials and magnetic properties of ferrite prepared by non-conventional processing methods[55,56,57]. Nevertheless, the great challenges in ferrite development exist in the area of improving process control to achieve product improvements using the less than ideal industrial conditions .The main preparation methods that can be used are conventional mixed oxides, sol-gel, coprecipitation and spray pyrolysis.

2.3.1.1 Conventional Mixed Oxide Processing

The mixed oxides processing method remains the predominant technology for most of the ferrite production industry. *Street*[58] has detailed a flow chart, *figure 2.7,* for the process. In this method the powder is prepared from raw materials

usually oxides or carbonates. Special care has to be taken in the preliminary stages because the mixing of raw materials is an inevitable and most important procedure as homogeneity is so significant in the finished product.

The mixed oxides should have enough reactivity, such that on mixing and prefiring, a homogeneous ferrite can be obtained. Utilising the wet mixing of the starting oxides in an attritor, in place of a ball mill, has shown that significant reductions in the mixing time are possible.

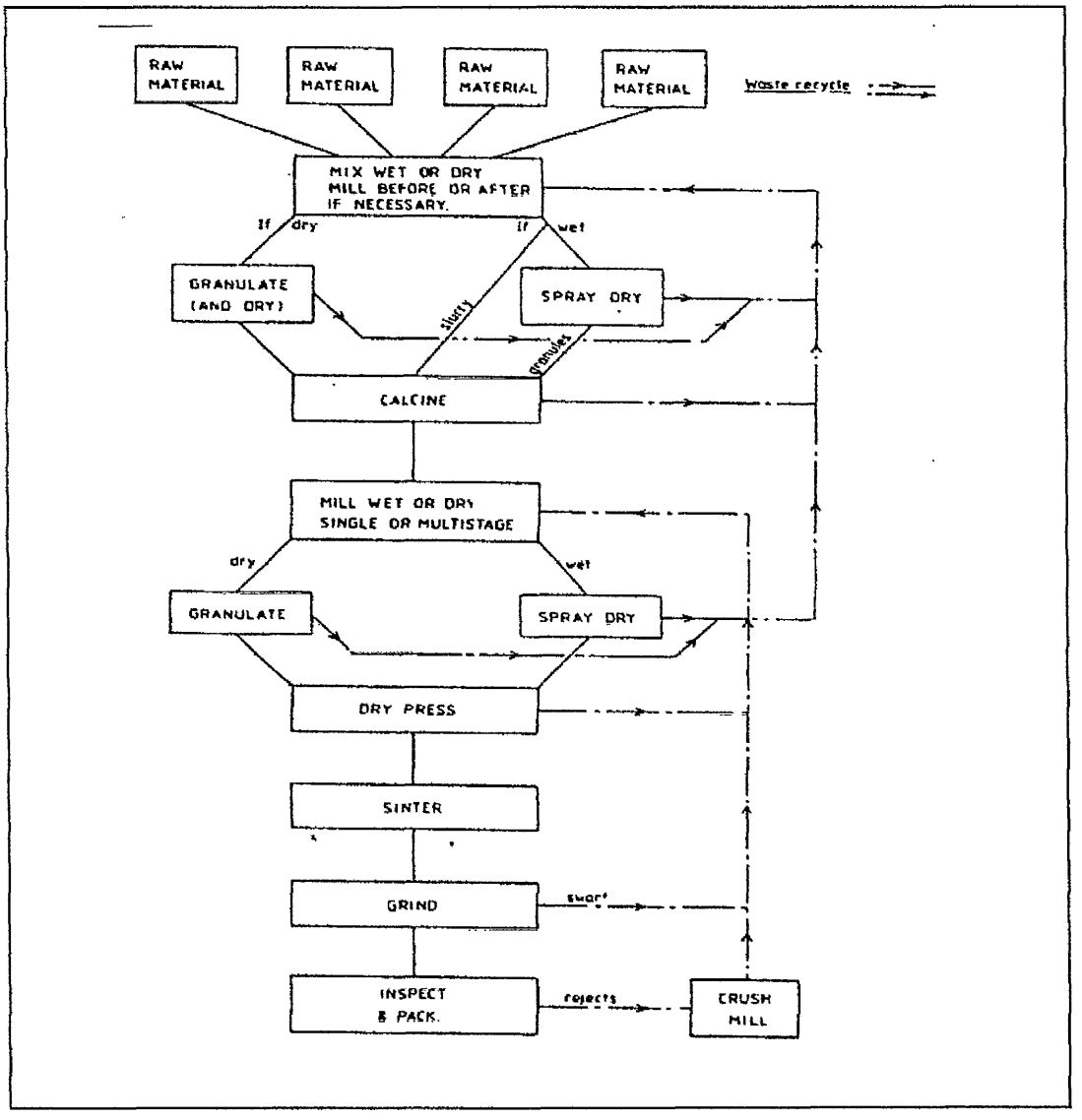

Figure 2.7. Production flow sheet for soft ferrite[58].

The mixture of oxides is calcined by heating in the temperature range of 900-1200 ^{0}C to form partially or fully ferrite as reported by many authors[59,60], to control shrinkage and to homogenise the mixture. The calcination is usually performed in a rotary kiln, and much care has to be taken because the calcination time and temperature have a great effect on the properties of the final product. The degree of reaction is much dependent on the time and temperature. If the prefiring temperature is too high, significant ferrite formation takes place during prefiring and the sintered agglomerates are difficult to break. These agglomerates can have a great effect on the final microstructure of the sintered ferrite. In the case where the prefiring temperature is too low, the reaction kinetics are very slow and the final powder is not homogeneous. The relationship between the spinel content and temperature of firing is linear for Mn-Zn ferrites and gives around 30% spinel formed at 800 ^{0}C and 100% at 1350 ^{0}C[61].

Milling is required after the prefiring stage to obtain powder with better sinterability and chemical reactivity, prior to the sintering stage. The milling process is to eliminate agglomerates and/or to reduce the particle size. Agglomerates which are present during the sintering process usually densify more quickly internally than with neighbouring particles with a resulting residue of voids in the spaces originally between the particles. Milling introduces defects into the crystals that may enhance diffusion and accelerate sintering, as well as breaking up agglomerates. The most conveniently utilised method of milling is wet ball milling. Attritor milling, instead of ball milling, has considerably reduced the milling time and gives a much more homogeneous particle size distribution. The milled powder is spray dried into spheroids ready for pressing or forming. The final stage of this method is the sintering stage that is discussed in section *2.3.3*.

2.3.1.2 Citrate Sol-Gel Method

Sol-gel processing is a relatively new technique, which has been used successfully for preparing ceramic powders. These days the sol-gel techniques are receiving much attention because they can be applied to an extremely wide range of materials. They offer the possibility of controlling not only the size and distribution of particles, but also their shape. The sol-gel processing technique has been developed to obtain fine ferrite particles and powders having homogenous chemical compositions and particle sizes.

The sol preparation process start by mixing concentrated solutions containing the cations of interest with an organic solvent as the dispersion medium. It is also possible to begin with a colloidal solution, instead of, or in addition to, the solutions. By adding water the sol is then destabilised. The presence of water modifies the pH of the sol and reduces the repulsion between particles, which results in a large increase in viscosity of the system, leading to formation of a gel. The amount of water has to be a minimum. *Delmon et. al.*[62]investigated the gel process using various nitrates and chlorides ,as starting chemicals, dissolved in citric acid in distilled water. The citric acid and metal ions quantities ratio can be expressed as[63]:

$$R = \frac{(gram\ equivalent\ citric\ acid)}{(gram\ equivalent\ metal)} \qquad 2.3$$

IR analysis has shown that even for calculated values of R less than 1, citric acid did not fully combine with metal ions until the ratio was increased to 1:1.

The homogeneity of the aqueous solution of salts is preserved in the amorphous precursor and may therefore be retained into the final solid oxide product. Consequently it is important to produce an amorphous precursor, in which case there is a need to form organo-metallic complexes during processing such that precipitation avoided.

The viscous liquid obtained is then dried, by applying heat and vacuum to form a dried organic, glass-like precursor. After drying, the precursor is subjected to a final calcination process to remove all organic substances to produce oxide powders. Due to the exothermic nature of Mn-Zn ferrite precursor decomposition/oxidation, a two stage calcination process has been recommended to prevent overheating and potential phase separation or loss of component by volatilisation[64]. The temperatures of the second stage calcination controls the particle size of the ferrite powders.

The decomposition of citrate precursors has been investigated by *Delmon et. al.*[62] and *Sale and Baythoun*[65]. At low temperatures, around 200 ^{0}C dehydration occurs and then with further increases of temperature to between 300-500 ^{0}C the precursor decomposes/oxidises rapidly producing a gas mixture of CO_2 and NO_2. *Delmon et. al.*[62] studied the decomposition of the precursor using different salts where the nitrate containing precursors have been shown to decompose more rapidly than the chloride containing precursor.

Courty et. al[63] have classified the decomposition of the amorphous precursors in the following manner.

Type 1. Precursors containing nitrates ions and metals having a strong catalytic activity in oxidation, such as iron, nickel, silver, copper or cobalt, which are characterised by continuous and often rather energetic reactions.

Type 2. Precursors of oxides such as spinels, perivskites, garnets and solid solutions, suggested to have pyrolysis behaviour which is characterised by an intermediary decomposition step. Depending on the type of decomposition the precursors decompose between 300 ^{0}C and 700 ^{0}C, but sometimes calcination up to 800 ^{0}C is required for full decomposition and oxide formation.

The main problem with the process is that, whilst high chemical homogeneity may be achieved, it is necessary either to prevent the formation of agglomerates or to remove agglomerates in the products that lead to unequal sintering characteristics and resultant high porosity. Such porosity in turn causes effects upon the magnetic properties of ferrites[66,67]. However the agglomerates that are formed during calcination may be removed during a subsequent milling process.

Sol-gel methods have been also used to produce a coating of additives on ferrite particles before sintering, in an effort to achieve good distribution. *Saimanthip and Amarakoon*[68] have made use of sol-gel processing to achieve a uniform distribution of CaO and SiO_2 in Mn-Zn ferrite powder. The ferrite powder was prepared chemically and suspended in tetra-orthosilicate dissolved in ethyl alcohol and then partially hydrolysed with hydrochloric acid. Calcium acetate, in aqueous solution form, was added and the solution was stirred. The CaO-SiO_2 thin films coated each particle. The final product showed much better microstructure than that of uncoated powder.

2.3.2 Mixing and Calcination Processes

2.3.2.1 Raw Materials and Mixing Processes

The starting components should be carefully chosen and characterised according to their purity, particle size, shape, degree of agglomeration, chemical reactivity, ease of supply and cost[59]. There is a necessity for correct selection of raw materials because the ferrite structure cannot be easily controlled other than when very pure raw materials are used.

The main component Fe_2O_3, especially its chemical quality, is of prime importance in controlling the magnetic properties of ferrite. The smallest amount of impurities which already exist within the raw materials are added unintentionally during processing and may considerably affect the microstructure-sensitive

properties of the final product. The selection of the correct ratio of the raw materials is of dominant importance to the achievement of the required magnetic properties.

Kurukawa[69] has studied the influence of ferric oxide powders and found out that there is a relationship between the initial permeability and particle surface activity. *Alam et.al.*[70] have also reported that the formation of Mn-Zn ferrites is a function of the raw materials and process conditions and is strongly dependent on the purity of raw materials. *Kimura and Chiba*[59] observed a dependence on the type of manganese oxide powder used with particular respect to the ferrite formation reaction sequence. *Toolenaar*[71] has also studied the influence of raw materials, especially the iron oxide, on the ferrite reaction and powder sinterability of manganese zinc ferrites. He discovered that the iron oxide has a significant affect on the magnetic properties.

Nakamura and Okano[72] have used $FeCl_3.nH_2O$ and $FeSO_4.7H_2O$-$NaOH$ salts as starting materials to prepare Mn-Zn ferrites, and to examine their properties. The results showed that much improved magnetic and electrical properties can be achieved by using $FeSO_4.7H_2O$-$NaOH$ salt as a raw material. However, the use of $FeCl_3.nH_2O$ as raw material gave a product with smaller grain sizes and higher resistivity and lower eddy current loss. *Zenger et. al.*[41] discussed the importance of high purity raw materials, especially iron oxides, and their effects on the final properties of high quality ferrite. They concluded that a high presence of SiO_2 would increase the power losses due to inhomogeneous grain growth.

The particle size of raw materials greatly affects the mixing process, the compressibility, the shrinkage and the reactivity of the compact. The primary objective of the mixing process is to combine the starting material into a homogeneous mixture. This process can be wet or dry mixing and the aim is to form a uniform composition throughout the bulk material. It is hard to avoid unmixing in some regions of the mass because of particle size or density differences. The most common mixing method for the starting oxides is the ball mill, which consists of a

lined pot with hard spheres or rods inside. Milling happens by impact of the spheres or rods on the powder. For an efficient tumbling, there is a limiting rotation speed imposed by centrifugal forces.

To increase the degree of mixing, the milling can be carried out in a wet medium by forming a liquid suspension of the raw materials. The limiting size of the mechanical milling is around 0.2 μm even after long periods of milling, and extended milling times have disadvantages as the spheres of the mill become worn and the introduction of undesired impurities into the powder, while the distribution in particle size becomes extremely wide.

Chol et. al.[73] reported that the vibratory mill produces more a homogeneous mixture than those obtained by ball milling. They also reported that manganese and iron oxide components become more homogeneous with milling time up to twelve hours, but the zinc component reached the maximum homogeneity after four hours of milling. Continuing the milling for more than four hours gave homogeneity decreases presumably due to some form of zinc oxide agglomeration.

Small particle sizes of the reactant powders provide a high contact surface area for initiation of the solid state reaction and short diffusion paths that lead a to more efficient completion of the reaction. The initial pore size is very important for the porosity elimination, while the narrow size distribution of spherical particles together with a dispersed state is important for compaction of the powder. Grain growth during sintering can be better controlled if the initial particle size is small and uniform.

Auradon et. al.[74] found that the initial permeability of Mn-Zn ferrite increased with the milling time. *Zaspalis and Mauczuk*[75] have reported that there were significant improvements in the magnetic properties associated with the homogeneity index increment. *Shibuya et. al.*[76] have debated that the coercivity of

Mn-Zn ferrite particles is originated by virtual shape anisotropy which is generated by groups of chained particles formed along the direction of magnetic field.

Lin and Nadiv[77] suggested that changes caused by intensive grinding of non-metallic materials include the following.

- Polymorphic transformations and alterations in magnetic properties of the bulk phase;
- mechanical activation and changes in solid surface properties;
- recrystallisation and amorphisation, and
- mechanochemical solid state reactions either at the surface or in the bulk.

Kosmac and Courtny[78] reported that while the understanding of the nature of mechanochemical reactions involving non-metallics has advanced somewhat, the fundamental processes controlling the evolution of structure, kinetics, and the thermodynamics of resulting chemical or physical transformations are still incompletely understood.

Kaczmarek and Ninham[79] have shown that complete phase transformation of hematite, Fe_2O_3, into magnetite, Fe_3O_4, may be achieved by room temperature ball milling. It was found that milling in air does not promote transformation while the use of the same milling conditions in vacuum, pure nitrogen or argon atmosphere, gives rapid reaction. The reduction of oxygen partial pressure was the main factor determining the process effectiveness.

2.3.2.2 Calcination Process

The calcination process is an important part of the control of powder properties during the formation of Mn-Zn ferrite. Calcination, or pre-sintering, is a process in which the temperature of the powder is elevated to the region of 1000 ^{0}C. The main objectives of calcining are to start the process of forming the ferrite lattice.

During the calcination process, the particles are combined by solid state reaction to form, partially or fully, ferrite structure. The magnitude to which ferrite is formed depends on the reactivity of the particles and the oxidation during the cooling stages of the cycle. The chemical reactions control the final product quality and the calcining process is usually employed to control the reactions[80].

Stijntjes et. al.[81] reported that for Mn-Zn ferrites when the calcined materials were cooled slowly in air, the magnetite will reoxidise according to:

$$4Fe_3O_4 + O_2 \Leftrightarrow 6Fe_2O_3 \qquad 2.4$$

which is followed by the oxidation of the divalent manganese in the mixed Mn-Zn ferrite as is shown in the following chemical reaction:

$$MnFe_2O_4 + \tfrac{x}{2}O_2 \Leftrightarrow MnO_{1+x} + Fe_2O_3 \qquad 2.5$$

The value of x will be 1/3 at temperatures higher than 1000 ^{0}C due to the formation of Mn_3O_4. Mn_2O_3 forms at temperatures of 500-1000 ^{0}C, while MnO_2 will form at temperatures below 500 ^{0}C. Thus the reactions depend on the cooling conditions and this results in a mixture of the ferrite with all these manganese oxides. The spinel phase remains in material, which has been fast quenched from the top temperature, preventing any reoxidation from occurring.

The calcination process is basically one of interdiffusion of the constituent oxides into a chemically and crystallographically homogeneous structure. The concentration gradient is the driving force for the interdiffusion. Some of the ferrite is created at the interface, as the individual oxides interdiffuse. This achieved phase decreases further diffusion. In the centre of each of the oxide particles, the materials have difficulty diffusing through the ferrite due to the diffusion distances becoming larger. If the powder is subsequently broken up exposing the inside of the particles, the driving force for diffusion is established again.

Another benefit of calcination is that it reduces or controls the shrinkage that occurs during the final sintering. This allows better control of the final dimension when this control is needed. Furthermore, calcining helps in decomposition of oxides and therefore it reduces the evolution of gases in the final sintering.

Krysicki and Lubanska[80] studied the influence of calcination on the initial permeability of the product and concluded that the cooling sequence following calcination affects the initial permeability of ferrite. *Živič and Lakner*[82] suggested that calcination at 850 to 950^{0}C, although providing less calcined homogeneity, results in better electromagnetic properties due to the higher reactivity and higher oxidation degree that enables the higher final sintered density. It was explained that the calcination basically affects the nature and dynamics of microstructure development. Better homogenisation is achieved through calcination at higher temperatures between 950 to 1050 ^{0}C and may produce a uniform and dense microstructure, but the reactivity and the oxidation level decrease significantly.

2.3.3 Sintering Processing

Sintering is an extremely complex process with many interaction factors as shown in *table 2.4.* The perfect sintering process results in a fully dense material by elimination of the porosity[14].

Sintering is a technical term for the densification of a particulate ceramic compact. Sintering is basically a removal of the pores between the starting particles, accompanied by shrinkage of the component, combined with inter-growth and strong bonding between touching particles. There are certain principles that must be met before sintering can occur:

- a mechanism for material transport must be existing, and
- a source of energy to activate and sustain this material transport must be present.

Interaction Factor	*Characteristic*
Powder	*Chemical composition*
	Average particle size
	Particle shape
	Particle distribution
	Pressing.
Additives	*Melting temperature*
	Solubility in product phase
	Cations vacancies
Sintering condition	*Heating rate*
	Sintering temperature
	Sintering time,
	Cooling rate
	Oxygen partial pressure

Table 2.4. Variables of sintering[14].

The main mechanisms for transport are diffusion and viscous flow. Heat is the main source of energy, in conjunction with energy gradients as particle to particle contact and surface tension. The sintering temperatures and heating rate have a great influence on the final properties of Mn-Zn ferrite.

2.3.3.1 Solid State Reaction

Pure Mn-Zn ferrites have a solid state sintering mechanism, where the material is in the solid state during the whole sintering process. The simplest way of representing solid state sintering is shown in *figure 2.8*.

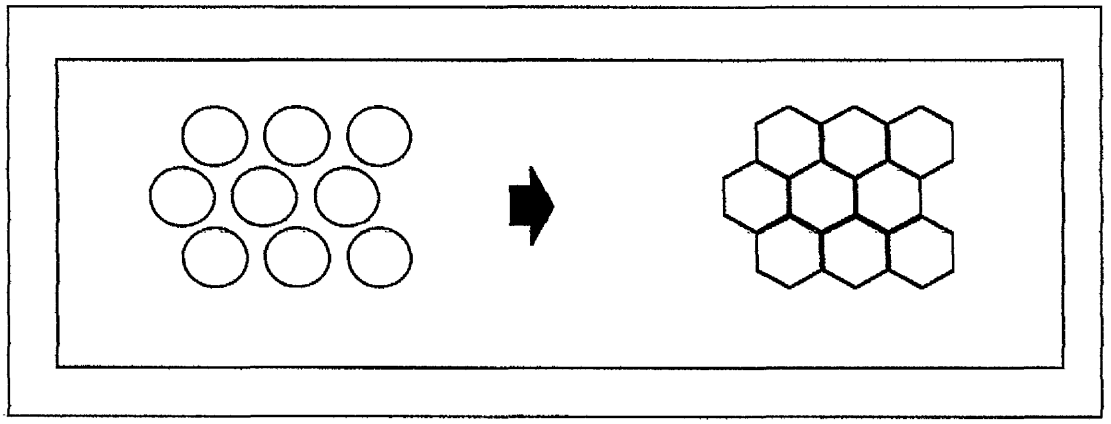

Figure 2.8. Sintering mechanism of sold-state sintering[83].

The series of solid state reactions leading to the mechanism of formation of spinel ferrites is shown in *figure 2.9.*, which shows the simple diffusion couples involving divalent metal oxide Me^{2+} and Fe_2O_3. The solid state reaction begins with the initial configuration where there is only one phase boundary between the reactants. Following the nucleation of ferrite, this boundary is replaced by two different phase boundaries, one between Me^{2+} oxide and ferrite $Me^{2+}Fe_2O_4$, and another between Fe_2O_3 and $Me^{2+}Fe_2O_4$. At this stage additional progress of reaction can only occur by movement of reactants through the ferrite phase. The difficulty is to determine which of the different ions of the components migrate across the ferritic phase and are mainly responsible for the reaction.

The ion diffusion means the simultaneous movement of electrical charges. This put limitation on the diffusional fluxes of the ions because in the steady state the net electrical charge flowing across the reaction layer must be zero. This state allows for a number of different balancing fluxes that are often referred to as different reaction mechanisms.

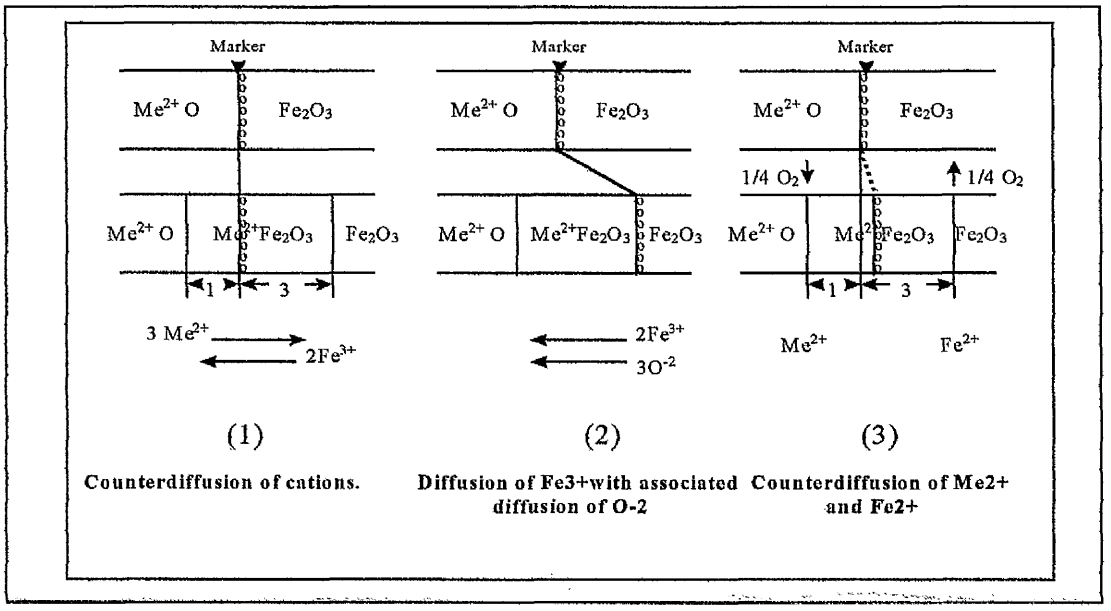

Figure 2.9. Schematic representation of possible reaction mechanisms involved in ferrite formation[84].

The theoretical relationships were deduced under the following assumptions.

- A thermodynamic equilibrium was maintained at the phase boundaries; therefore the phase boundary reaction rates were lower than those of the diffusion processes through the reaction product layer.

- The reaction product Mn-Zn ferrite layer was assumed to be highly dense and free of cracks. The contribution of diffusion at grain boundaries and dislocations was held to be very small and the only lattice defects present in the Mn-Zn ferrite reaction layer were those that were in thermodynamic equilibrium.

- The fluxes of pores, ions and electrons were mutually independent and were connected through the requirement of the electroneutrality.

In *figure 2.9.* three possible reaction mechanisms in which $MeFe_2O_3$ can be formed are given schematically indicating ionic and electronic fluxes, in addition to the position of the inert markers before and after ferrite formation. *Wagner*[85] and

Reijenen[86] considered the material transport mechanisms in solid state reaction shown in *figure 2.9.* In example 1, only cations migrate in the opposite directions, while the oxygen ions were basically stationary. Under these environments the position of inert markers does not change. As predicted, the ratio of ferrite formed on the both sides of the marker was 1:3.

In the second example, *figure 2.9.* part 2, the anions take part in the diffusion process, and in an extreme case there was a reaction in which the diffusion of one cation, either Me^{2+} or Fe^{3+}, was compensated for entirely by an associated flux of anions instead of a counter-current of other cations, as in the previous example.

In the third example *figure 2.9.* part 3, Fe^{2+} diffused through the ferrite layer. In that case, oxygen is transported through the gas phase, being supplied at the $MeFe_2O_4/Fe_2O_3$ interface and taken up again at $MeO/MeFe_2O_4$ boundary. The inert marker displacement was proportional to the amount of oxygen transported through the external phase. Practically, these experimental techniques have been found to be difficult when significant changes in density are involved and shrinkage of the ferrite may lead to fracture of the reactant-product interface[84].

2.3.3.2 Mn-Zn Ferrite Sintering Reactions

Other factors to be considered in ferrite sintering are the chemical reactions which occur between the constituent oxides. These reactions are known to affect the final product properties and the calcining stage is usually used to control these reactions[57,81,82]. The sintering process of pure Mn-Zn ferrite starts with the rapid burn-out of organic binder which can be limited due to the formation and escape of gases by the combustion processes.

Broussaud et. al.[87] reported that the sintering atmosphere during the binder burn-out is very crucial as it affects the final properties of Mn-Zn ferrite. In situations where the organic binder is burnt-out in a reduced oxygen atmosphere, the

ferrite will be reduced because of the consumption of oxygen from the ferrite by the organic binder. The primary sources of oxygen in that case may be MnO_2 and some Mn_2O_3, that formed during cooling after calcination process.

Stijntjes et. al.[81] using DTA found that strong exothermic reactions which form carbon dioxide and water at temperatures between 200 and 290 ^{0}C occurred during the burn-out of the organic binder. Hence the temperature increases rapidly as a result of the exothermic reactions that will accelerate at higher temperatures. As a result chemical homogeneity of Mn-Zn ferrite may be affected due to zinc evaporation.

The removal of organic binder at low heating rate and high oxygen atmospheric pressure results in higher green strength. The oxides reactivity during sintering depends on the co-ordination of the various cations because of the stronger covalent bonding of the divalent manganese ions in the tetrahedral '*A*' sites as compared to the ionic bonding of the divalent iron and trivalent manganese[81].

Perriat et. al.[88] have given a complete model for oxidation and reduction reactions that occur at low temperatures for spinel oxides. They suggested that when the iron based spinel oxides contains one or more oxidizable cations, such as Me^{3+} and Me^{4+} in ferrites, each cation oxidises in a well defined range of temperature in close relation with the cation-oxygen distance of the cation. The cation-oxygen distance depends on both valence state and the location in the spinel structure, tetrahedral '*A*' or octahedral '*B*' site. The model of oxidation and reduction involves both thermodynamics and kinetics considerations where:

- thermodynamics involves the minimisation of the Gibbs free energy, and

- the kinetics of oxidation are explained on the basis of a diffusion-affected stress effect.

Kimura and Chiba[59] studied in detail the formation of commercial Mn-Zn ferrites and produced a reaction sequence and assessed the effect of raw materials and compositional changes on the process. They concluded that the reactions between ZnO and Mn_2O_3 and between $ZnFe_2O_4$ and $ZnMn_2O_4$ play no role in the formation of Mn-Zn ferrite. In the initial stage of the final sintering process, the binder added during milling, i.e. of the calcined product, decomposes and volatilizes. The first reaction to form zinc ferrite starts at around 600 ^{0}C, as shown in *equation 2.6*:

$$ZnO + MnO_\alpha + Fe_2O_3 \overset{600^0C}{\Longleftrightarrow} ZnO + ZnMn_2O_4 + Fe_2O_3 \overset{800^0C}{\Longleftrightarrow} ZnMn_2O_4 + ZnFe_2O_4 + Fe_2O_3 \qquad 2.6$$

Experiments observing changes in the lattice constants of the spinel, showed that in the ZnO-Fe_2O_3 system, the lattice constant remains the same between 700 ^{0}C and 1100 ^{0}C which suggests that the zinc ferrite formation goes to completion at around 700 ^{0}C. The reactions to form Mn-Zn ferrite start at 800 ^{0}C, through slow dissolution of the manganese into the zinc ferrite. The reaction rate increases at higher temperatures, around 1000 ^{0}C. Alteration in the spinel lattice constant in the system MnO_2-ZnO-$2Fe_2O_3$, thought to be due to an increasing Mn content into the zinc ferrite spinel, reaches a maximum at around 1100 ^{0}C. The final reaction is thought to reach completion at 1200 ^{0}C, according to *equation 2.7*:

$$ZnMn_2O_4 + ZnFe_2O_4 + Fe_2O_3 \underset{900^0C}{\overset{800^0C}{\Longleftrightarrow}} Spinel + Fe_2O_3 \overset{1200^0C}{\Longleftrightarrow} Mn_{\frac{1}{2}}Zn_{\frac{1}{2}}Fe_2O_4 \qquad 2.7$$

Perriat et. al.[88] noticed that during the rise in sintering temperature, the oxidation and reduction reactions occurred up to 1000 ^{0}C and had an influence on the grain growth and the densification, but too violent reaction could lead to cracks during this stage. *Neijts*[29] studied the chemical reactions of the Mn-Zn ferrite that

been used as a base composition in the present study. The heating and cooling reactions are given in *table 2.5.*

Heating Cycle	
Temperature Range (^0C)	***Reaction***
0-400	$Adsorption.of.H_2O,.CO_2.releases,.and.thermal\ expansion$
500-700	$MnO_2 \Leftrightarrow Mn_2O_3 + O_2$ $MnO_x + ZnO \Leftrightarrow ZnMnO_4$
700-800	$MnO_2 \Leftrightarrow Mn_2O_3 + O_2, Ends$ $Mn_2O_3 \Leftrightarrow Mn_3O_4 + O_2, Starts$ $ZnO + Fe_2O_3 \Leftrightarrow ZnFe_2O_4$
800-1000	$Mn_2O_3 \Leftrightarrow Mn_3O_4 + O_2$
1000	$Mn_2O_3 \Leftrightarrow Mn_3O_4 + O_2, Ends$ *Shrinkage begins*
1000-1400	$Mn_3O_4 + Fe_2O_3 \Leftrightarrow MnFe_2O_4 + O_2$
1200-1400	$Fe_2O_4 \Leftrightarrow Fe_3O_4 + O_2$
Cooling Cycle	
1400-1200	$Fe_3O_4 + O_2 \Leftrightarrow Fe_2O_3$
1400-600	$MnFe_2O_4 \Leftrightarrow MnO_x + Fe_2O_3$

Table 2.5. Reaction sequence of a commercial Mn-Zn ferrite[29].

The ferrite reactions during cooling following sintering are similar to those of the oxidation reactions found during cooling after the calcination process. The chemical composition achieved during sintering is not stable in an oxidising atmosphere at lower temperature and reoxidation occurs. As a result at temperatures

lower than 900 ^{0}C, ferrites pick up oxygen from the atmosphere and form a reoxidised material. *Kim et. al.*[89] found that the oxidation of manganese zinc ferrite produces hematite, α-Fe_2O_3, which precipitates on the close-packed lattice planes, as plate shaped particles. The relationship between platelet length and time indicates that the rate of formation is limited by diffusion. It was found that around the hematite plates pores were produced as an after effect of hematite formation.

2.3.3.3 Effect of Partial Oxygen Pressure during Sintering Process

As indicated above, during the sintering process, not only densification but ferritisation also takes place. Mn_2O_3 and excess Fe_2O_3 release a large amount of oxygen on reaction during heating and in order to control this reaction, it is essential to select adequate oxygen partial pressure in the sintering atmosphere. As a result it has been recognised that one of the main parameters during ferrite preparation is the control of the atmosphere as function of temperature. Particularly, conditions during the sintering and cooling of these materials are critical and have a most important influence on the magnetic properties. Ferrite compositions vary from one another by the amount of oxygen they contain and by the distribution of valences among their cations. Generally, a particular composition can be obtained at high temperature by the suitable choice of oxygen content in the sintering atmosphere. Oxidation mechanisms of Mn-Zn ferrites are interpreted as:

- the reaction $Fe^{2+} \Rightarrow Fe^{3+}$ forming cation vacancies in the spinel at higher temperature and α-Fe_2O_3 below the grain boundary, and

- the reaction $Mn^{2+} \Rightarrow Mn^{3+}$ with the formation of β-Mn_2O_3.

The oxygen partial pressure in the gas phase in equilibrium with trivalent iron ions is a function of Mn-Zn ferrite composition and sintering temperature. Reduced oxygen partial pressure leads to a reduction of trivalent iron into divalent iron ions, which result in increased oxygen vacancy in the ferrite. This process intensifies

volume diffusion which leads to a higher sintered density. However, an unsuitable oxygen partial pressure alters the oxidation degree of the ferrite, the grain boundary energy, and can generate a heterogeneous composition by cations migration.

Blank[90] began the work of constructing a phase diagram, including contour lines of constant Fe^{2+} content at certain oxygen partial pressure as a function of temperature. He proposed a universal equilibrium diagram for all ferrites, *figures 2.10* and *2.11*, with particular sections of it appropriate for specific ferrites, and was able to define boundaries enclosing temperatures and oxygen content within which a relatively stable spinel phase was achievable.

The universal diagram was designed to apply for all ferrite compositions, where interaction with oxygen occurs via redox reactions of ferric and ferrous ions. The diagram was intended to represent ferrites which maintain their spinel structures. Melted ferrites, or those which form second phases were not included. As such, only specific parts of the diagram were expected to be appropriate for certain ferrites.

Slick[91] has determined a composition-atmosphere-temperature diagram for the equilibrium in a Mn-Zn ferrite based on the principles given by *Blank*[90], as shown in *figure 2.12*. *Morineau and Paulus*[92] determined the relation between the equilibrium oxygen pressure and oxygen nonstoichiometry of Mn-Zn ferrites using of thermogravimetry and determination of Fe^{2+} content, but they showed only the cation-deficient region of positive δ. δ is dependent on oxygen pressure at constant temperature. *Morita and Okamoto*[93] concluded that the achievement of a desired oxygen content requires simultaneous control of the deoxidation and sintering rates by adequate adjustment of the oxygen partial pressure in the sintering atmosphere.

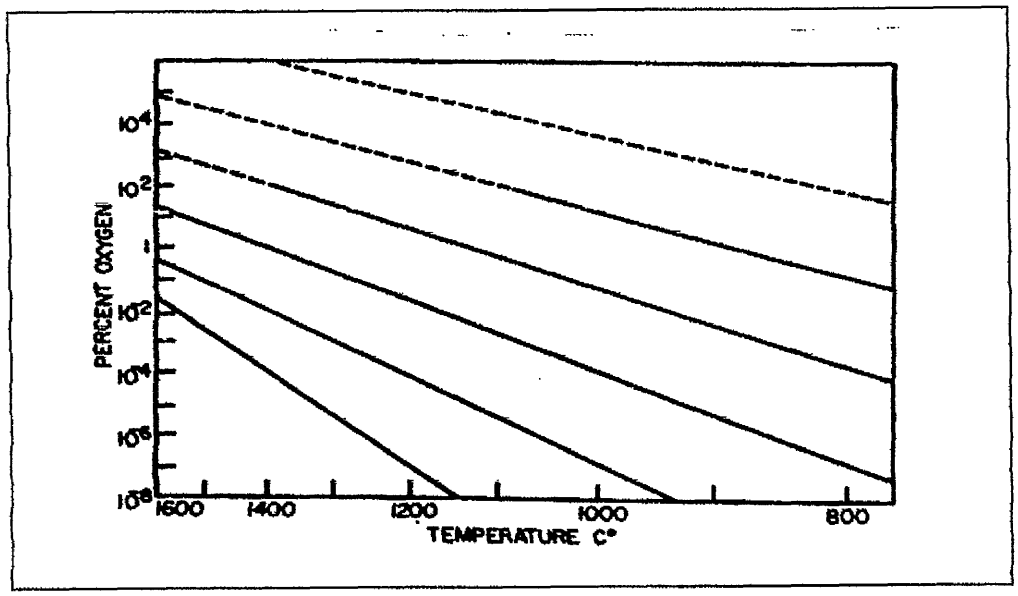

Figure 2.10.Universal equilibrium atmosphere diagram[90].

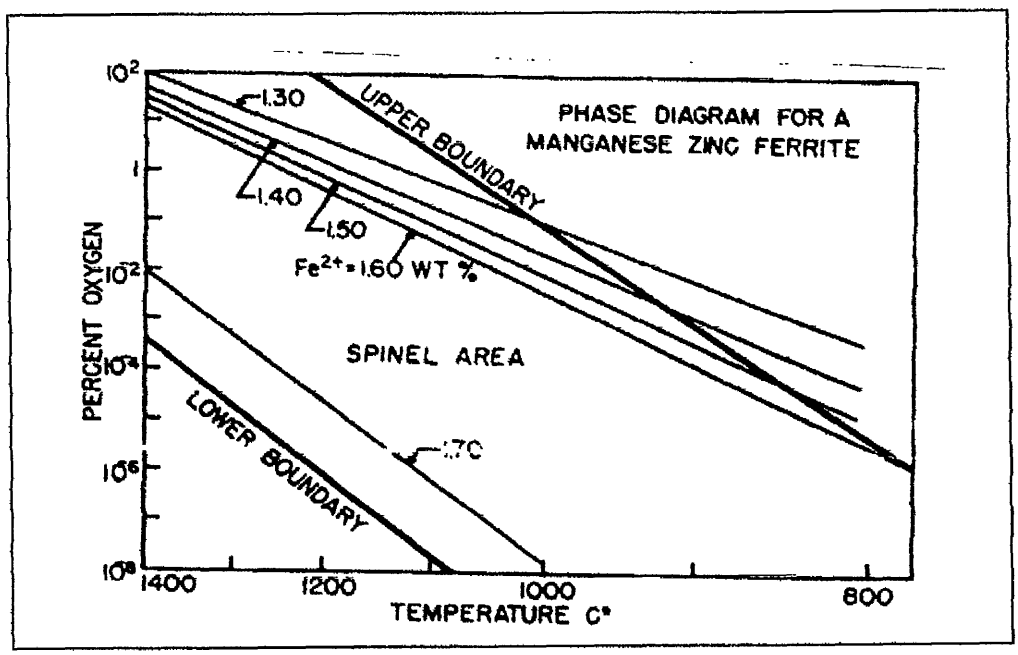

Figure 2.11. Phase diagram of Mn-Zn ferrite[90]

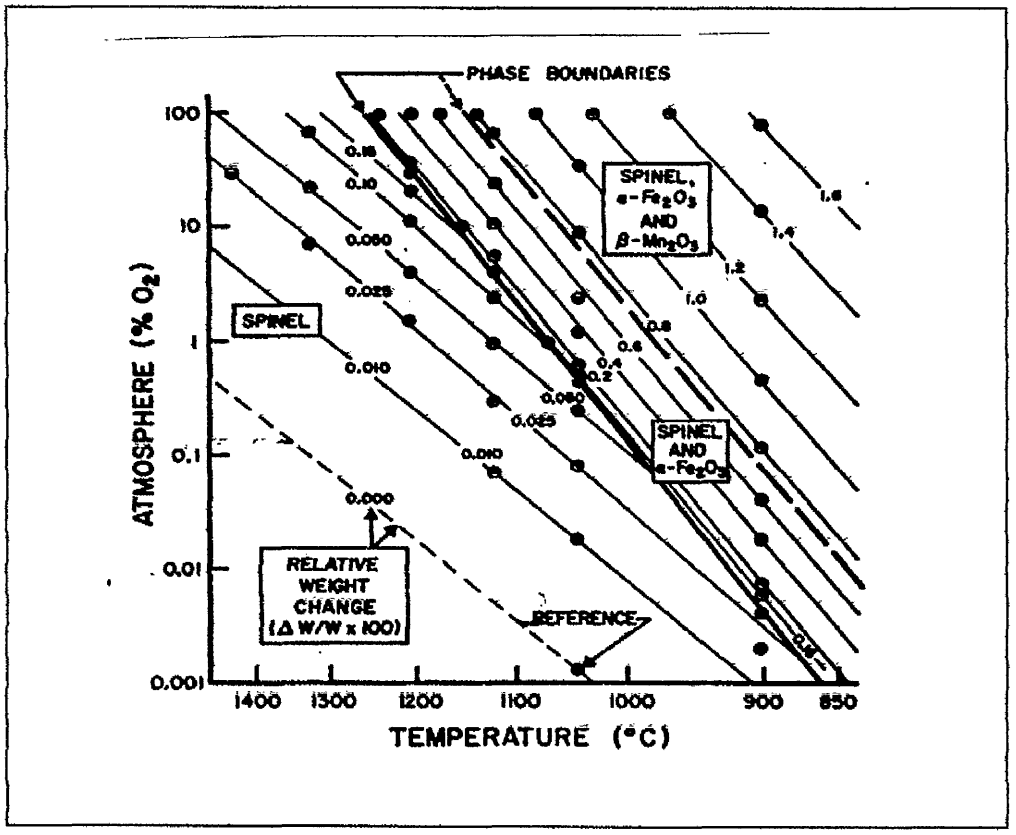

Figure 2.12. Equilibrium oxygen partial pressure, P_{O2}, as a function of temperature for Mn-Zn ferrites[91].

Nomura and Mori[39] have correlated the oxygen partial pressure of the sintering atmosphere with oxygen content of ferrite powder and suggested that the oxygen partial pressure should be adjusted according to the oxygen content.

Inaba[94] has studied the effect of oxygen nonstoichiometry on the physical and magnetic properties of Mn-Zn ferrite. In summary his results are as follows.

- It has been suggested that the dependence of oxygen nonstoichometry on disaccommodation and the change of Fe^{2+} content at the stoichiometric composition were due to the presence of two different defects structures of Mn-Zn ferrites.

- The lattice parameters became a maximum at the stoichiometric composition, which suggested that the major defects were cation vacancies in cation-deficient regions and oxygen vacancies in anion-deficient regions.

- The electronic conduction was deduced to be of *p*-type for the cation-deficient region and *n*-type for the anion-deficient region.

- The magnetic properties were significantly improved at the stoichiometric composition which suggest the importance of the number of point defects for the initial permeability as well as for the power loss.

In order to engineer the Mn-Zn ferrite microstructure, the concentration of oxygen during sintering may be varied from 21 vol% to 1 vol%. It was established that a higher amount of oxygen, ≥21 vol%, increases the pore mobility and induces exaggerated grain growth, while a lower oxygen concentration increases the concentration of the slowest moving species, i.e., oxygen vacancies, and promotes volume diffusion and therefore the grain boundaries mobility[95]. Conversely, the pore-grain boundary interaction during sintering has an absolute influence on the microstructure development[96]. Depending on the pore size-grain size ratio, the grain growth is largely determined by the attachment or separation of the pores from the grain boundary. In cases where this ratio is small the pores will be left behind and the conditions for the formation of grains with exaggerated grain size and trapped pores will be present. Hence, to manage effectively the microstructure of Mn-Zn ferrites, exaggerated pores must first be developed by applying a high partial pressure of oxygen during sintering.

Carpay[97] emphasised that if these pores are large enough they can effectively pin the grain boundaries, and hinder grain growth at lower oxygen partial pressure, which decreases densification and promotes pores mobility. *Mochizuki*[5] indicated that maintaining a reduced oxygen partial pressure from 600 ^{0}C during

heating stages increases the mobility of the cation vacancies that would result in ferrites of higher sintered density.

The influence of the oxidation and reduction reactions occurring during the cooling stages of sintering on the properties of ferrites can be explained by the fact that the reactions, which are determined by the atmosphere conditions, lead to a deviation from stoichiometry of the spinel oxides, which considerably affects the electrical and magnetic properties[88].

Žnidaršič and Drofenik[98] investigated the effect of oxygen partial pressure during sintering on the magnetic properties of Mn-Zn ferrites. Their investigation revealed that a lower oxygen concentration in the sintering atmosphere modifies the ferrite microstructure and its magnetic properties, and as a result of the combined effect of the increase of the Fe^{2+} concentration in the spinel lattice and the decrease of the average grain size improved performance of M-Zn ferrite results.

Han[99] has reported that the power losses of Mn-Zn ferrites were improved significantly with the reduction of oxygen partial pressure in the atmosphere at lower temperatures. *Dawson*[100] related the initial permeability and strength upon the formations of Mn^{2+} and Fe^{2+} for Mn-Zn ferrites sintered in air. He compared the consequences of cooling a Mn-Zn ferrite in nitrogen and air, and found that the cooling in nitrogen resulted in improvement in permeability without a significant decrease in strength compared with that cooled in air. *Tung et. al.*[50] have reported that samples sintered at 1250 ^{0}C and cooled in a nitrogen atmosphere have a significant improvement in power losses compared with samples sintered at 1150 ^{0}C which were cooled in air.

2.3.3.4 Mechanisms of Zinc Loss during Sintering

High sintering temperature may lead to partial volatilisation of zinc, due to its low vapour pressure. Zinc ions present at the surface of a ferrite are in direct or

indirect contact with the sintering atmosphere and can volatilise easily according to *equation 2.8*:

$$ZnO_{(solid)} \Leftrightarrow Zn_{(gas)} + \tfrac{1}{2}O_{2(gas)} \qquad 2.8$$

Paulus[19] found that a decrease in the number of Me^{2+} ions at the surface due to Zn^{2+} loss would oxidise the surface. Although the change of oxygen content combined with open porosity cannot in this situation give an equal degree of oxidation in the matrix itself and in the surface of the body.

Beer et. al.[101] reported that decreases in the oxygen content in the sintering atmosphere will increase the zinc evaporation. This effect could occur during heating stages, but it increases during the cooling stages. Depending on the oxygen content in the sintering atmosphere, the equilibrium zinc partial pressure can be given as:

$$P_{(Zn)} = \frac{K_1}{\sqrt{P_{O_2}}} \qquad 2.9$$

where K_1 is the equilibrium constant.

Zinc and oxygen diffusion to the surface occurs through the grain boundaries and the interiors of the outer grains. *Sainamthip et. al*[68]. reported that a zinc oxide microscopic layer had been found on the outside of examined core. The microscopic zinc oxide layer was caused by zinc reduction throughout the grains and the grain boundaries.

The zinc loss decreases the lattice parameters of the affected materials. Because the zinc loss mainly occurs at the grain boundaries, the microstresses are concentrated in their neighbourhood, which increases the grain boundary energy. This results in a higher driving force for grain growth that increases the grain boundary velocity. The Zn^{2+} ion migration to the grain boundaries, before

evaporation, simulates a Fe_2O_3 defect condition with high oxygen vacancies. The high level of oxygen vacancies accelerates the grain boundary mobility which leads to exaggerated grain growth[102].

The loss of the zinc is not dependent only on sintering conditions. *Chen et. al.*[103] studied the zinc loss during sintering of ferrite using alumina cover plates. The process of zinc sublimation changed significantly when the sintered ferrite was in contact with alumina. In this case zinc and oxygen ions migrated to the alumina and formed an alumina-zinc spinel. The driving force for this process was presumed to be the lower chemical potential of zinc cations in alumina-zinc spinel as compared with that of the ferrite. The chemical reaction of zinc and alumina is given in *equation 2.10:*

$$ZnO + Al_2O_3 \Leftrightarrow ZnAl_2O_4 \qquad 2.10$$

Zinc loss could be significantly decreased by sintering the pressed ferrite on zinc rich ferrite particles[102,103,104].

Zinc loss seriously affects the magnetic properties, especially the initial permeability as reported by many authors[102,103,104]. *Tasaki and Ito*[105] studied the effect of zinc loss during sintering at low oxygen pressure on the initial permeability. They emphasised that at sintering temperatures below 1200^0C, promotion of sintering, as caused by the lattice imperfection relating to oxygen partial pressure in the atmosphere, determines the permeability of the sintered ferrite. Hence, high permeability was obtained in atmosphere without oxygen. Conversely, ferrites sintered at temperature higher than 1300 ^{0}C have lower permeability values due to the volatilisation of zinc, and the highest value was obtained by sintering in pure oxygen. *Tsay et. al.*[106] have also addressed the same issue and related the zinc loss to the reduction of the initial permeability of Mn-Zn ferrite during long time sintering at reduced oxygen partial pressure. They suggested that the zinc loss could be substantially reduced by precise control of oxygen partial pressure and flow rate.

2.4 Factors Affect the Magnetic properties of Mn-Zn Ferrites

Mn-Zn ferrites are characterised by their electromagnetic properties.

- High saturation magnetic flux density (B_m).
- High initial (μ_i) and/or amplitude permeability.
- High Curie temperature.
- Secondary peak maximum , SPM, located at 100 ^{0}C.
- High resistivity.
- Low power loss.

These various characteristics of Mn-Zn ferrites are very sensitive to composition and/or microstructure. In general, saturation magnetic flux density (B_m), Curie temperature (T_c), or the temperature (T_p) which affects power loss is more dependent on the ferrite composition than on the microstructure of the sintered Mn-Zn ferrite. *Nomura and Mori*[39] reported that the (T_p) temperature increases with the increase of *MnO* content, while the Curie temperature (T_c) increases according to the decrease in *ZnO* content and the increase of Fe_2O_3 content. *Ochiai and Okutan*[107] produced a model for Mn-Zn ferrites which relate the magnetic properties to composition as shown in *figure.2.13.*

Nomura et. al.[108] have given a relationship, *equation 2.11.*, which shows that the saturation magnetic flux density (B_m) is dependent on temperature and sintered density.

$$B_{mt} = \left(\frac{d}{dt}\right).\left(1-\left(\frac{T}{Tc}\right)^{n}\right).\left(B_{mo}\right) \qquad 2.11$$

where B_{mt} is the saturation magnetic flux density at $T\,^0K$,

B_{mo} is the saturation magnetic flux density at $0\,^0K$,

d is sintered density of Mn-Zn ferrite,

dt is theoretical density,

T is temperature,

Tc is Curie temperature, and

n is constant.

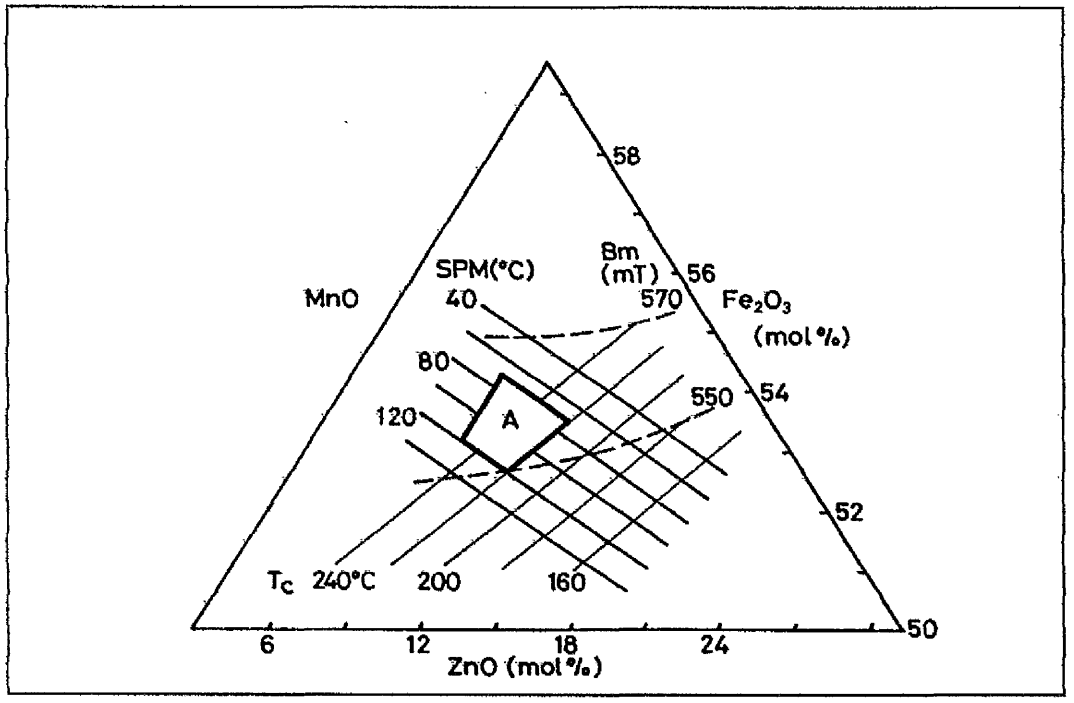

Figure 2.13. Magnetic properties of Mn-Zn ferrites represented in miscibility diagram

2.4.1 Effect of Microstructure

Even though the raw materials and additives may be carefully chosen, the microstructure of Mn-Zn ferrite is always markedly affected by sintering conditions [109]. Generally it is expected that a lower heating rate will result in Mn-Zn ferrites with higher sintered density. In cases where the sintering temperature is reached too rapidly, the grain size is not uniform and the pores can be found not only on the grain boundaries, but also in the grains. On the other hand, if the heating rate is low, the grain size is uniform and the pores are relatively distributed on the grain boundaries.

This is due to the increasing mobility of pores, that is in turn due to the oxygen ions movements through the vapour phase and the creation of cation vacancies under the controlled oxygen partial pressure. Therefore it is essential to control the oxygen partial pressure in the sintering atmosphere and the heating rate in order to obtain a high density sintered Mn-Zn ferrite composed of fine and uniform grains.

It is well known that the magnetic properties of a fired ferrite of a given composition depend on the microstructure of ferrite. The desirable microstructure of Mn-Zn ferrites can be summarised as follows.

- The homogeneity of each grain should be similar.
- The grain interior should be of high purity and high permeability.
- The grains should be fine and uniform.
- Any added impurities of high resistance should be concentrated on the grain boundaries.
- Pores should be eliminated or minimised and any remaining should be located on the grain boundaries.

Adequate selection of additives, sintering program, and the ferrite powder processing methods enable the production of such desirable Mn-Zn ferrite microstructures to be achieved. The microstructural features of ferrites include grain boundaries, pores, inclusions and other imperfections. The grain boundaries are well known acting as impediments to domain wall movement which means that the larger grains the fewer grain boundaries there are with the result that the permeability will be high.

The first determination of the relation of grain size and initial permeability for Mn-Zn ferrites was made by *Roess*[110] and it has been confirmed by *Beer and Schwartz*[101], and *Perduijn and Peloschek* [111]. The relationship between the grain size and initial permeability will generally be linear only if the grain growth is

normal, that is, if all grains grows at the same time and same rate which leads to a rather narrow range of final grain sizes.

The high quality Mn-Zn ferrites, which are used mainly at high operating frequencies, require a precise control of the microstructure, especially the grain size and grain size distribution. Better initial permeability values were found in ferrites with higher density and homogeneous grain composition. However the presence of triple points and the isolation of grains by high-resistance ultrathin amorphous layers, due to the additions of CaO and SiO_2, reduces the permeability, but improves the eddy current losses in frequency range 100-1000 kHz. Also a high level of chemical inhomogeneity, inclusions or other structural imperfection, and most importantly the high level of pores would prevent the attainment of high permeabilities[19].

The presence of pores in the ferrite microstructure acts as a pinning for domain walls which prevents their movements. There are two types of pores, which can be found in the microstructure of Mn-Zn ferrites. The first type called intergranular type and can be found on the grain boundaries. The second type, referred to as intragranular pores, can be found in large grains as a result of many pores being swept over by grain boundaries during rapid grain growth.

The effect of the intragranular porosity on the initial permeability is larger than that of the intergranular type. The distance between intragranular pores rather the grain size accounts for variations in permeability. Mn-Zn ferrites with large grains with intragranular pores due to exaggerated grain growth may have higher permeabilities than those with normally grown grains. Provided the distances between pores are the same, a Mn-Zn ferrite with a large grained microstructure is less sensitive to grain boundary effect[102].

In addition to the strong effect of the intergranular and intragranular pores on the initial permeability, the coercivity and hysteresis of Mn-Zn ferrite are also affected. *Kingery et. al.*[112] and *Chiang et. al.*[113] have suggested that the pores give

rise to demagnetising fields that can cause either rotation of the magnetisation away from easy directions or nucleation of reverse domains, in which case it is surprising that the ratio of the remanence to the saturation magnetic flux density has been found to be greater for more porous ferrites.[112,113].

Van der Zaag et. al.[114] have studied the microstructural influence on the coercive field of Mn-Zn ferrites. They found that the coercive field (H_c) depends on the grain size (D) as:

$$H_c \propto D^{-1} \qquad 2.12$$

They suggested that this dependence can be accounted for by assuming a grain boundary with unit permeability, which also accounts for the influence of the grain size on the initial permeability of Mn-Zn ferrites.

Besides the grain size, grain boundaries and pores, there are other ceramic imperfections, which occur due to the processing, or the effect of additives, which can obstruct domain wall movement. These imperfections which include microcracks, residual strains and inclusions as well as second phases act as energy walls that pin the domain walls and therefore lead to a need for higher activation energy for the detachment of walls.

2.4.2 Analysis of Power Loss

The core losses value (P_L) usually consists of three contributions, the hysteresis losses (P_h), eddy current losses, (P_e) and the residual losses (P_r). The hysteresis losses and eddy current losses predominate up to frequencies of 500 kHz. Above this frequency residual loss, which are a combination of relaxation and resonant losses caused by the delay of magnetisation equilibrium become important. The total power losses can be shown as[115, 116]:

$$P_L = P_h + P_e + P_r \qquad 2.13$$

2.4.2.1 Residual losses

The residual power loss (P_r) is caused by intrinsic damping and is a result of diffusion in the lattice, i.e., diffusion of metal ions or cation vacancies. *Snelling and Giles*[117] suggested that these losses are important only at low induction levels and can be ignored for the high induction levels in power application. *Visser*[118] reported that the residual power loss may be much suppressed by utilising ferrites that do not contain ferrous ions and are sintered stoichiometrically. *Snelling*[56] and *Visser et. al.*[119] have expressed the residual loss as:

$$P_r = 2.5x10^6 . f . B^2 . \frac{\tan\delta}{\mu_i} \qquad 2.14$$

where f is frequency (kHz),

B is flux density (T),

$\frac{\tan\delta}{\mu_i}$ is loss factor, and

δ is the loss angle.

As the residual power loss depends on low induction level and/or high frequency (> 500 kHz), for applications involving yoke ring materials the total power loss can be expressed as:

$$P_L \approx P_h + P_e \qquad 2.15$$

2.4.2.2 Hysteresis Losses

The hysteresis loss can be defined as the energy lost in magnetising and demagnetising the material. The hysteresis loss occurs when a magnetic field (H) is applied to a ferrite. Two types of magnetisation process take place.

1. There is a rotation of the magnetisation inside each magnetic domain, from the preferred direction towards the direction of the magnetic field (H) until the sum of

the magnetostatic energy and the anisotropy energy has reached its minimum value.

2. The second process depends on the domain wall movements as the domains having preferable magnetisation directions with respect to the direction of magnetic field (H) increase at the expense of others. In the case where the magnetic field is sufficient large, irreversible jumps of domain walls occur between pinning points, such as grain boundaries, internal pores or inclusions. These obstructions to domain walls give rise to dissipation of magnetostatic energy in the ferrites. In the case of an alternating magnetic field (H), a hysteresis loop of magnetic induction (B) vs. (H) results. During each cycle one loop is completed and the loss per cycle is given by the area of the loop.

The hysteresis power loss for Mn-Zn ferrite used for yoke ring which operating in low frequency condition can be shown as:

$$P_h = f.\oint B.dH \qquad 2.16$$

where: H - the magnetic field strength,

B - flux density (mT), and

f - frequency (kHz).

The reduction in hysteresis loss depends upon the following factors[120]:

- Small internal or external stresses (σ),
- Small volume fraction of inclusions (v), which includes pores, dislocations, cavities and impurities,
- Small magnetocrystalline anisotropy (K_1),
- Small magnetostriction (λ), and
- High saturation magnetisation (M_s)

The latter three are determined by the chemical composition of the ferrite. The magnetocrystalline anisotropy (K_1) can be controllable with the compensation of Ti^{4+} ions[9]. The most suitable ferrite materials for applications where hysteresis losses play an important role are clearly Mn-Zn ferrites. *Ohta*[121] and *Stoppels*[122] reported that the magnetocrystalline anisotropy of Mn-Zn ferrites with small excess of Fe can be minimised by anisotropy compensation due to the Fe^{2+}ions.

The other factors are determined by microstructure, which indicates that microstructure largely govern hysteresis loss except for the control that is obtained by the chemical composition. The inner parts of the grains should be homogeneous and free of impurities, pores or other defects. There should not be a variation in chemical composition on a microscale, neither within grains, nor from grain to grain it would result in stresses and in deviation of the magnetocrystalline anisotropy from the minimum values.

Berger et. al.[123] have observed that in the case of discontinuous variations in chemical composition on a microscale, e.g., titanium from grain to grain, higher power losses resulted in Mn-Zn ferrites. All these microstructural requires point to the need for the utilisation of pure, high quality raw material and a very well controlled preparation process

2.4.2.3 Eddy current losses

The eddy current loss (P_e) is generated by the electrical resistance losses within the core caused by an alternating magnetic flux. Eddy current loss is determined by frequency, the amplitude of the magnetic induction and the resistivity as is given in *equation 2.17*[118, 124]:

$$P_e = c.f^2.\frac{B^2}{\rho} \qquad 2.17$$

Bogs and Holubarsch[116] and *Sano et. al.*[120] showed that the grain size has a crucial effect on eddy current losses at high frequencies and modified the previous equation as follows:

$$P_e = c.f^x.B^y.\frac{d^2}{\rho} \qquad 2.18$$

where c is the proportional constant,

f is frequency (kHz),

x values is depends on grain size, for small grain size = 2,

B is the flux density (mT),

d is the average grain size (μm),

y values correspond to the values of eddy current losses, and

ρ is the resistivity at frequency (f), (Ω.m).

The following methods may be used to reduce the eddy current loss of Mn-Zn ferrites[46].

1. *Suppression of electron hopping* $Fe^{2+} \Leftrightarrow Fe^{3+}+e^-$ *inside grains.* It well known that the resistivity can be improved by titanium ion substitutions[9]. As indicated earlier titanium ions usually tend to occupy the octahedral site adjacent to Fe^{2+} and are able to suppress the electron movement between Fe^{2+} and Fe^{3+} to some extent. *Otsuka et. al.*[6], *Otsuki et. al*[125], and *Inaba et. al.*[126] have reported that of the other additives such as HfO_2, Ta_2O_5, V_2O_5 and Nb_2O_5 which have been found to be effective in increasing the resistivity by forming layers at grain boundaries and triple points, V_2O_5, has been found to be partly substituted in the ferrite spinel lattice and therefore reduces the electron hopping from Fe^{2+} ions.

2. *Formation of* $CaSiO_3$ *thin insulating films at the grain boundaries to raise the apparent resistance.* A very efficient way to improve the resistivity is to provide the grains with electrically insulating layers on the grain boundaries. For this purpose, additives such as CaO and SiO_2, are added. These additives diffuse

toward the grain boundaries during the cooling stages of the sintering process and create an electrically insulating layer of 1-10 nm thickness[45,127]. *Snelling*[56] stated that as the frequency increases, the boundary resistance becomes short circuited by the boundary capacitance. *Stijntjes*[128] confirmed the previous suggestion by illustrating this with experiment data. For the majority of power ferrites the electrical resistivity is decreased to half its value at frequencies between 100-1000 kHz.

3. *Improvement by making homogenous and small grain size ferrites.* In case where the grain size is large, the fraction occupied by the domain wall part will increase. This will result not only in the increase of microscopic eddy current, but also in the increase of the hysteresis loss, though it causes a rise in the permeability. Furthermore, if there is a variation in grain size or difference in the composition of grains, the magnetic flux distribution becomes in each grain diverse because initial permeability differs amongst the grains. Consequently, the relation between the magnetic flux (B) and the power loss (P) is non-liner ($P \alpha B^{2.2\text{-}2.4}$) as suggested by *Ohta et. al.*[129]. The inhomogeneity of the distribution of magnetic flux brings about an increase of total losses of the sample. The addition of impurities which enhance grain growth must be avoided in order to produce a ferrite having homogenous grains with appropriate size. Consequently, raw materials with high purity must be used, and additives that prevent grain growth must be selected.

4. *Production of higher density ferrites. Reijnen*[95] reported that the presence of pores not only creates demagnetising fields and lower initial permeability, but also increases the substantial magnetic flux density which leads to an increase of the total power loss. Hence, the reduction of pores must be maintained as much as possible and any pores must be located at the grain boundaries.

Chapter 3

3. Experimental Procedures

3.1 Production of Powders

3.1.1 Mn-Zn Ferrites Prepared by the Citrate Gel Processing Route

High purity 'Analar' grade citric acid and nitrates of manganese, zinc and iron were individually dissolved in distilled water and mixed together to make solutions for gel production, *figure 3.1.*

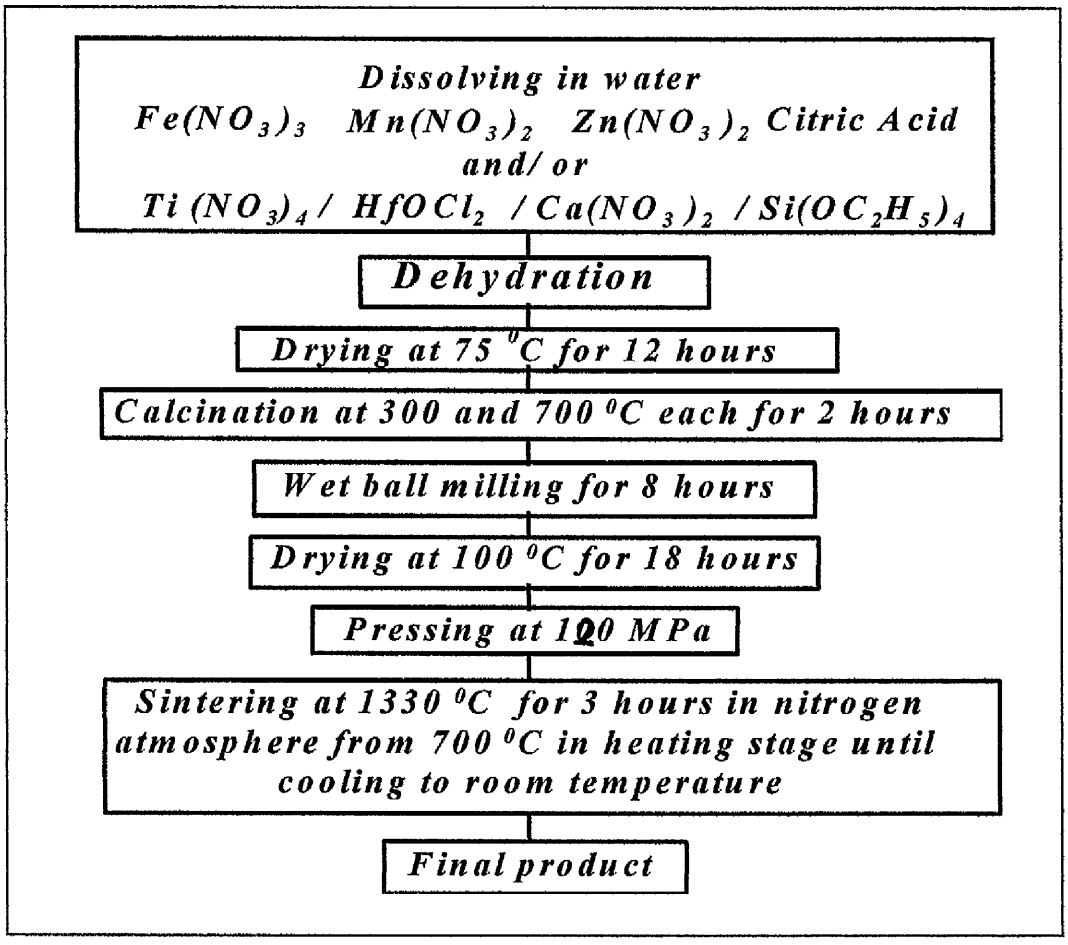

Figure 3.1 Overview of Mn-Zn ferrite citrate-gel processing route

The titanium ions were added to the solution as titanium nitrate. Titanium tetrachloride was dripped into deionized water to form 0.1M aqueous solution, $TiCl_{4(aq)}$. Titanium tetrachloride forms hydroxide precipitates very easily in water at room temperature so chilled deionized water, $<4^0C$, placed in an ice bath was essential. The resultant solution was a white turbid-like solution, and it was necessary to store it in the refrigerator for 24 hours before it became clear and stable. A titanium hydroxide precipitate was obtained by addition of the aqueous $TiCl_4$ solution to ammonia solution, followed by triple filtering and washing with deionized water to remove any residual chloride ions. The titanium nitrate solution was obtained by dissolving the titanium hydroxide precipitate in highly concentrated nitric acid in a chilled environment. The resulting titanium nitrate was then diluted to the required concentration determined by simple gravimetric analysis[67,130,131].

The effect of calcia and silica additions on Mn-Zn ferrite prepared by citrate gel processing was studied and an assessment was made of the effect of these impurities on the magnetic properties. Silicon was added to the mixed metal nitrate solution as tetraethyl orthosilicate $Si(OC_2H_5)$ and calcium was added as high purity Analar grade calcium nitrate solution. Desired amounts were added to give the basic ferrite chemical composition with 0.02 wt% SiO_2 and 0.04 wt% CaO. The amount of citric acid was kept to the minimum necessary to provide a $(COOH)$ group for each (NO^{3-}) ion in the nitrate solution. The dissolved citric acid was added to the solution, which was transferred to a two litre evaporation flask. The evaporating flask was connected to a rotary glass sleeve and was immersed in a hot water bath kept at 75±5 ^0C. The excess water from the solution was evaporated and condensed by means of a water jacketed condenser and was collected in a distillate receiver flask. A water pump generated the rotary evaporating system, figure 3.2, operating under vacuum, which. This drying process was continued until the solution became gel-like. At this time the product was transferred to a vacuum oven at 65±5 ^0C for 12-18 hours in order to produce the final dried precursor which was a reddish-brown, brittle and porous glass-like substance.

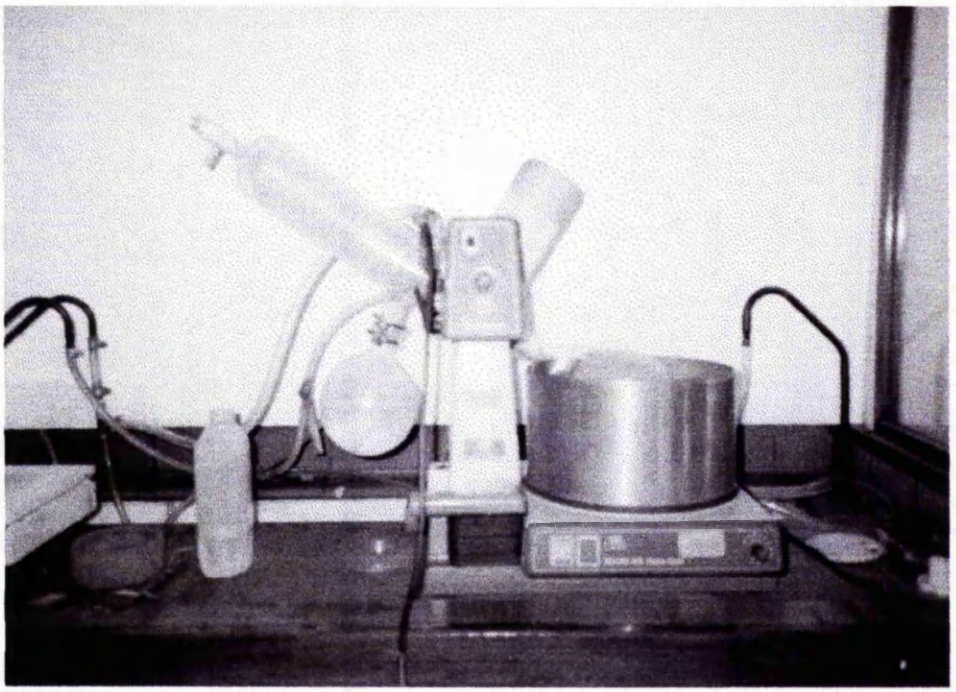

Figure 3.2 The rotary evaporating system

3.1.2 Mn-Zn Ferrites Prepared by the Mixed Oxides Method

Ferrite samples with Hf^{4+} ion substitutions and SiO_2 and/or CaO additions were also prepared using the mixed oxides processing method. Two preparation routes were employed to examine the effect of preparation method on the homogeneity, distribution and interactions between the additives and ferrite.

In the first route, *figure 3.3*, high purity 'Aldrich' grade iron, manganese and zinc oxides were weighed, and mixed mechanically in an Erich mixer for 8 hours, and then calcined in air at 300 and 950 ^{0}C each for 2 hours respectively to form the spinel phase and to ensure the chemical homogeneity of the ferrites. The desired amounts of high purity Aldrich grade HfO_2, SiO_2 and/or CaO were added to the spinel powder and then wet ball milled for a further 8 hours. After wet ball milling, the homogenous mixture was pressure filtered prior to oven drying to remove water. This route was used because some studies have indicated that the introduction of the

additives after the calcination stage improves the chemical homogeneity as well as the impurities-ferrite interactions due to the reduction in particle size during the milling and calcination processes[132].

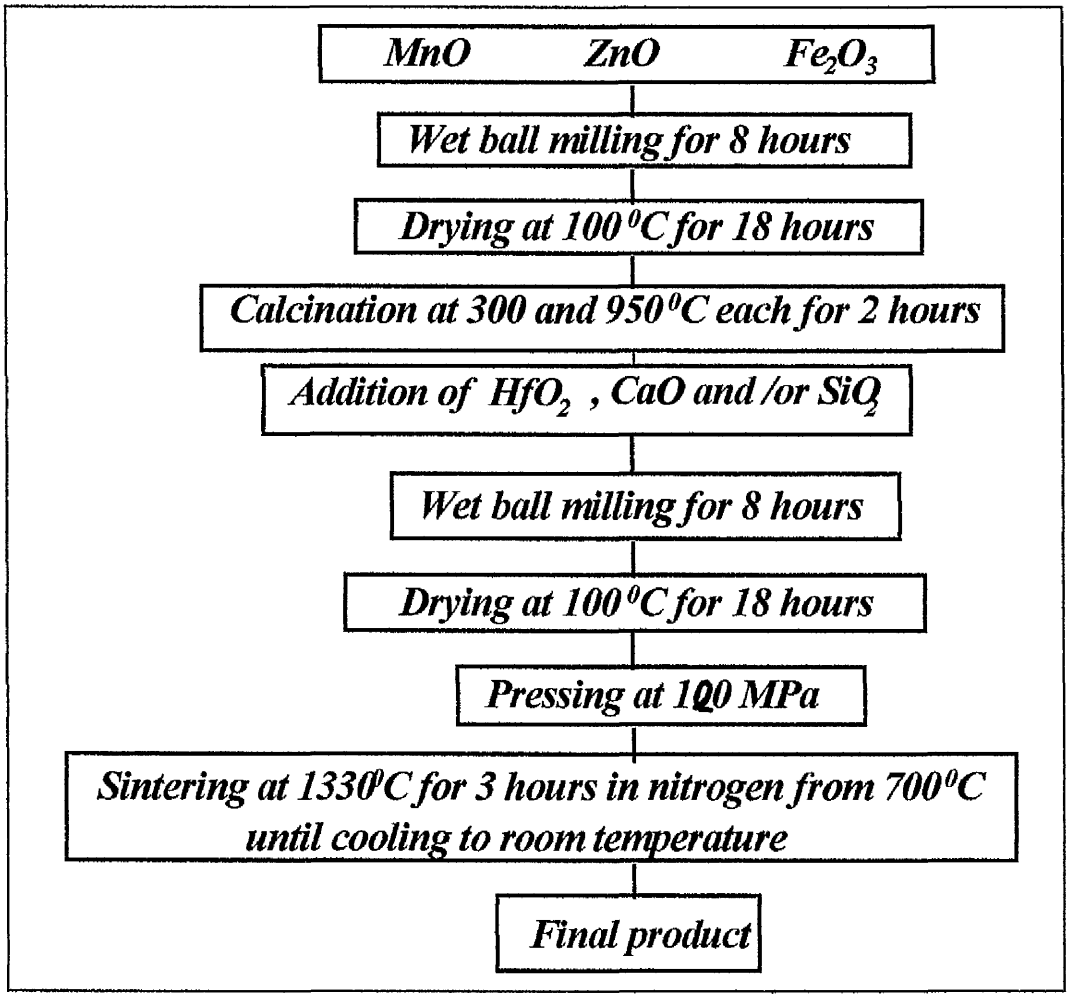

Figure 3.3 Overview of Mn-Zn ferrite mixed oxides processing route 1

The second mixed oxide processing route, *figure 3.4*, involved the mixing of all the oxides and the additives from the start of the process. Consequently, the additives had the chance to become involved in the reaction which occurred at calcination, i.e., they could possibly become incorporated with the spinel or could possibly effect the reactions and powder size by acting partially as sinter aids at the temperature of calcination.

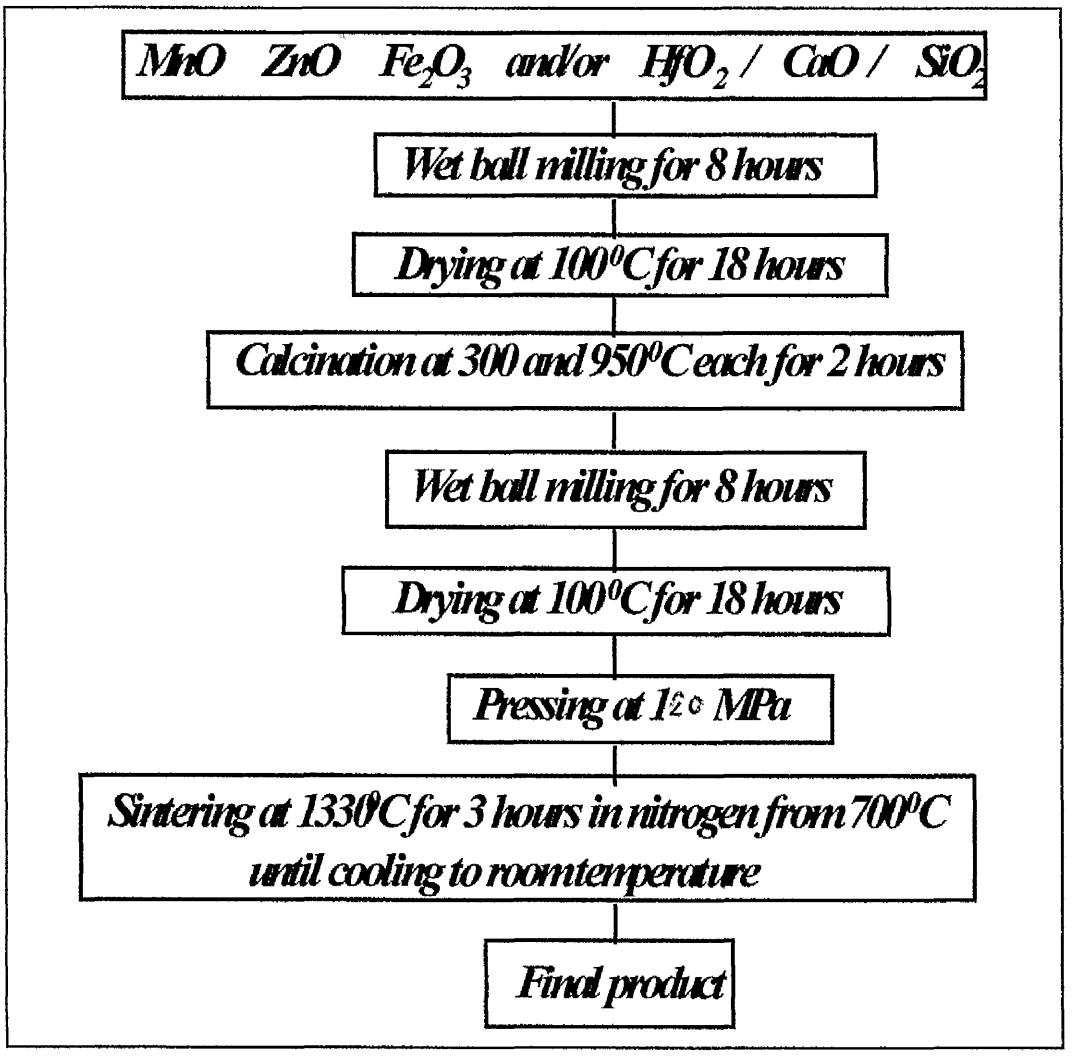

Figure 3.4 Overview of Mn-Zn ferrite mixed oxides processing route 2

3.2 Characterisation of Precursor, Powder and Sintered Ferrite Samples

3.2.1 Thermal Analysis

Thermogravimetric (TG) and Differential Thermal Analysis (DTA) of the precursors was carried out using a Seiko series SSC/5200 simultaneous thermal analyser. The necessity of these analyses was to gain some understanding of the relationships between the temperature and the decomposition and reaction

mechanisms, such that optimum conditions could be established for production of the ferrite powders.

In the Seiko system the reference Al_2O_3 and the Mn-Zn precursor sample balance beams are supported separately by individual driving coils. Any change in the sample weight results in a movement of the sample balance beam, which is carried through the driving coil to the opposite end of the beam. Optical sensors detect the movement and send signals to the balance circuit which supplies enough feedback current to the driving coil to return the beam to the balance position. Small amounts of precursor were heated from room temperature to 800 and 1200 ^{0}C, depending on the preparation method of the powders, at a heating rate of 10 ^{0}C/min under a 100 ml/min flow rate of air. The amounts of powders were varied according to the expected weight loss. The weight of the sample was continuously recorded as a function of time and/or temperature during the heating and cooling sequences.

As a result of thermal analysis and previous experiences, two stages of decomposition of the citrate gel precursor were used to prevent overheating and possible segregation of oxide components, which leads to chemical inhomogeneity. Temperatures of 300 and 700 ^{0}C each for 2 hours were selected for the gel processing precursors. For the mixed oxide route calcinations at 300 and 950 ^{0}C, each for 2 hours, were implemented.

3.2.2 X-Ray Diffraction Analysis (XRD)

X-ray diffraction analyses were carried out using a Philips diffractometer type PW 3710 with a programmable control unit and nickel filtered copper ($K\alpha$) radiation. The radiation source was made up of two components:

- $K\alpha 1$ with a wavelength of 0.1540 nm, and
- $K\alpha 2$ with a wavelength of 0.1544 nm.

The relative intensity ($K\alpha 1$) to ($K\alpha 2$) is approximately 2:1. A continuous scan rate of 2θ= 10-80 at 0.1 ^{0} s^{-1} was used primarily to examine the structure of the powders or sintered samples and to detect the presence of extra peaks caused by the impurities

The wavelength of copper ($K\alpha$) (λ = 0.154 nm) was used for the measurement of the interplaner spacing (d) which was used to determine the theoretical density of ferrite. The areas of the peaks were measured accurately by a set of programs stored in the control unit of the X-ray diffractometer. Data and x-ray patterns associated with the measurements were analysed automatically by the computer attached as part of the data acquisition system.

To carry out the X-ray analysis small amounts of precursors and 300, 700 and 950 ^{0}C calcined powders were ground and placed in the round recess of a sample holder, then levelled using a glass slide taking special care to ensure that the powder surface was flat to minimise errors in gonimeter alignment. To improve powder cohesivity, a few drops of collodian binder were added. Sintered pellet samples were also analysed using a dished sample holder and care was taken to ensure that the flat surfaces. As small an ammount as possible of plasticine was used to stick the sintered pellet in the sample holder, and to ensure the flatness of the surface. Again, a glass slide was used to level the sample surface with the sample holder's edges.

3.3 Milling and Pressing of Powders

The calcined, citrate-gel and mixed oxide powders, were milled using a wet ball milling route in order to deagglomerate and reduce the particle size prior to compaction to restore their compaction behaviours and reactivities before the final sintering process. The powders were placed into polypropylene bottles with low carbon steel balls and deionised water and milled for 8 hours. The weight ratio of powder, water and steel balls was 1:1:10. In order to reduce the amount of water needed for fluidity and to improve grinding efficiency, ammonium citrate was used as a surface-active agent (dispersant).

Following the milling stage the slurry was dried in an oven at 100±5 ^{0}C for 18 hours. The dried powder was ground in a mortar and sieved using a mesh of nominal opening of 300 μm to produce a homogenised aggregated particle size. Toroid specimens with dimensions of 24 mm OD, 18 mm ID and 4 mm thickness were pressed at 100 MPa using a Moore hydraulic press. Pellets with 16 mm outer diameter and 4 mm thickness were produced using a cylindrical, single action push rod die.

3.4 Sintering Process

Sintering of the ferrites was carried out using a Vecstar tube furnace with a programmable temperature controller. Samples were sintered at temperature setting of 1300 and 1330 ^{0}C for 2 and 3 hours respectively. A schematic diagram representing the heat treatment profile initially used is shown in *figure 3.5*. The samples were heated isothermally in air at 200 ^{0}C/h up to the peak temperature of 1300 ^{0}C and held for two hours and then cooled in a nitrogen atmosphere to room temperature.

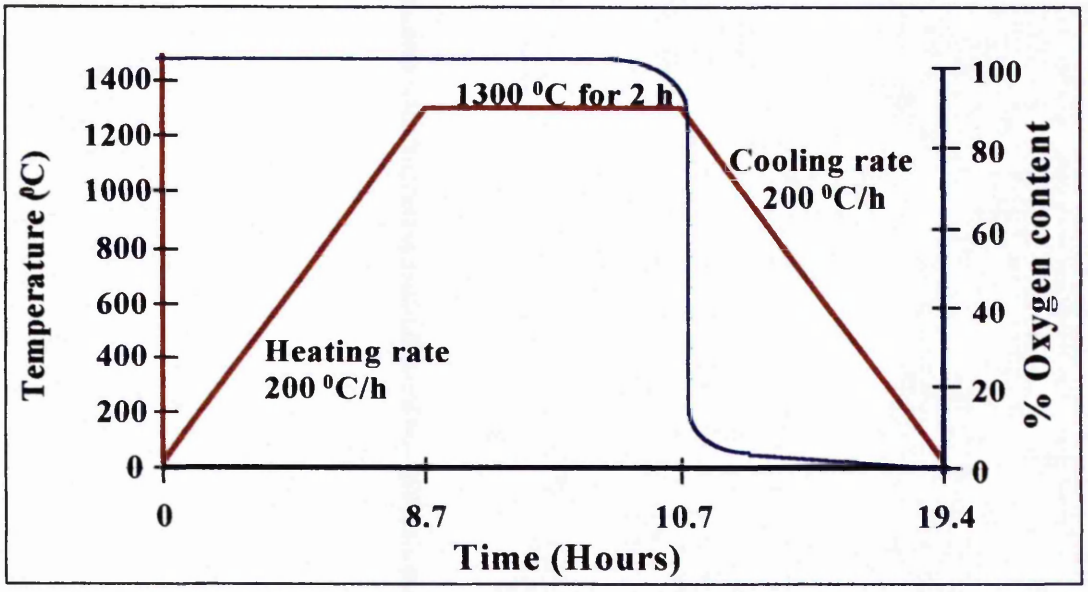

Figure 3.5 First heat treatment process profile

The second heat treatment method used in this work is shown in *figure 3.6.* Pressed samples were heated in air up to 700 ^{0}C, and then nitrogen was introduced into sintering atmosphere. The peak sintering temperature was 1330 ^{0}C for three hours. The cooling process had two cooling rates, the first was -75 ^{0}C/h until 900 ^{0}C, while the second was -300 ^{0}C/h to room temperature

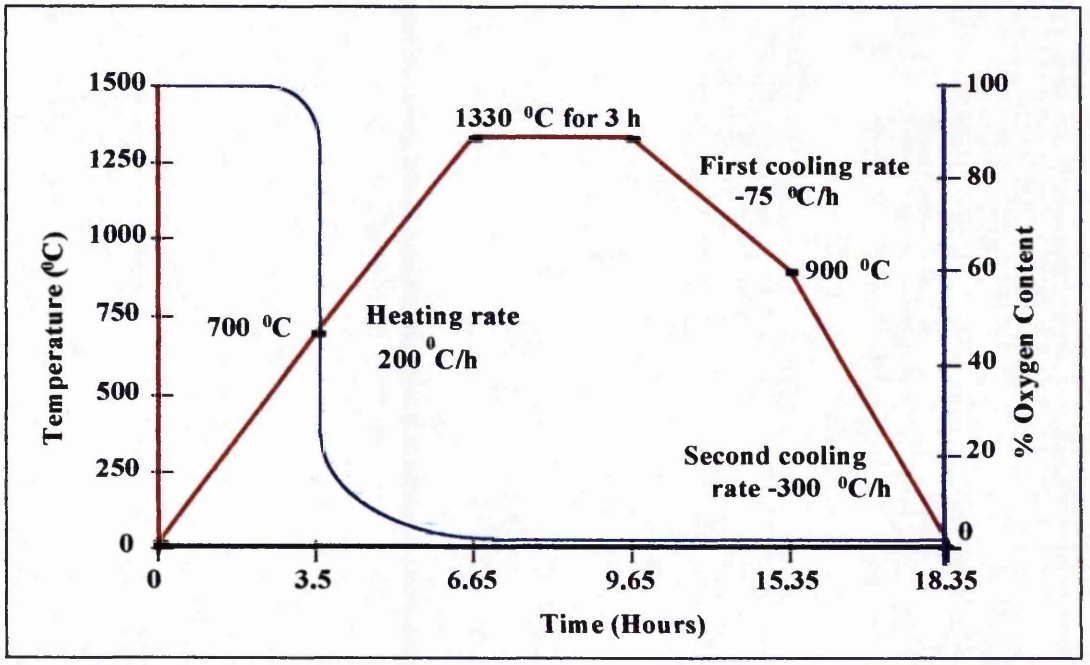

Figure 3.6 Profile of the second heat treatment process

3.5 Scanning Electron Microscopy (SEM)

The particle sizes and morphologies of precursors were analysed using a Philips 505 scanning electron microscope. The powder particles were attached onto double sided adhesive tape on the sample holder. To prevent "charging up" of the particles within the microscope, the samples were gold coated using an Edwards S150B sputter coater, to make them electrically conducting. The gold coat layer also improved the image quality due to the high secondary electron emission coefficient. Silver paint was used to provide a conducting path between the exposed areas of the adhesive tape and the sample stub. The scanning electron microscope was operated at an accelerating voltage of 20 kV, and the images were recorded on 35 mm film.

3.6 Transmission Electron Microscopy (TEM)

Transmission electron microscopy analyses were carried out on specific specimens to obtain more details about their crystal structure, chemical compositions and the location of additives within the ferrite.

The specimens were prepared from 3 mm diameter and 1 mm thickness sintered discs. The specimens were glued to a thick glass slide using wax, and were ground on silicon carbide paper grade 1200 to thickness of 250 μm. The ground samples were then transferred to a dimpling machine which was used to flatten the specimens to an approximate thickness of 100 μm, after which the flattening wheel was changed to a dimpling wheel which thinned the samples to around 40 μm at the centre. The dimpled samples were removed and cleaned with acetone to remove debris and wax prior to drying. The samples were supported by gluing them to a 3 mm copper reinforcement grid with a single large hole in the centre. This provides good support for it to be handled by tweezers without any of the thinned area being obscured.

The final stage before TEM analysis was to thin the sample to near transparency using an Edwards IONTEC ion beam thinner. Prepared samples were analysed using a Philips 400 transmission electron microscope fitted with an EDAX 9100/60 energy dispersive x-ray spectrometer operated at an acceleration voltage of 120 kV. The particles were highly magnified and their compositions were measured using the nano-probe mode in the TEM. The material volume testing during chemical analysis approximated to a cylinder with a diameter that was equivalent to the beam diameter, with the depth being a function of sample thickness. The minimum available beam diameter was defined by the current available in the focused probe. Practically, the lower limit was 10 nm below which sensible x-ray count rates could not be achieved. To analyse the individual ferrite grains a beam diameter was chosen which enabled the acquisition of statically significant data in time of the order of 60 seconds. For grain boundary analyses the minimum diameter

beam used was 10 nm, and longer analyses times utilised to achieve the required sensitivity. The x-rays were collected for 100 seconds. Twenty readings were taken for each particle geometry, and standard software was used to quantify the collected spectra.

3.7 Magnetic Property Measurements

3.7.1 Initial Permeability Measurements

The initial permeability measurement values were calculated from the inductance values over the frequency range of 1 to 100 kHz and a current of 10 mV using a multifrequency LCR HP 4274 meter. The sintered toroids were winded with 30 turns of plastic insulated wire.

The inductance reading was used to calculate the initial permeability values using a Hewlett Packard program:

$$\mu_i = \frac{\left(\frac{1}{a}\right).L}{4.10^{-7}.\pi.N^2} \qquad 3.1$$

where :L - inductance (mH),

N - wire turns, 30 turns, and

a - core factor.

3.7.2 Power Loss Measurements

Power loss measurements were carried out using a laboratory built B-H loop and power loss measuring system. The power losses of sintered toroids were measured using 20 wire windings, 10 primary and 10 secondary, at frequencies of 16, 32, 64, 100 and 128 kHz and flux densities of 50 and 100 mT. The ranges of

frequencies were selected due to the operating environments of Mn-Zn ferrite yoke ring which operates at a relatively low frequency range. The voltage needed to accomplish the required flux density was obtained from *equation 3.2*:

$$V = 4.B.A_e.N.f.10^{-9} \qquad 3.2$$

where: V - required voltage (V),

B - flux density (T),

A_e- effective area (mm^2),

N - number of turn of wire, and

f - frequency (kHz).

3.8 Microstructure Analysis

Microstructure analyses were carried out using an Olympus BH optical microscope. Sintered toroids were cut into halves by a mechanical Buehler Isomet machine using a diamond cutting wheel. A low cutting speed was maintained to minimise any damage that may occur during the cutting process and to obtain as smooth a surface as possible. One half was cold mounted. Cold mounting used to avoid cracks that may initiate during hot mounting due to high temperature and pressure applied to the samples.

The mounted samples were surface ground using 1200 and 2400 silicon carbide papers for a few minutes. Coarser papers were avoided because they cause can excessive damage to the samples. Further grindings were carried out on 4000 grade silicon carbide paper for 10 minutes and the specimens were washed and dried to clean the surface from debris.

The polishing process was carried out using Buehler grinding and polishing machines, type Motopol 12. Samples were polished on self adhesive Buehler polishing microcloths for few hours using different micron sizes of oil based

polishing diamond suspensions followed by washing and drying subsequent to etching immersion for 60 to 90 seconds in the etching solution and subsequently washed by running water and dried with ethanol solution. The etching solution has a ratio of 15% *HF*, 5% HNO_3 and 80% distilled water.

The grain size of ferrite was measured using the mean linear intercept method. Two circles having diameters of 70.5 mm and 32 mm with total circumference length of 322 mm were superimposed on optical micrographs and number grains intercepting the circle, N_T, were counted. Then the mean linear intercept ($m.l.i$) (grain size was calculated as:

$$m.l.i = \frac{L_T}{N_T . M} \qquad 3.3$$

where M is the magnification of the micrograph, L_T is the sum of perimeters of the circles. At least five different fields were used for each measurement.

The sintered density of the ferrites was determined using the Archimedes principle technique. Iodoethane was used because of its high density (1.935 gm/cm^3) and low surface tension. The weight to volume relationship was used to calculate the sintered density.

Chapter 4

4 Results and Discussion I

4.1 Characterisation of Powders

The base composition was a commercial grade pure Mn-Zn ferrite with chemical formula of $Mn_{0.57}Zn_{0.35}Fe_{2.08}O_4$, and may be described through a formula unit of the spinel structure as, $Mn^{2+}_{0.57}Zn^{2+}_{0.35}Fe^{2+}_{0.08}Fe^{3+}_2O^{2-}_4$, making the assumption that the Mn^{2+} cations and Fe^{2+} ions remain in the divalent state at the tetrahedral site. Usually the divalent ions tend to move to the octahedral site and therefore the real divalent ions content in the ferrite can be smaller than the calculated one as part of the divalent iron ions would be in the trivalent state.

To compare the effect that *Ti* group oxides have on the properties of the ferrites, the Me^{4+} ion substitutions in Mn-Zn ferrites were introduced in two ways.

- The first method was to substitute the Ti^{4+} for the Fe^{3+} ions, and to keep the Fe^{2+} ion constant as $Mn^{2+}_{0.57}\ Zn^{2+}_{0.35}Me^{4+}_xFe^{2+}_{0.08}Fe^{3+}_{2-x}O^{2-}_4$, where the amount of ($x$) was equivalent to 0.61 wt%. Samples of this composition will be referred to as 3C21.

- The second method was to keep the Fe^{2+} ion concentration constant and simultaneously increase the Mn^{2+} and Ti^{4+} or Hf^{4+} ion content at the same time reducing the Fe^{3+}, as suggested by *Stijntjes et. al.*[9]. This gives the following composition $Mn^{2+}_{0.57+x}Zn^{2+}_{0.35}Me^{4+}_xFe^{2+}_{0.08}Fe^{3+}_{2-2x}O^{2-}_4$ for samples. The amounts of (x) were equivalent to 0.2, 0.4 and 0.6 wt% for the titania addition. The amount of hafnia addition was restricted to 0.4wt%. All samples produced according to this second method will be referred to as 3C22.

To examine the effects of CaO and SiO_2 as impurities and their interactions with the ferrites and the TiO_2/HfO_2 additions, small additions, 0.04 wt% CaO and 0.02 wt% SiO_2, were made in combination or on their own.

4.1.1 Thermal stability of Powders

Typical simultaneous curves for DTA/TGA analysis of a Mn-Zn ferrite powder prepared by the gel-processing method are shown in *figure 4.1*. The DTA curve shows that the decomposition process occurs between 20-356 ^{0}C, and can be divided into two main consecutive stages.

The first decomposition stage is between 105-220 ^{0}C. The DTA curve shows a steady exothermic event at the start of this stage, followed by small sharp exothermic reaction between 195-221 ^{0}C. Within this stage, the TG analysis shows a large weight loss of 37.8% that could be attributed to the start of decomposition of the organic substances and nitrates (decomposition/oxidation) and the beginning of crystalline phase formation. Both decomposition/oxidation and crystalline phase formation may be expected to be exothermic in nature.

The second decomposition stage is between 221-356 ^{0}C and it characterised by large sharp exothermic peak at 332 ^{0}C as is seen in the DTA curve. The multiple steps may be explained by the formation of transiently-stable semi-decomposed precursors. The occurrence of this stage may be explained as the final decomposition/oxidation of the organic materials, remaining after the second decomposition stage, and oxidation of residual carbon. These exothermic reactions were accompanied by the generation of a considerable amount of heat, and the liberation of nitrous oxide, H_2O and CO_2, which increases the local temperature in the precursor[64,133]. The nitrate ions provide an oxidising environment surrounding the metal ions and thus simplify the decomposition and oxidation of precursor. The TG curve shows a relatively high weight loss of 38.2% at this stage. The precursors have decomposed almost completely after the second exothermic reaction and heating between temperatures of 356-900 ^{0}C is accompanied by a weight loss of 1.74%, as seen on DTA and TG traces and the final removal of residual carbon occurs.

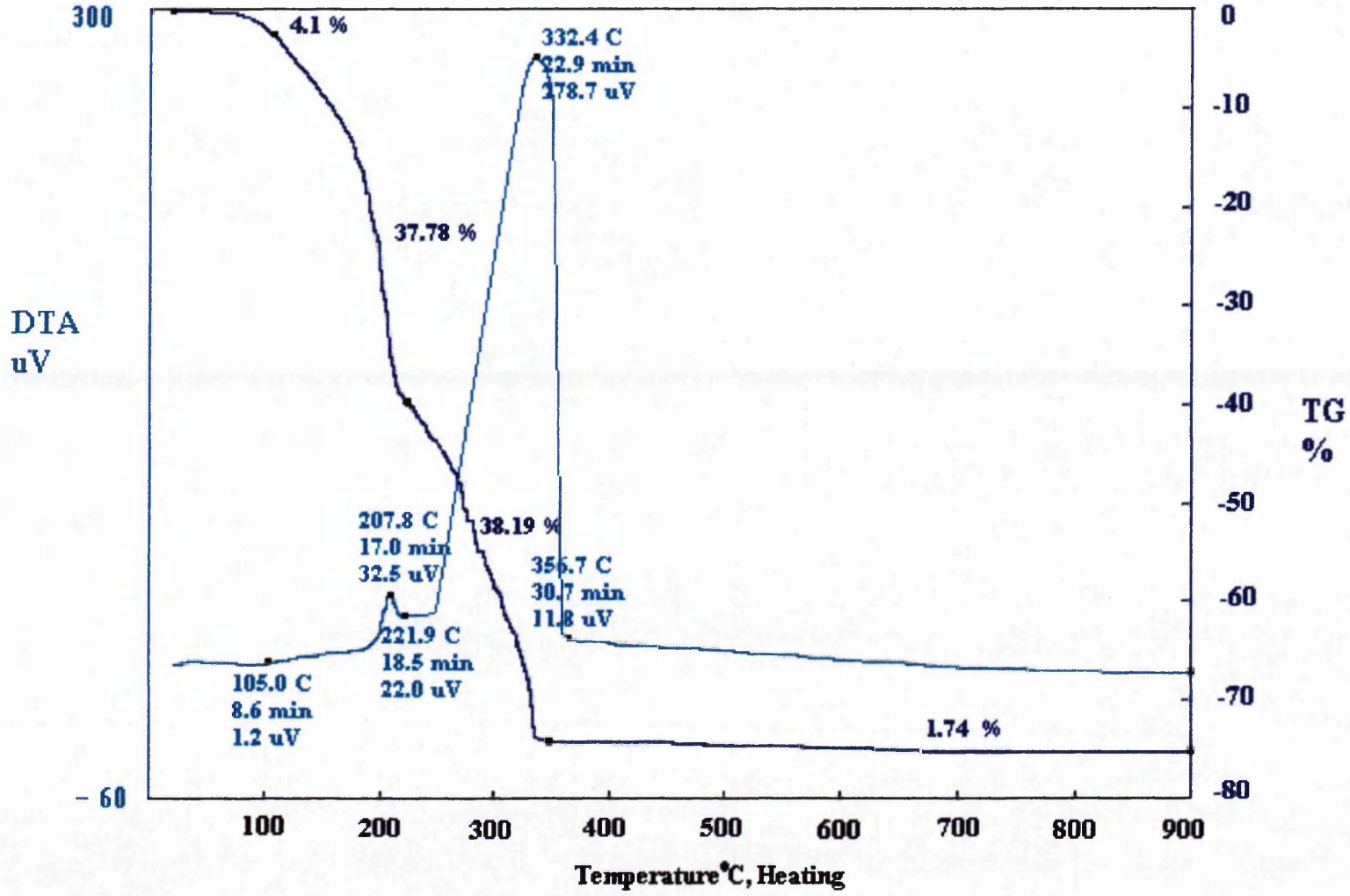

Figure 4.1. TG and DTA data for Mn-Zn ferrite precursor prepared by gel processing route

The total experimental weight loss during the formation of the spinel phase on heating up to 900 ^{0}C is found to be approximately 78%, excluding the dehydration stage. Supposing that all the chemical constituents involved in the ferrite have formed as oxides, the theoretical weight loss may be calculated as 77%, based on the stoichiometries of metal nitrates and citric acid utilised in the chemical solution. This calculation assumes assuming that all the water of crystallisation of the original nitrates is removed in the precursor drying stage. It further assumes that on decomposition of the completely dehydrated precursor, all the nitrate ions and citric acid are removed to give the ferrite.

Figure 4.2 shows a simplified possible complex formation arrangement where the citric acid has three bonds available to form a complex with metal ions, as presented by *Baythoun and Sale*[65].

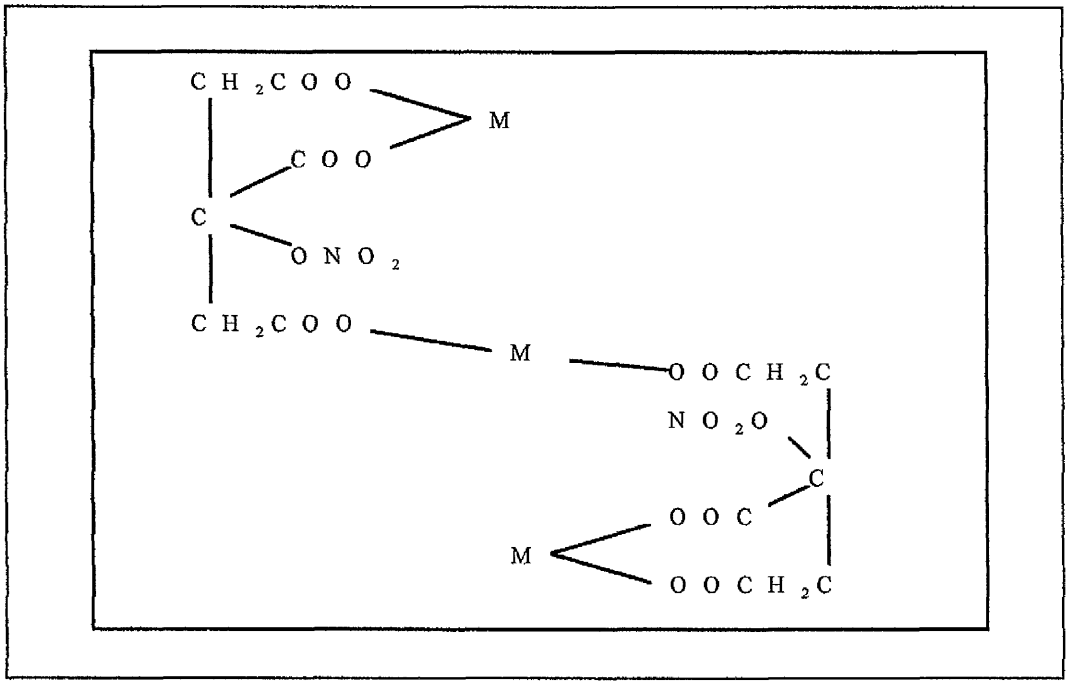

Figure 4.2 Possible complex formation arrangement between citric acid and metal ions[65].

According to this arrangement, the stoichiometric calculation for all metal ions to have successfully bonded in the complex and then decomposed to produce their

respective oxides may be predicted to be 77% weight loss, which is in very good agreement with experimental values of 78%.

The simultaneous DTA/TG traces of a Mn-Zn ferrite precursor prepared by the conventional oxide method is shown in *Figure 4.3*. The oxide decomposition-ferrite formation process occurs between 20-950 ^{0}C. The DTA curve shows only one broad exothermic reaction associated with this event as burning of binder, residual carbon and the formation of the ferrite. The TG curve shows a weight loss of 0.5% over the temperature range 20-250 ^{0}C which may be attributed to the loss of surface adsorbed water. The oxygen needed for the burning of the binder and residual carbon and for the formation of the ferrite is supplied either by the oxygen present in the surrounding atmosphere and/or by the reduction of the metal oxides, which react to give the ferrite. The higher oxidised manganese, such as Mn_2O_3 and especially MnO_2 will easily supply oxygen for the oxidation of binder and residual carbon. Consequently the oxidation process induces to a quick temperature rise, which promotes the chemical oxidation-reduction reactions[81]. *Stijntjes et. al.*[81] have explained that the decomposition below 500 ^{0}C is as a result of MnO_2 and small amounts of Mn_2O_3 are being decomposed according to:

$$2MnO_2 \Leftrightarrow Mn_2O_3 + \tfrac{1}{2}O_2 \qquad 4.1$$

$$3Mn_2O_3 \Leftrightarrow 2Mn_3O_4 + \tfrac{1}{2}O_2 \qquad 4.2$$

and this decomposition is complete at about 600 ^{0}C.

In the temperature range between 250-700 ^{0}C a weight gain of 0.24% occurred that could be as an indication for a considerable oxygen pick-up takes place at this stage and reaching its maximum at 700 ^{0}C. The oxygen produced through *equation 4.1* is highly reactive and leads to a speedy oxidation of any ferrite to Mn_2O_3 and Fe_2O_3 as shown in *equation 4.3*:

$$2MnFe_2O_4 + \tfrac{1}{2}O_2 \Leftrightarrow Mn_2O_3 + 2Fe_2O_3 \qquad 4.3$$

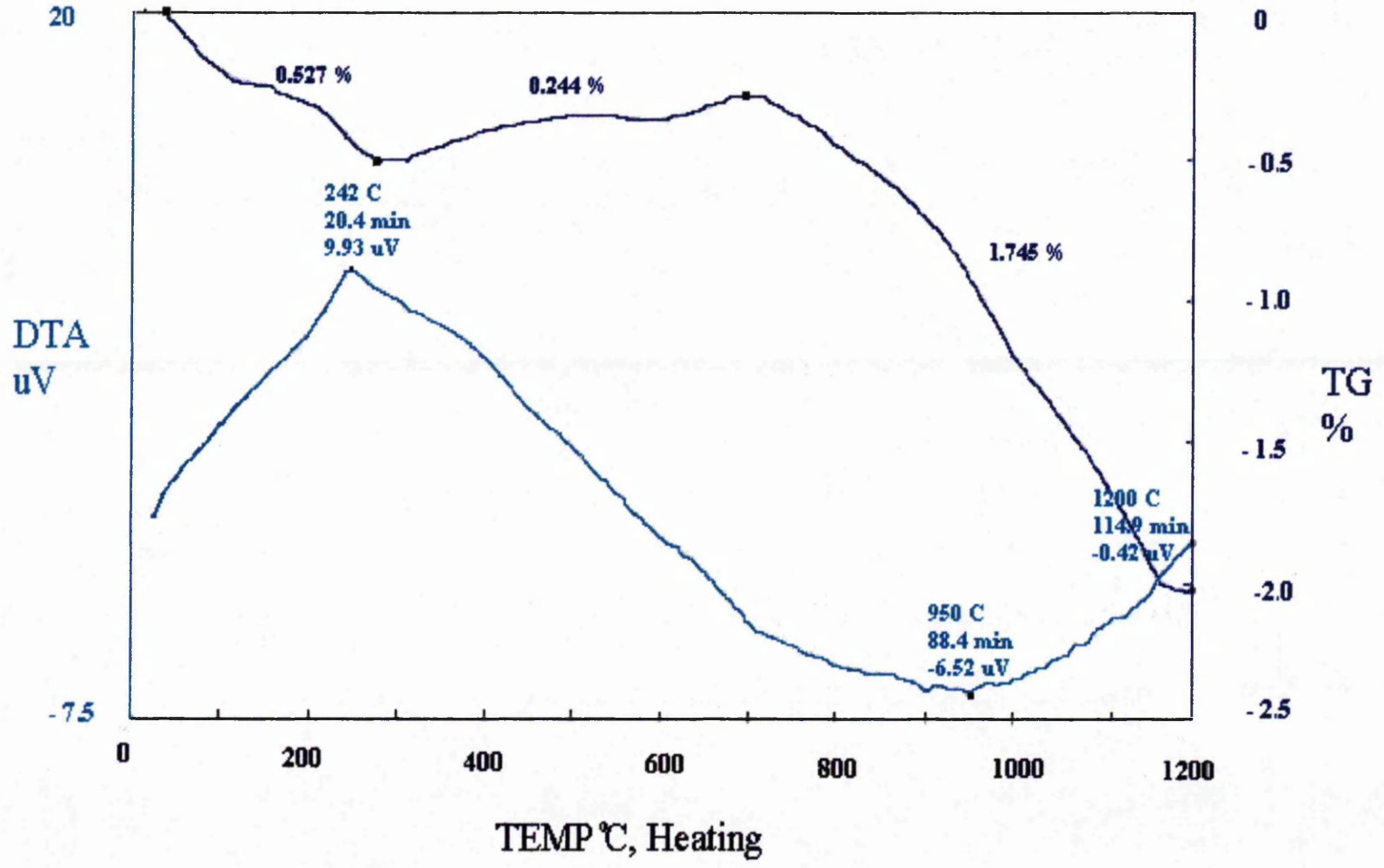

Figure 4.3. TG and DTA data for Mn-Zn ferrite powder prepared by mixed oxides processing route

The TG curve shows a weight loss of 1.75% as the temperature rises from 700 to 1200 ^{0}C, as a result of the reversal of the reaction given in *equation 4.3* as it proceeds to the left with the formation of Mn ferrite and/or mixed Mn-Zn ferrite-manganite. There was no evidence that the impurities and additions made to the ferrites had any effects on these reactions. It is therefore apparent that the amounts added were too small to have a major role and did not act as catalysts for either the decomposition or re-combination reactions.

4.1.2 X-Ray Diffraction Analysis

Figure 4.4 shows a series of XRD patterns obtained from the Mn-Zn gel and its products calcined at different temperatures. The "as prepared" gel precursor exhibits an amorphous phase. The XRD of the calcined gel was done to ensure single-phase ferrites were being produced after the exotherm that was associated with ferrite formation on the DTA plots. The first ferrite diffraction lines appeared after thermal decomposition of the gel precursor at 300 ^{0}C, and indicated a pure spinel phase. This indicates a clean single-crystalline phase material when compared to the gel precursor pattern, and a with small crystallite size due to the broadness of the peaks.

At higher calcination temperatures, 700 ^{0}C, in addition to these lines the X-ray diffraction pattern of α-Fe_2O_3 appears. The X-ray diffraction pattern indicates a relatively large amount of hematite phase along with smaller amount of spinel phase present in the calcined powder. The presence of hematite was due to the fact that $MnFe_2O_4$ oxidises and disintegrates, accompanied by the formation of α-Fe_2O_3, when the ferrite powder is calcined and cooled in air at temperatures higher than 500 ^{0}C[67]. *Ramesh et. al.*[134] reported that the hematite phase starts to appear at 450 ^{0}C and the presence increases dramatically at 550 ^{0}C when the ferrite powders are heat treated in an oxidising atmosphere. *Rozman and Drofenik*[135] proposed the reaction scheme for the disintegration/oxidation of manganese zinc ferrite as:

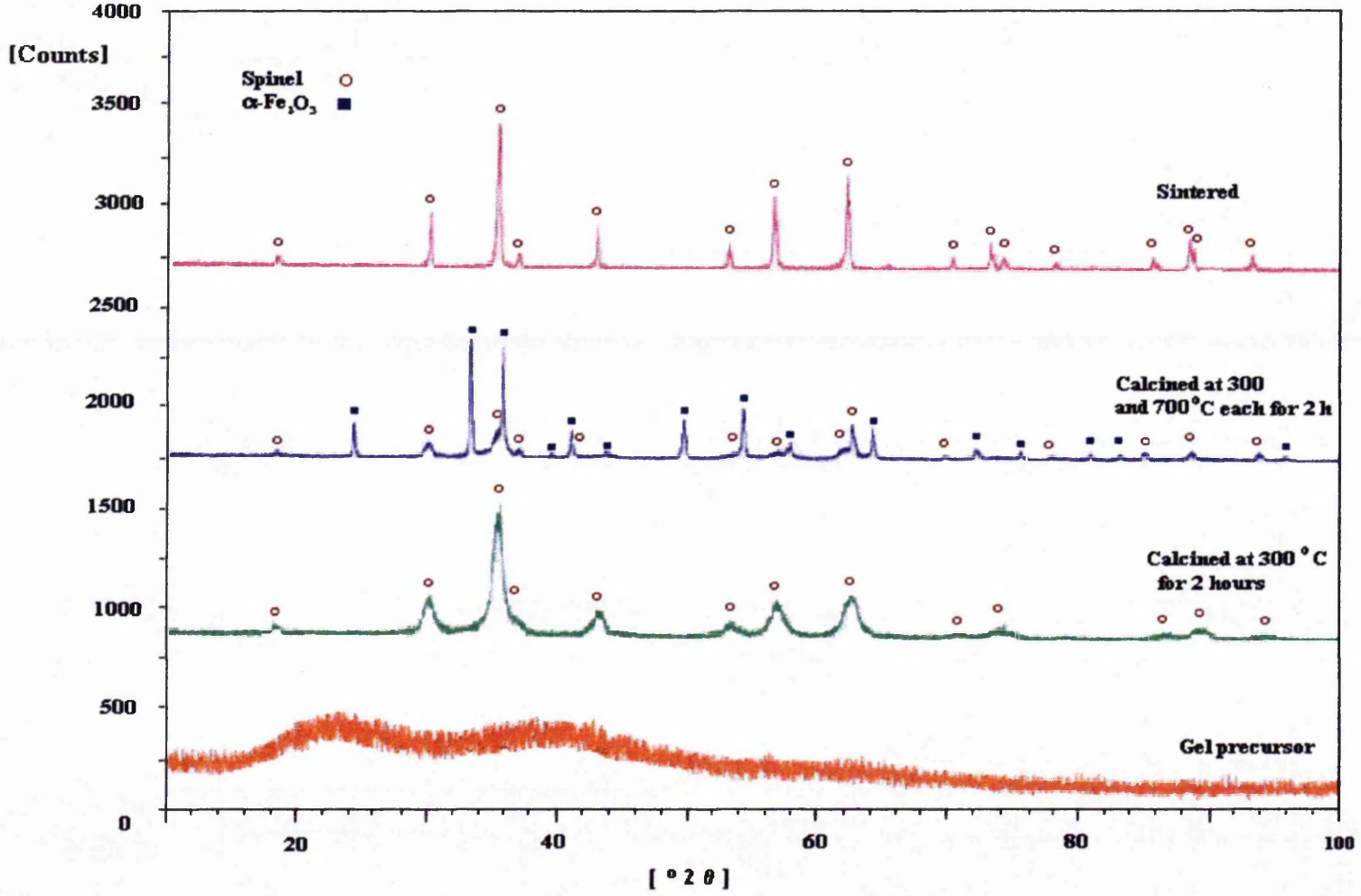

Figure 4.4 X-ray diffraction pattern of Mn-Zn ferrite produced by gel processing method

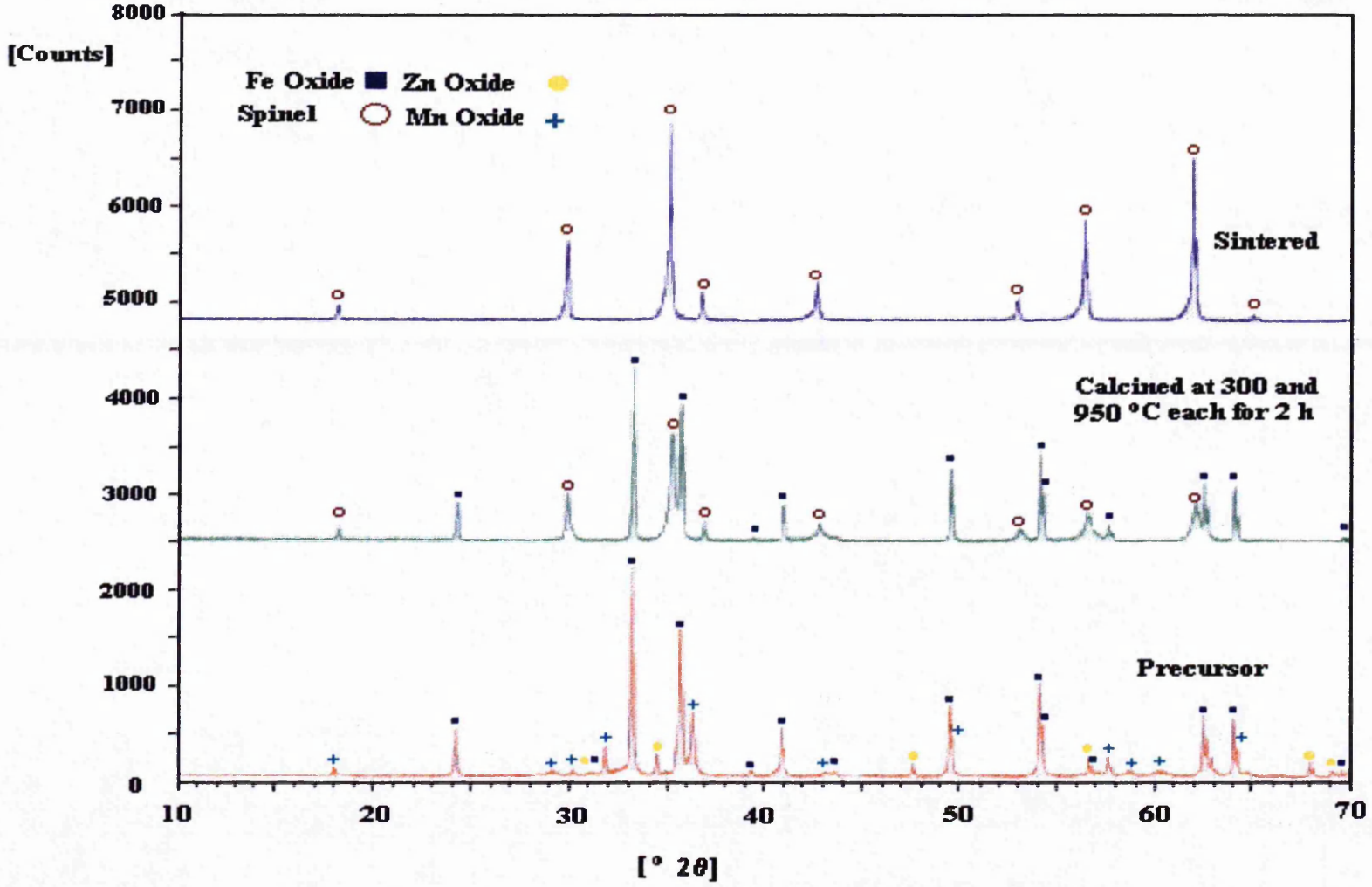

Figure 4.5 X-ray diffraction pattern of Mn-Zn ferrite produced by mixed oxides processing method

$$Zn_{1-x}Mn_xFe_2O_4 + \frac{x}{4}O_2 \rightarrow (1-x)ZnFe_2O_4 + \frac{x}{2}Mn_2O_3 + xFe_2O_3, \quad 4.4$$

The strong tendencies of Mn^{2+} ions to oxidise to Mn^{3+} at elevated temperatures make the Mn-Zn ferrite powders very prone to oxidation. When the calcination temperature in air is further increased, Mn^{2+} ions become more stable again above 900^0C and Mn-Zn ferrite starts to reform. Therefore at higher sintering temperature, 1350 ^{0}C, the XRD peaks corresponding to the spinel phase became more clear and sharp and no intermediate phase, such as α-Fe_2O_3, was observed.

The XRD patterns of the Mn-Zn ferrite prepared by mixed the oxide method is shown in *figure 4.5.* The X-ray diffractogram of the mixed oxide precursor indicates a strong presence of Fe_2O_3, which corresponds, with the proportion of Fe_2O_3 added to the mixture. Small peaks of MnO and ZnO are also detected which confirms their presence in the oxide mixture. An α-Fe_2O_3 phase, together with the spinel phase was formed after calcination at 950 ^{0}C and cooling in air. No traces of the substitutes or impurities were detected, as the amount of these additions was less than 5%, a typical detection limit of this experimental technique.

4.1.3 Scanning Electron Microscopy Analysis

The citrate gel precursor was friable and porous in texture with a glassy irregular-shaped morphology that on decomposition at low temperatures produces a porous network that also has a glassy appearance under SEM, *figure 4.6a.* SEM micrographs in *figure 4.6* illustrate the morphological nature to consist of groups of agglomerates. As citrate gel processing produces fine, small submicron homogenised particles, the probability of agglomeration formation is very high. Agglomeration occurs because of a high surface area and the action of one of the weak forces. The common weak forces are *van der Waals* attraction, electrostatic charges, capillary liquid forces, or magnetic forces. The *van der Waals* force acts over a distance of approximately 100 nm and is most significant for particles below 0.05 μm in size. As the calcination

temperatures were increased, the network structure was retained as aggregates of larger particles formed *figures 4.6b* and *4.6c.*

The morphology of 950 ^{0}C calcined ferrite powders prepared by the mixed oxides method is shown in figure *4.6d.* The powders exhibit equiaxed submicron size particles which were agglomerated. However, the agglomerates were easily broken up during the ball milling process.

Figure 4.6 a

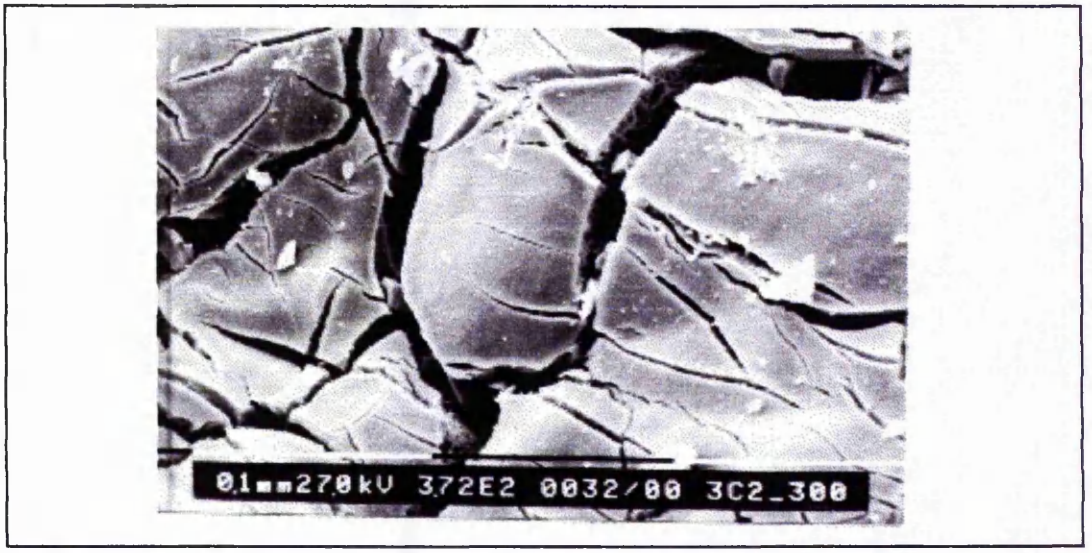

Figure 4.6 b

Continiued/

Concluded/

Figure 4.6 c

Figure 4.6 d

Figures 4.6. SEM micrographs of: (a). precursor prepared by gel processing; (b). calcined at 300 ^{0} for 2 hours; (c). calcined at 300 and 700 ^{0}C each for 2 hours; (d). powder prepared by mixed oxides method and calcined at 300 and 950 ^{0}C each for 2 hours

4.2 Sintered Density Measurements

4.2.1 Effect of Compaction on Density

Manganese zinc ferrites are very much influenced by processing conditions even for a fixed starting composition which should yield a high permeability and low power loss. To achieve optimum properties the sintered density has to be as high as possible. The sintered density depends on many factors such as particle size, pressing pressure, compressibility of particles, sintering time and sintering temperature. Generally, the parameters of the sintering process need to be held constant during manufacture in order to minimise variations in the properties of the final products.

Table 4.1 shows the compaction data for selected gel processed powders and its effect on the sintered density. It is evident that the sintering densities have increased with increase in pressing pressure. All three compositions show higher densities as a result of higher pressing pressure. Pure Mn-Zn powders pressed at 120 MPa gave 1.4% improvement in sintering density compared with those pressed at 100 MPa. 3C21 composition powder also has an improved sintered density by 0.4% at 120 MPa, while only 0.2% theoretical density improvement was achieved for 3C22 composition.

During the pressing process the particles are subjected to loading which produces re-arrangement of the particles within the compact. The re-arrangement process depends on the particle size, shape and pore size distribution. *Stuijts*[136] reported that to achieve high density ferrite, care has to be taken to ensure homogeneous build-up of the green compact, which means a small pore size distribution and no density gradients. The homogeneity can be improved by reducing the friction between the powder particles and the die surface, which largely depends on the relative hardness of the die wall and the presence of lubricants on the particle surface. Therefore to reduce the possibility of density gradients resulting from pressing a small amount of *Zn*-stearate lubricant was added to the powder. *Chien and Sale*[137] reported that better sintered

densities were achieved for *Mg* based soft ferrites prepared by the citrate gel method when pressed at higher pressing pressure of 160 MPa after being milled for 6 hours.

Composition	*% Theoretical Density*	
	100 MPa	*120 MPa*
Pure Mn-Zn	*94.1*	*95.5*
3C21 Mn-Zn with 0.61 wt% TiO_2	*96.8*	*97.2*
3C22 Mn-Zn with 0.6 wt% TiO_2	*97.2*	*97.4*

Table 4.1. Effect of applied pressing pressure on the sintered density of Mn-Zn ferrites

The presence of agglomeration in the calcined powder and its effect on sintered density is well known. The agglomeration can cause inhomogeneous shrinkage during sintering resulting in a large percentage of pores surrounding the sintered agglomerates. The relationships between the compaction and sintering densities depend on the homogeneity of the particle size and the degree of porosity of the pressed powder. Powders with high percentages of agglomerates are more often have poor final density, as one of the sintered density functions is the shape of particles. *Chien*[30] has observed that the presence of agglomerates causes voids in the sintered ferrite. The relationship between the agglomerates and the voids were attributed to inhomogeneous shrinkage as the agglomerates sinter to produce a higher density than their surroundings and in turn produce trapped, closed pores and, moreover, pull away from their surroundings leaving a porous and badly cracked area in the immediate vicinity of the agglomerates.

4.2.2 Effect of Sintering Time, Temperature and Atmosphere on Sintered Density

Sintering time, temperature and atmosphere have all been shown to have significant effects on sintered density. *Table 4.2* shows that the sintered density is determined predominantly by the increase of the peak sintering time and temperature corresponding to increases of the sintered density for all compositions. The pure Mn-Zn ferrite had improvements in its sintered density of 0.4%, as the peak sintering time and temperature increased by one hour and 30 ^{0}C respectively. However a significant increase in the final density of both 3C21 and 3C22 compositions by 1.1% and 1.2% respectively, were recorded after the duration of the sintering time and temperature was increased.

Composition	*% Theoretical Density*	
	1300 ^{0}C for 2 hours	*1330 ^{0}C for 3 hours*
Pure Mn-Zn	*95.5*	*95.9*
3C21 Mn-Zn with 0.61 wt% TiO_2	*97.2*	*98.3*
3C22 Mn-Zn with 0.6 wt% TiO_2	*97.4*	*98.6*

Table 4.2 Final densities of sintered 3C2 Mn-Zn ferrites

With increasing temperature and sintering time the sintering and crystal growth proceeds where the particles are in contact. The free surfaces containing the pores decrease and the particles grow together to form crystalline grains with the associated

rise in density. The sintering time combined with the increase of temperature play a crucial factor in the improvement of sintered density by allowing the residual pores and any non-soluble particles enough time and mobility to migrate to the grain boundaries. As the temperature is increased, the rate of motion of grain boundary increases. The breakaway of the boundaries from the pores often occurs because the pores are slower moving than the grain boundaries. At lower temperatures, the rate of grain growth is small and pores remain attached and impede it. Under the tension of a moving grain boundary, pores move by volume diffusion, surface diffusion, or evaporation-condensation across the pore. However at a high temperature the rate of grain growth increases to a point where the boundaries break away from the pores.

As a result of the break away of boundaries from pores, the pores can occupy sites on the grain edges or inside the grains. The system energy is lower when pores occupy grain edges, since the total interface area and energy is reduced. In the event of the pore and boundary becoming separated, the system energy is increased in proportion to the amount of newly created interface area. Consequently, the pore has a binding energy to the grain boundary that increases as porosity increases. Therefore, at the beginning of the densification process, little separation of boundaries from pores is expected. As the densification process continues, the slower mobility of pores combined with the reducing of pinning force allows breakaway.

In the early stages of sintering process, the large pores are immobile and pin the grain boundaries, maintaining a small grain size. In the late stages of sintering, there are fewer pores, which are small due to shrinkage and the grains are relatively large. In this situation separation can be avoided if the pores are sufficiently mobile to migrate with the boundaries. Hence, the sintering process requires precise manipulation of the heating cycle, since several factors can inhibit final pore elimination[138].

Miyoshi et al[139] reported that the sintered density of Mn-Zn ferrite increased significantly by almost 10% when the sintering temperature was increased by 100 ^{0}C, from 1100 ^{0}C to 1200 ^{0}C. However, *Hon and Ko*[140] noted that the sintered density is not

only dependent on the sintering temperature, but also on the heating rate. Their suggestion was that, as the sintering process starts at relatively lower temperatures, between 900-1100^{0}C, it is beneficial to hold the material at 900 ^{0}C for 30 minutes, prior to reaching to the final sintering temperature, to improve the sintered density of Mn-Zn ferrites significantly.

The effect of sintering atmosphere on the sintering density has been reported by many authors[5,94,141]. This effect is well known as "reaction sintering with an atmospheric control". The importance of controlled oxygen partial pressure in the sintering process of Mn-Zn ferrites has been recognised to obtain ferrites of excellent properties. Lattice imperfections, relating to the oxygen partial pressure in the sintering atmosphere, promote the sintering. At high sintering temperatures and low oxygen pressure sintering atmosphere, the imperfections in the lattice caused by the reduction of the oxygen ion content promotes sintering as the mobility of the cation vacancies is increased.

The effects of changing the sintering atmosphere from air to nitrogen on the density results of the Mn-Zn ferrites in this study are shown in *table 4.3*. It can be seen that densities have increased with the introduction of nitrogen in the sintering atmosphere at 700 ^{0}C in the heating stage, *figure 3.6*, and the density improvement differs depending on the chemical composition. The improvement for the pure Mn-Zn ferrite was 0.6%, compared with increases in density of 0.3% and 0.5% theoretical respectively for compositions 3C21 and 3C22 with 0.6 wt% TiO_2. *Drofenik and Rozman*[142] reported that the sintering of nanosized Mn-Zn ferrite powders in a nitrogen atmosphere leads to sintering densities higher than 99% theoretical. *Tasako and Ito*[143] reported that at sintering temperature below 1200^{0}C, promotion of sintering as caused by the lattice imperfection relating to oxygen partial pressure in the sintering atmosphere determines the sintered density of *Ni-Zn* ferrites.

In summary, *tables 4.2 and 4.3* shows that the final sintered densities are mostly determined by sintering temperature, time and atmosphere.

Composition	*% Theoretical Density*	
	1330 ^{0}C for 3 hours in air and cooled in nitrogen atmosphere	*1330 ^{0}C for 3 hours. Nitrogen atmosphere from 700 ^{0}C in heating stage and sintering and cooling stages*
Pure Mn-Zn	*95.9*	*96.5*
3C21 Mn-Zn with 0.61 wt% TiO_2	*98.3*	*98.7*
3C22 Mn-Zn with 0.6 wt% TiO_2	*98.6*	*99.1*

Table 4.3. Effect of sintering atmosphere on the sintering densities of Mn-Zn ferrites

4.2.3 Effect of Substitutes and impurities on Sintered Density

The sintered density of ferrites depends not only on the sintering temperature, atmosphere or time but also upon the additions that have been made. Generally, the additions influence the density positively when they are present as a liquid phase or approach a liquid state at the sintering temperature. To examine the effect of various levels of Ti^{4+} ion substitutions on the sintered density of Mn-Zn ferrites three 3C22 samples were prepared. These three 3C22 compositions, with 0.2, 0.4 and 0.6wt% TiO_2, were sintered according to the second heat treatment cycle, *figure 3.6,* with nitrogen introduced at 700 ^{0}C in the heating stage. The obtained results are shown in *table 4.4* and *figure 4.7.*

Table 4.4 shows the relationship between the TiO_2 addition and the sintered density. The density has increased slightly by 0.8% with the addition of 0.2wt% TiO_2 to the base composition with further increase of TiO_2 to 0.4wt%, the density continued to rise significantly, giving an extra 2.1% in comparison with the 0.2wt% addition, and reached its highest value of 99.4% theoretical. Increasing the addition to 0.6 wt%, resulted in a decrease in sintered density by 0.3% theoretical compared to that achieved by 0.4wt% TiO_2 addition. It is clear that the sintered density reached its highest level with 0.4wt% TiO_2 addition as the titanium ions appear to have reached their solubility limit in the ferrite lattice.

wt% TiO_2	*% Theoretical Density*
0	*96.5*
0.2	*97.3*
0.4	*99.4*
0.6	*99.1*

Table 4.4 Sintered density as a function of TiO_2 addition

To explain these observations it is known that an increase of Ti^{4+} substitution within ferrite lattice increases the anion vacancy concentration[5,6,9], which in turn should enhance any sintering process via bulk diffusion of the anions. Diffusion may occur by assuming that a Ti^{4+} ion dissolves into the ferrite lattice and replaces either Fe^{3+} or Fe^{2+} ions. Such a replacement creates excess cation sites. Continuing this process may create more excess cation vacancies in the spinel. Generally, the created vacancy has an excess charge, equal and opposite to the charge of the ion removed, associated with the neighbouring ions of opposite sign. The interstitial ions are attracted electrostatically to a vacancy and can dissociate from it only if the temperature is sufficiently high to supply the dissociation energy. This phenomenon will be discussed in the following section.

From the obtained results it is clear, that this effect was observed for 0.2 and 0.4wt% TiO_2 additions.

Similar effects of Ti^{4+} ions in promoting grain growth and therefore increasing the density have been reported by *Yan et. al*[25]. However, they reported that the grain boundary velocity could be increased by segregation to the boundary of cations with little effect on grain growth. *Mulin et. al.*[144] reported that the sintering mechanism depends on the Ti^{4+} substitution level and the oxygen partial pressure of the sintering atmosphere.

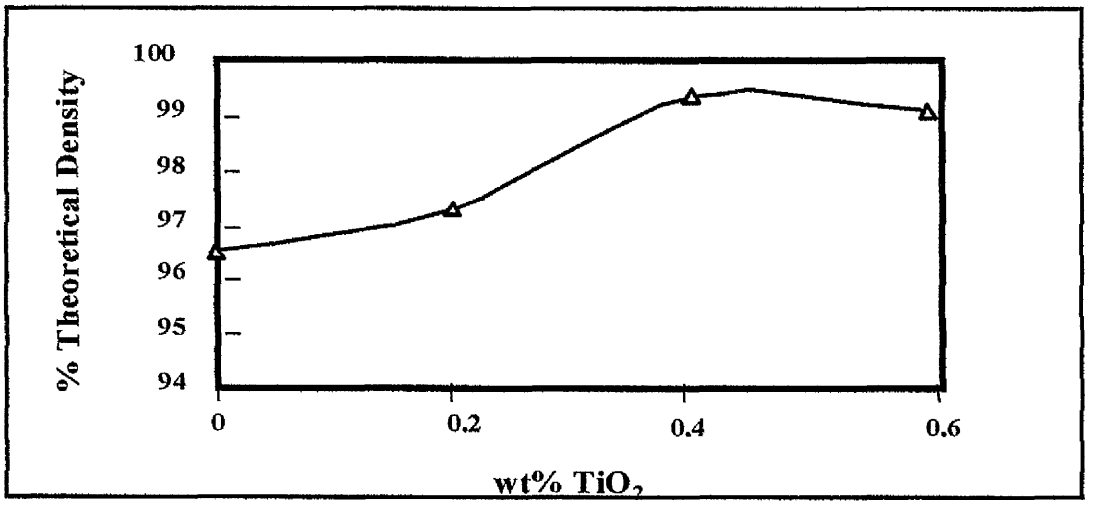

Figure 4.7 Effect of TiO_2 additions on sintered density

Table 4.5 shows the effect of small additions of impurities on the Mn-Zn ferrite sintered density. It shows that the samples with only 0.04 wt% *CaO* additions have the lowest density values for all compositions investigated. This may be explained by the fact that additions of Ca^{2+} in Mn-Zn ferrites will segregate at the grain boundaries and not become substituted in the ferrite lattice due to its larger size. Such segregation is known to inhibit grain boundary mobility due to the impurity drag effect. The drag effect can be explained as the result of *CaO* particles, which remain attached to the boundary as it moves. The *CaO* particles gradually become concentrated at boundary intersections and concentrate into large particles as grain growth continues. Hence, second-phase

inclusions, which move along with boundaries, offer hindrance to mobility. As grain growth proceeds, the driving force for reduction of grain boundaries diminishes, and any inclusions dragged along by the boundary increases in size so that mobility almost halted. As a result, *CaO* as a second phase acts as a grain growth inhabitant[112]. As a result the presence of *CaO* in the ferrite samples causes a decrease in density, a high porosity and small grain size.

Ghata[4] also reported that *CaO* tends to segregate at grain boundaries and hinder grain growth such that pores will be trapped on the grain boundaries and result in a ferrite with a high percentage of porosity. This behaviour has been observed for the additions of *CaO* to pure ferrite and the rest of the 3C22 compositions with Ti^{4+} ion substitutions (compare *Tables 4.4* and *4.5*). Conversely the results of SiO_2 addition shows that all compositions achieved better densities. *Giles and Westendorp*[36] reported that samples of Mn-Zn ferrite with relatively small SiO_2 addition achieved full sintering density at relatively low sintering temperatures, around 1140 ^{0}C. The presence of a SiO_2-based liquid phase is thought to enhance densification at 1150 ^{0}C. The study of the effects of combined 0.02 wt% SiO_2 and 0.04 wt% *CaO* additions on the sintered density revealed that all compositions achieved better density than those of samples containing *CaO* alone. However the density values were all lower than those obtained with equivalent compositions with only silica additions.

Table 4.6 shows the results of the sintering tests for the Mn-Zn ferrites with Hf^{4+} ion substitutions prepared by both gel processing and conventional mixed oxide method. For comparison, the pure Mn-Zn ferrite composition has been also prepared by the two methods and processed under the same conditions as the compositions containing the additives.

wt% TiO_2	*% Theoretical Density*		
	0.04 wt% CaO	*0.02 wt% SiO_2*	*0.4 wt% CaO & 0.02 wt% SiO_2*
0	*94.2*	*96.8*	*95.9*
0.2	*96.8*	*97.9*	*97.3*
0.4	*98.8*	*99.5*	*99.3*
0.6	*98.7*	*99.2*	*99*

Table 4.5 Sintered density as a function of TiO_2, CaO and SiO_2 additions

All samples with HfO_2 and CaO and/or SiO_2 additions showed density values in excess of 95% theoretical regardless of preparation method. It was observed that the substitution of Hf^{4+} ions improved the sintered density slightly compared with that achieved for the pure Mn-Zn composition prepared by the same method and processed under the same conditions.

The presence of Hf^{4+} ions in the ferrite powder prepared by gel processing has improved the sintered density by almost 0.3% theoretical compared with the base composition. The most improved sintered density was for the composition with HfO_2 and both CaO and SiO_2 additions which has improved significantly by 1.9% theoretical compared again with the base composition. Based on the data obtained for TiO_2 additions, the lowest sintered density obtained was as expected for the composition with HfO_2 and CaO additions. However, in this case it was still better than that obtained for the base composition by 0.3% theoretical. The presence of SiO_2 with HfO_2, which

always gave the highest sintered density, improved the density by 0.6% theoretical which is lower than expected on the basis of data obtained for TiO_2 additions.

In order to examine the effect of processing method on the physical properties of Mn-Zn ferrite, two routes have been utilised to prepare powders by the conventional mixed oxides process, as is given in *Chapter 3*, section *3.1.2.* All compositions prepared by the first route, where the additives were introduced after calcination, gave better sintered density than those prepared by the second route where the additives were introduced from the start of processing

Chemical Composition	*% Theoretical Density*		
	Mixed Oxides Method		*Citrate Gel Method*
	Additives Introduced Before Calcination	*Additives Introduced After Calcination*	
Mn-Zn with 0.4 wt% HfO_2	*96.2*	*96.8*	*97.7*
Mn-Zn with 0.4 wt% HfO_2 and 0.02 wt% SiO_2	*95.6*	*95.9*	*97.1*
Mn-Zn with 0.4 wt% HfO_2 and 0.04 wt% CaO	*95.5*	*95.7*	*96.8*
Mn-Zn with 0.4 wt% HfO_2 and 0.02 wt% SiO_2 and 0.04 wt% CaO	*97.8*	*98.1*	*98.4*
Base Mn-Zn composition	*95.9*	-	*96.5*

Table 4.6. Density Measurement Results of Mn-Zn ferrite with HfO_2, SiO_2 and/or CaO additions.

Mn-Zn ferrite powders prepared by the 2nd route shows sintered densities between 95.5-97.8% theoretical, while the same powders prepared by the 1st route and sintered in the same sintering environments showed an improved sintered density between 97.7-98.1% theoretical. Powders with HfO_2, CaO and SiO_2 addition prepared by the 1st route gave the best level of densification and achieved 98.7% theoretical, while the same powder prepared by the 2nd route gave a lower sintered density of 97.8% theoretical. As expected the lowest sintered densities were for powders with HfO_2 and CaO addition. 95.5% theoretical density was achieved for powders prepared by the 2nd route and 95.7% theoretical for powders prepared by the 1st route respectively. However, the additions of SiO_2 in combination with the HfO_2 additions resulted in an unexpected decrease in sintered density of 0.6% for the 2nd route and 0.9% for the 1st route respectively, compared with powders containing only Hf^{4+} ions that had been prepared in the same way.

In summary, the presented experimental data show that the all compositions prepared by the gel processing method achieved higher sintered densities than the same composition prepared by the mixed oxides method. On the other hand, results presented for the compositions prepared by the 1st mixed oxide route showed better final sintered densities than those prepared by the 2nd processing route.

It is well known that the calcination process is used to form partially or fully spinel ferrite by combining the ferrite constituents through solid-state reaction[56]. During this process the calcined powders react forming Mn-Zn ferrites, Zn ferrite, manganites and other mixed oxides. Since the additions were made in the early stage of powder mixing, for powders prepared by 2nd processing route, they have the opportunity to react with the ferrite as it forms during the calcination stage. Consequently, these additives will have opportunities to diffuse into the ferrite during calcination and hence their presence at grain boundaries. In particular, it may be considered that the hafnia can substitute partially in the ferrite leaving a more concentrated CaO-SiO_2 based glassy phase at grain boundaries. Such a phase could promote grain growth and lead to pores

trapped within grains. The presence of trapped pores within grains decreases the final sintered density values. On the other hand, the improvements in the sintered density of compositions prepared by the ' 1s- . route could be as a result of the higher concentration of additives at the ferrite grain boundaries. As the additives were introduced after calcination process, during secondary ball milling, they will be distributed relatively uniformly around grain boundaries and may act in conjunction to inhibit grain boundary motion. As a result a more uniform microstructure with less trapped pores inside the produced grains. Microstructural examination presented in the following section will confirm this hypothesis.

4.3 Microstructure Developments of Mn-Zn ferrites

4.3.1 Effect of Temperature and Time

High quality Mn-Zn ferrites with improved magnetic properties require careful microstructural control of the final sintered products. The quality of a Mn-Zn ferrite microstructure depends on the grain size and grain size distribution, the chemical composition and the structure of the grain boundaries. These microstructural characteristics may also reflect the effect of impurities and minor addition and the sintering conditions such as temperature and atmosphere during heating and cooling.

Figures 4.8.a, b and *c*, shows the relationship between the sintering conditions and microstructural development of Mn-Zn ferrite. The main features of the microstructure obtained by gel processing of the base composition sintered at 1300 ^{0}C for 2 hours, *figure 4.8.a*, shows small average grains of 3μm with some evidence of porosity. However, *figure 4.8.b* shows a sample of the same chemical composition sintered at 1330 ^{0}C for 3 hours when a nitrogen atmosphere was introduced from 700 ^{0}C on heating. This sample exhibits a denser microstructure with larger grain sizes of 4 μm with all the residual porosity being located at grain boundaries. Microstructural observation of a Mn-Zn ferrite sample of the same composition prepared by the mixed oxides method, *figure 4.8.c.*, sintered at 1330 ^{0}C for 3 hours shows a non-uniform microstructure with average grain size of 19 μm with porosity located within grains and at grain boundaries. The grains appear to have grown much faster than in the same

composition ferrite prepared by the gel method and sintered under the same conditions. That could be related to the initial particle size and homogeneity of the prepared powder. It is well known fact that powders prepared by citrate gel processing method possess small homogenised particle size, while powders prepared by mixed oxides method showed wide diversity of particle sizes[30]. As indicated above, it is notable to observe that the smaller grains do appear to be pore free, while the larger grains have pores trapped within the grains, where the grain boundaries have migrated faster than the pores when the grain growth occurred.

Pore-grain boundary interaction during sintering has a decisive influence on the microstructural development. Depending on the pore size/grain size ratio, the grain growth is largely determined by the attachment or separation of the pores from the grain boundary. If the ratio is small then the pores will be left behind and the conditions for the formation of grains with exaggerated grain size and trapped pores will be present. To achieve Mn-Zn ferrite with fine microstructure, exaggerated pores are developed by applying a high oxygen partial pressure during sintering. However, if these pores are large enough they can pin the grain boundaries[97] and hinder grain growth due to drag effect[98]. It is well known that a higher amount of oxygen in the sintering atmosphere, ≥21 vol%, increases the pore mobility and induces exaggerated pore growth, while a lower concentration of oxygen increases the concentration of the oxygen ion vacancies, and promotes volume diffusion and therefore grain boundary mobility[95,98]. In order to obtain a dense polycrystalline body it is necessary to eliminate the voids between the original particles of the ferrite and the pores from the grain boundaries. The continuous evolution of microstructure during sintering can be divided into three stages[145]. During the first stage the contact area between particles increases, where neighbouring particles form a neck by surface diffusion and also at higher temperatures by an evaporation condensation mechanism. Grain boundaries then start to form at the interfaces between particles with various crystallographic orientations. Subsequently, pores are seen as voids between three or more adjacent particles, and finally, shrinkage of the ferrite bulk begins.

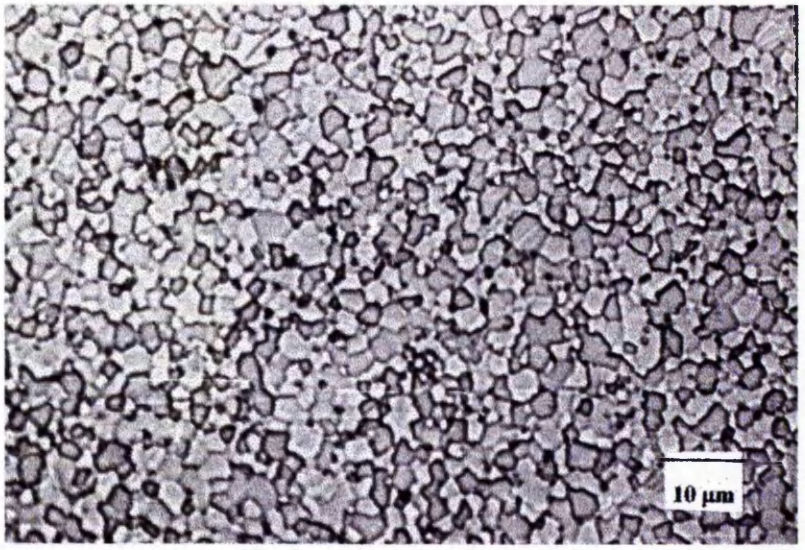

(a)

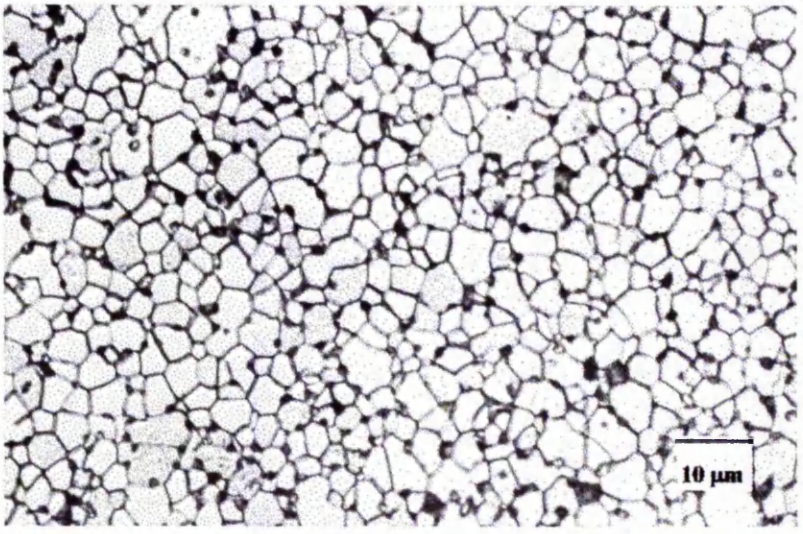

(b)

Continued/

Concluded/

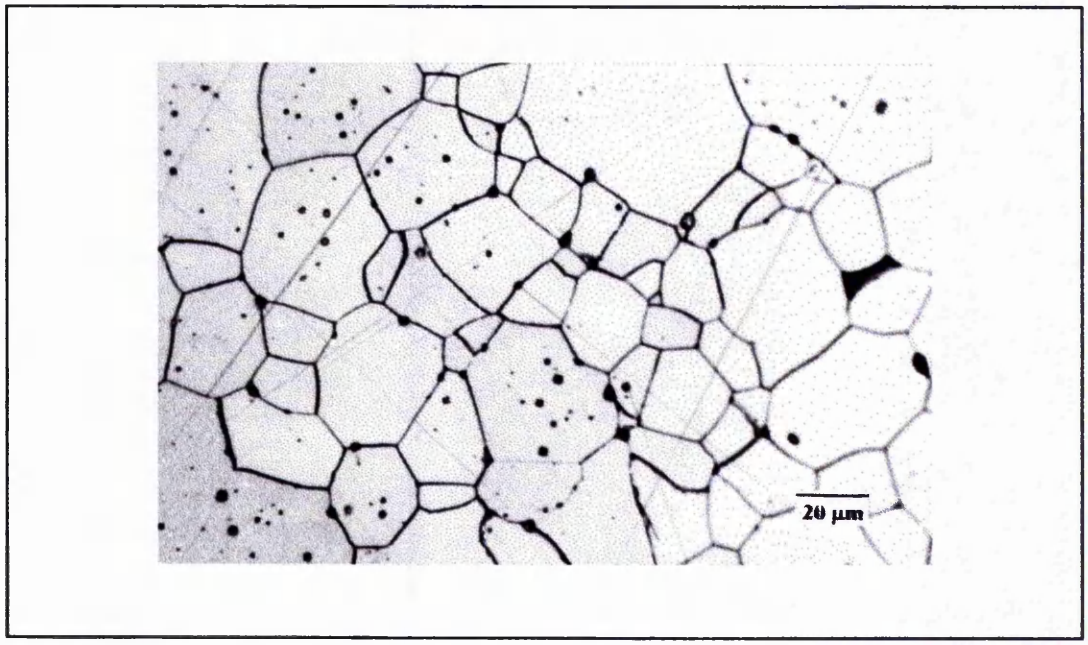

(c)

Figure 4.8. Optical micrographs of the base Mn-Zn ferrite composition samples prepared by the gel method. (a). sintered at 2hours at 1300 ^{0}C, (b) sintered at 1330 ^{0}C for 3 hours, and(c) prepared by conventional mixed oxides method and sintered at 1330 ^{0} for 3 hours.

The second stage of the microstructural evolution begins when a three dimensional system of necks is achieved and during this stage, most of the increases in density take place. To increase the density and eventually eliminate pores, a net transport of material to the pores by volume diffusion is essential. The transportability of the ions is acutely intensified by the presence of lattice defects. The sintering mechanism involves creation of vacancies in the curved surfaces of the pores, their mobility through the grain and their absorption at the grain boundaries, which act as sinks. The pore elimination mechanism is such that the pores experience a compressive stress due to the formation of grain boundary area and the disappearance of surface area during shrinkage. The trapped gas inside the pores acts as a resistance to their elimination. The decrease in pore volume continues until both the external and internal pressures become equal[(146)]. In the third and final stage, grain growth occurs and all remaining pores become isolated.

Paulus[19] suggested that the grain growth in an aggregate of similar grains depends strongly on the sintering temperature and the oxygen content in the sintering atmosphere. The grain growth rate relies on the surface energy of the grain boundaries and the relationship between the two factors can be explained by one of the following models[19]:

- The first model assumes that the grain boundary surface energy is the total of two energies; elastic and disordered energy. The elastic energy extends into the adjoining grains for several ionic distances while the second energy is due to the disordered ionic structure of the grain boundary. The disordered nature of grain boundary permits a rearrangement of ions, which lowers the grain boundary surface energy.

- The second model states that the grain boundary surface energy is actually the difference between the surface energy of a monocrystal and the surface energy of a larger number of crystals, of the same total volume, separated by air. By increasing the temperature, the number of crystal lattice defects also increase, which decrease the grain boundary surface energy. This model does not explain the sudden change of surface energy at certain transition temperature.

In the case where the grain growth process is very rapid, pores may be left inside the grains by the rapidly moving grain boundaries and not between the grains. *Stuijts*[137] reported that ferrites sintered in a nitrogen atmosphere have low concentration of cation vacancies that leads to the materials transport from one side of the pore to the other not being fast enough to allow the pores to move along with grain boundaries. Consequently, the grain boundaries tend to move much faster than the pores, leaving them trapped within the grains.

4.3.2 Effect of Titania Additions

Grain growth kinetics also depends very strongly on the addition levels of minor additives, such as TiO_2, that could effectively change the nature and concentration of defects in the matrix. Thus, they could affect the grain boundary mobility, pore transportability and pore elimination[25]. The effects of three different levels of TiO_2 additions on grain size were studied in the present work and are given in *table 4.7.* As indicated in *Chapter 3, section 3.9* these grain sizes were determined for low magnification micrographs using the general intercept procedures. All compositions with titania additions were sintered at 1330 ^{0}C for 3 hours. The 0.2 wt% TiO_2 additions increased the grain size by 40% compared with the base composition sample processed under the same conditions on increasing the titania additions to 0.4 wt%, the grain growth improved considerably compared with both base and 0.2 wt% TiO_2 samples and the average grain size of was found to be 8.6 μm as shown in (*figure 4.9*). However, further increases of titania additions up to 0.6 wt%, (*figure 4.10*) resulted in grain size decreases compared with 0.4 wt% TiO_2. The 0.6 wt% TiO_2 addition sample was shown to have a high sintered density and larger grain sizes than those of both 0.2 wt% TiO_2 and base composition samples.

Composition	*Average Grain Size (μm)*
Base Mn-Zn ferrite	*4.1±0.3*
Mn-Zn ferrite with 0.2wt% TiO_2	*5.7±0.2*
Mn-Zn ferrite with 0.4wt% TiO_2	*8.6±0.3*
Mn-Zn ferrite with 0.6wt% TiO_2	*6.9±0.2*

Table 4.7. Grain size dependence on TiO_2 additions

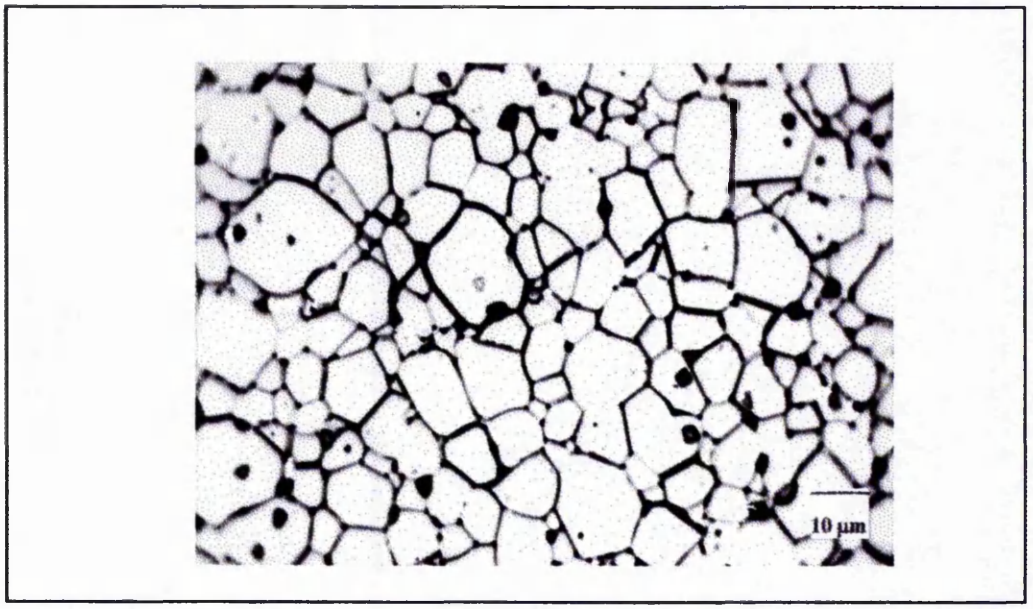

Figure 4.9. Optical micrograph of Mn-Zn ferrite with 0.4 wt% TiO_2 additions sintered at 1330 ^{0}C for 3 hours.

The grain sizes of ferrites have been found to increase with titania additions up to the solubility limit in the ferrite, beyond which the grain size decreases[25]. Evidence in this study, suggests that for the Mn-Zn ferrite used the solubility limit for titania is 0.4 wt%, and any further increase will result in decreases in grain size. The possible mechanism for the reduction of grain size in Mn-Zn ferrite by excess TiO_2 is related to the presence of high a concentration of impurities on or near grain boundaries region that results in reduction in the grain boundary motion by a simple drag effect.

It has been reported that titania act as a grain growth promoter and has been classified to dissolve in the host lattice[4] where it increases the transport rate of the slow moving ions, such as oxygen, by increasing the appropriate defect concentration. The vacancy mechanism can be explained as an excess vacancy formation as Ti^{4+} ion substitutions to the ferrite can be related to the site and charge balance as well as the oxidation-reduction equilibrium of iron. In the case of titanium substitutes for an

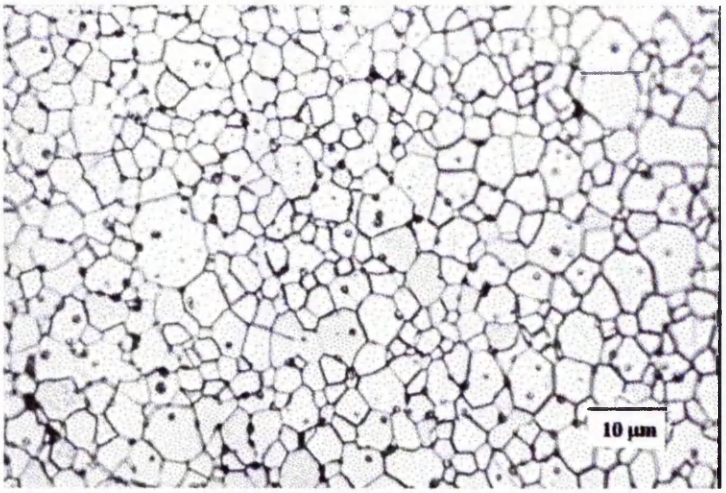

Figure 4.10. Optical micrograph of Mn-Zn ferrite with 0.6 wt% TiO_2 additions sintered at 1330 ^{0}C for 3 hours.

occupancy

addition of three $^{VI}Ti^{4+}$ ions, four Fe^{3+} ions are reduced to Fe^{2+} to satisfy site and the charge balance, which means that the $[Fe^{2+}]/[Fe^{3+}]$ ratio increases. But, the oxidation-reduction equilibrium of iron requires that[35]:

$$Fe^{2+} + \tfrac{1}{4}O_2(g) \Leftrightarrow Fe^{3+} + \tfrac{3}{8}V_{Fe} + \tfrac{1}{2}O_0^{2-} \qquad 4.4$$

and,

$$[V_{Fe}]^{1/4} = K_{23}\frac{[Fe^{2+}]}{[Fe^{3+}]}\frac{P_{O_2}^{1/4}}{[O_0^{2-}]^{1/2}} \qquad 4.5$$

where V_{fe} donates iron vacancy, and K_{23} is the redox equilibrium constant. Therefore, any increase in $[Fe^{2+}]/[Fe^{3+}]$ ratio creates excess iron vacancies, *equation 4.5*. Consequently, it may be concluded that iron vacancies must be created by Ti^{4+} ions to be consistent with both site and charge balance and the redox equilibrium of iron. Hence as titania initiates excess cation vacancies, a model of increased pore mobility can be

rationalised, according to *Reinjnen*[95]. During the pore movement both anions and cations have to be transported. As indicated earlier, oxygen existing in the ferrites can be transported through the gas phase in the pores because of the differences in curvatures on the opposite surfaces of the pore. As the gas-phase diffusion of the oxygen is rapid, the pore movement is rate-limited by the slower cation diffusion. Consequently, the cation vacancy flux generated by Ti^{4+} ions increases the pore mobility resulting an increase in the mobility of pore-loaded grain boundaries[25]. *Franken*[24] has also examined the effect of Ti^{4+} ion substitutions on the microstructure of Mn-Zn ferrites prepared by the mixed oxides method and concluded that the presence of titania enhances significantly the grain growth. Conversely, *Lebourgeois et. al.*[51] reported that TiO_2 has a small influence on the grain growth as all the Ti^{4+} are incorporated in the spinel phase of the ferrite and do not precipitate on or next to grain boundaries.

4.3.3 Effect of Hafnia Additions

The effects on hafnia additions on the microstructure were also studied in the present work. The addition level of hafnia was maintained at 0.4 wt%, because this amount appeared to be close to the solubility limit of titania substitutions. *Figure 4.11a* shows the microstructure of Mn-Zn ferrite with 0.4 wt% HfO_2 additions prepared by the gel method. Microstructural observation shows that there was significant grain growth and a uniform microstructure with an average grain size of 8 μm was produced compared with the base composition prepared by the same processing method. The microstructures of the Mn-Zn ferrite prepared by the mixed oxides processing method are shown in *figures 4.11b.*, and *c.* The presence of 0.4 wt% HfO_2 in the ferrites prepared by the first processing route, *figure 4.11b,* results a in homogeneous microstructure with a larger grain size compared to the base material processed under the same conditions. However, a non-uniform microstructure with a significant grain growth was observed as the main feature of the ferrite sample prepared by the second route *figure 4.11c,* in which the hafnia addition was introduced before the calcination stage, compared again with the base composition. It is clear, that the presence of Hf^{4+} ions increases the mobility of grain boundaries and therefore enhances the grain growth regardless on the

introduction stage. However, the addition stage of HfO_2 is shown to have an important effect on the microstructure of analysed samples. In the case where HfO_2 additions were introduced during milling of the ferrite (route one) the hafnia and ferrite subsequently have opportunity to react during sintering and a small amount of hafnia dissolves into the ferrite lattice, while the remainder either forms a secondary phase located at the grain boundaries or is captured during discontinuous grain growth. However, the introduction of HfO_2 before the calcination process (route two) allows the possibility of two reaction processes with the ferrite. The primary reaction is during the calcination process while the secondary reaction is during the sintering process, which results in more grain growth than in the ferrite prepared by the route one as a result of more diffusion into the ferrite spinel. The rapid hafnia dissolution, diffusion and precipitation result in rapid grain growth, which allows faster grain growth than would normally occur as in route 1. The Hf^{4+} ion dissolution in Mn-Zn ferrite grains and the consequenial increase in the Fe^{2+} ions an increase of Fe^{2+}/Fe^{3+} was associated with the increased grain growth. However, the oxidation/reduction equilibrium of iron requires that the number of iron vacancies must also increase. An increase in cation vacancy concentration and the possibility of vapour phase transport may also increase the grain boundary mobility[147], which leads to intragranular porosity. However, the introduction of hafnia during ball milling led to a finer microstructure compared to samples prepared by route 2. The hafnia deposited at grain boundaries decreased the grain boundary mobility. The intrinsic grain boundary mobility corresponds to motion limited by the movement of ions . the boundary. However, when the grain boundary was pinned with hafnia second phase, then its motion became slower and grain growth slowed down. This can be seen when one compares the microstructures of samples prepared by both mixed oxides processing routes (*figures 4.11.a and b*).

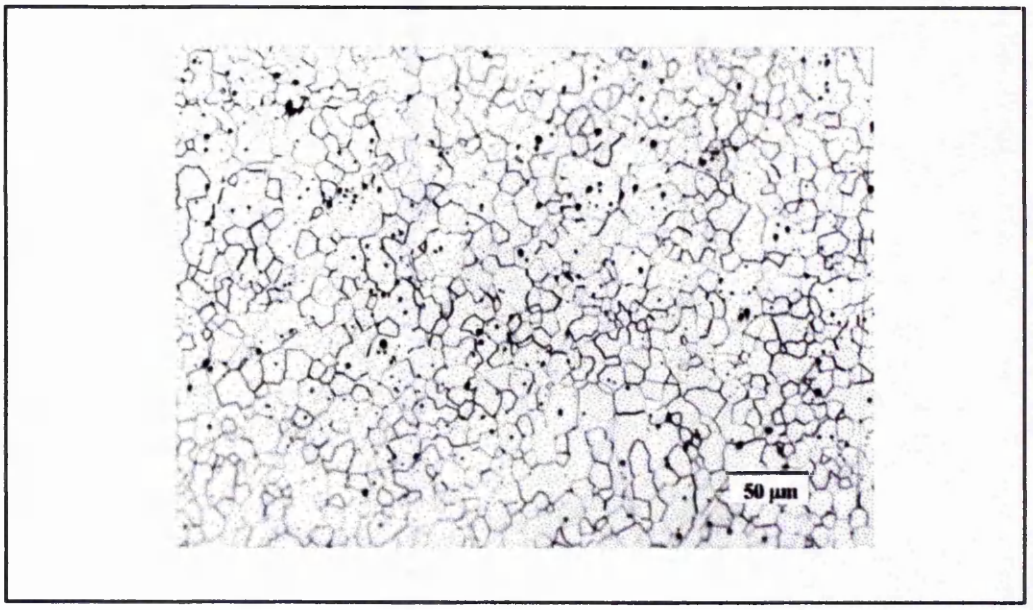

(a)

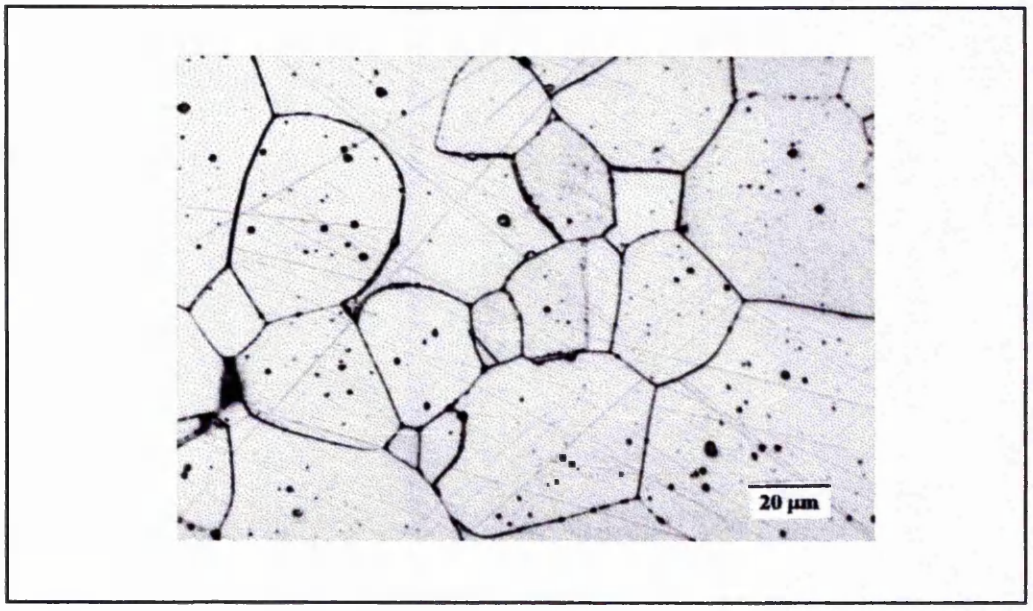

(b)

Continued/

concluded/

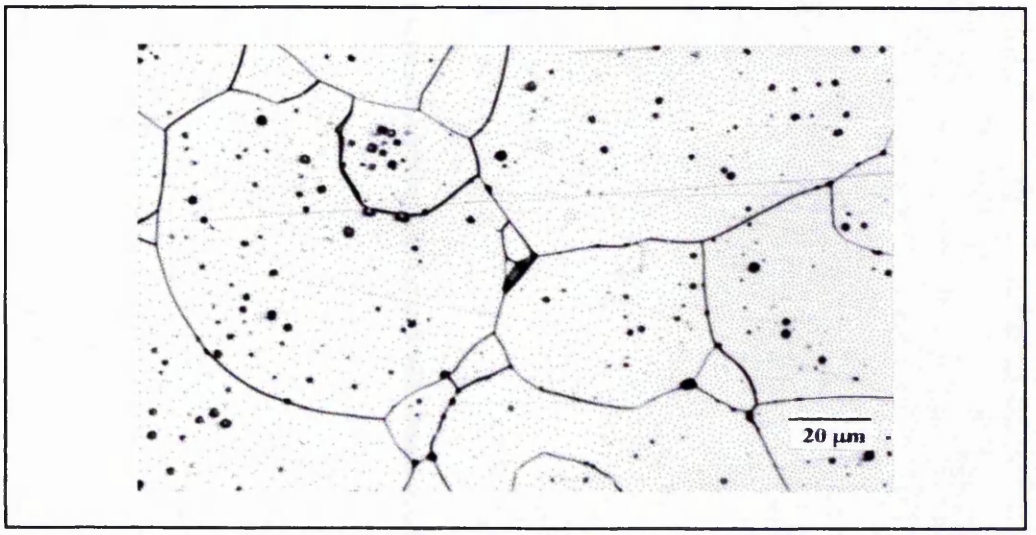

(c)

Figure 4.11. Optical micrograph of Mn-Zn ferrite with 0.4 wt% HfO_2 additions, (a) sample prepared by citrate gel processing method, (b) sample prepared by mixed oxide methods, hafnia introduced after calcination (route 1), and (c) sample prepared by mixed oxide methods hafnia introduced from start of processing (route 2).

4.3.4 Effect of Calcia and Silica Additions

The effects of different additives, such as *CaO* and/or SiO_2, on the base composition and compositions with TiO_2 and HfO_2 microstructures were also studied. HfO_2, *CaO* and SiO_2 addition levels were maintained at 0.4 wt%, 0.04 wt% and 0.02 wt% respectively, while the TiO_2 additions were varied as stated earlier.

The effect of the impurity additions on grain size of the base composition and compositions with TiO_2 additions of the Mn-Zn ferrite microstructures is given in *table 4.8*. The presence of *CaO* reflects similar trends of small non-uniform and with more porous microstructures for all compositions, but with various effects depending on the quantities of TiO_2 additions. The most notable effect of *CaO* additions on the microstructure is on the base composition with very small grains, 3.5 μm, and high

intergranular porosity level. Combined additions of TiO_2 and CaO results in smaller non-uniform grain size with a more porous microstructure than that without CaO additions. Combined effect of 0.2 wt% TiO_2 additions and 0.04 wt% CaO addition shows that it has similar but less effect on the microstructure of sintered ferrite. The latter mentioned composition showed less porous, with more uniform microstructure than the base composition with CaO addition. While, the microstructure of the other two compositions, 0.4 wt% and 0.6 wt% TiO_2 additions with 0.04 wt% CaO addition, shows less porosity and less reduction in grain size. *Figure 4.12.* shows a typical microstructure of Mn-Zn ferrites with 0.4 wt% TiO_2 and 0.04 wt% CaO where the grains became significantly smaller than those of Mn-Zn ferrites with 0.4 wt% TiO_2.

Existing evidence in this study (*figure 4.12 and table 4.8*) suggests that the CaO does not dissolve in the ferrite lattice and it is strong possibility that it precipitated at the grain boundaries. The grain sizes of CaO added samples are smaller than these of sample containing titania only that could be due to the pinning effect of calcia as it precipitate on the grain boundaries. *Paulus et. al.*[19] using autoradiography and preforential chemical etching methods of ferrite samples containing calcia, high presence of calcia on and next to the grain boundary regions. They related this phenomenon to the fact those calcia segregates at the grain boundaries during cooling as it leaves the ferrite matrix toward the grain boundary areas.

Figures 4.13a, b, and *c,* shows that the presence of CaO along with HfO_2 inhibits grain growth. As a result the grains are smaller in size compared with HfO_2 only. It is interesting to notice that the samples prepared by the first route of mixed oxides processing and gel processing method show more uniform grain sizes than the same composition prepared by the second route which could be as a result of more homogenous distribution of CaO in the microstructure. Similarly, microstructures obtained of the same composition prepared by citrate gel processing showed small but uniform grain sizes compared with the compositions prepared by conventional mixed oxide method. *Table 4.9.*, shows comprehensive results of the effect of HfO_2 and CaO

Composition	*Grain Size (μm)*		
	0.04 wt% CaO	*0.02 wt% SiO_2*	*0.04 wt% CaO and 0.02 wt% SiO_2*
Base Mn-Zn ferrite composition	*3.4±0.2*	*4.9±0.3*	*4.5±0.2*
Mn-Zn ferrite with 0.2 wt% TiO_2	*5.1±0.3*	*6.7±0.3*	*6.2±0.2*
Mn-Zn ferrite with 0.4 wt% TiO_2	*8.1±0.3*	*9.1±0.4*	*8.9±0.3*
Mn-Zn ferrite with 0.6 wt% TiO_2	*6.4±0.2*	*8.2±0.3*	*7.9±0.2*

Table 4.8. Grain size dependence on impurity additions

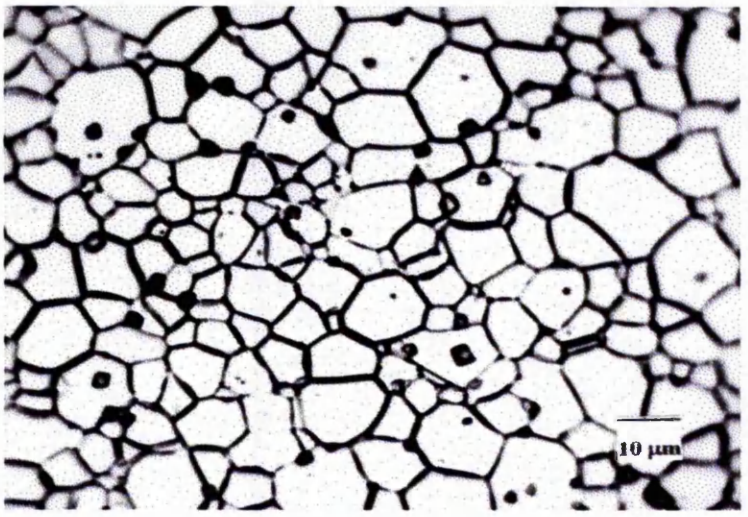

Figure 4.12. Optical micrograph of Mn-Zn ferrite with 0.4 wt% TiO_2 additions prepared by gel processing method in combination with 0.04 wt% CaO.

and/or SiO_2 additions on the microstructure of Mn-Zn ferrites. *Otsuka et. al.*[6] studied the effect of HfO_2 with CaO additions on the Mn-Zn ferrite microstructures and found a HfO_2-CaO complex to have a tendency to be precipitated next to, or at, the grain boundaries. *Johnson et. al.*[148] investigated the effect of CaO on the microstructure of Mn-Zn ferrite and they found that the CaO generally segregates on the grain boundaries and decreases grain boundary mobility that results in reduction of grain growth. *Bando et. al.*[42] reported that the additions of CaO to the Mn-Zn ferrites prevents the grain growth process, while SiO_2 enhances it.

The effect of SiO_2 additions on the microstructures of Mn-Zn ferrites has been also analysed. Generally, the presence of Si^{4+} ions in the microstructure of the studied compositions results in significant increase in grain size. The largest increase in grain size been found in the composition with 0.6 wt% TiO_2, while similar tendency with less effect on grain growth been found for the other compositions, *table 4.8*, especially composition with 0.4 wt% TiO_2, *figure 4.14*. While the presence of silica along with hafnia results in very large uniform grains with pores inside the grains as a result of a secondary grain growth.(*figures 415a, b* and *c*). This observation suggests that the HfO_2 and SiO_2 form a chemical complex and do not dissolve in the ferrite lattice and therefore it is possible that a liquid phase is formed at sintering temperatures which increases grain growth by a flux growth process[47].

Giles and Westendrop[36] observed exaggerated grain growth in Mn-Zn ferrites in the presence of SiO_2, while *Carpy and Stuijts*[47] also reported that SiO_2 promotes the grain growth through the formation of a silica based liquid phase and described a "flux growth" process where the liquid dissolves materials from the grain boundaries which then diffuse through the liquid phase and finally precipitates. Hence, rapid dissolution, diffusion and precipitation result in rapid flux growth that gives faster grain growth than would normally occur in the solid state. Consequently, the grain boundaries move faster than the pores, leaving them trapped within the grains. *Perdujin and Peloschek*[111] have also classified SiO_2 as a grain growth promoter and suggested that during sintering a

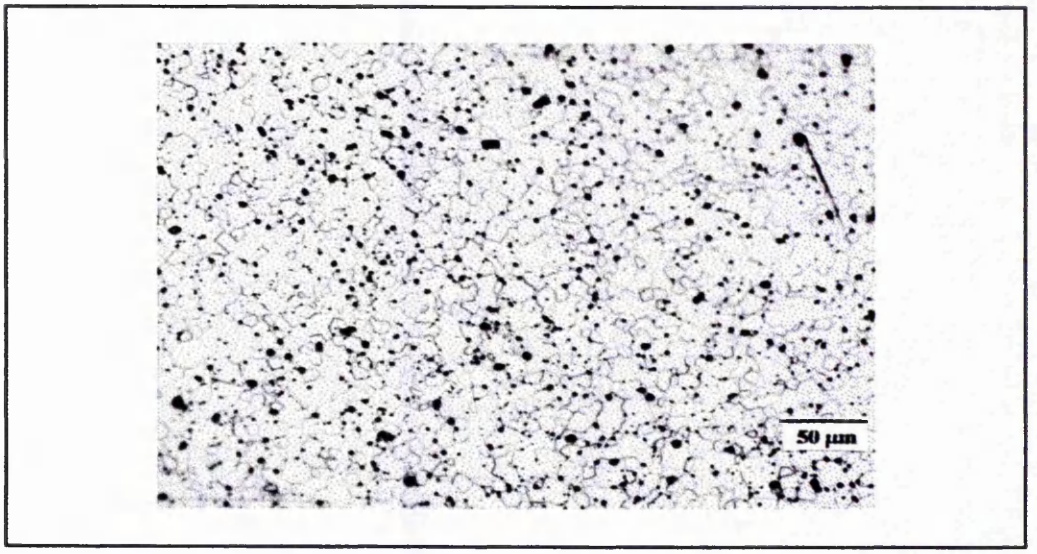

(a)

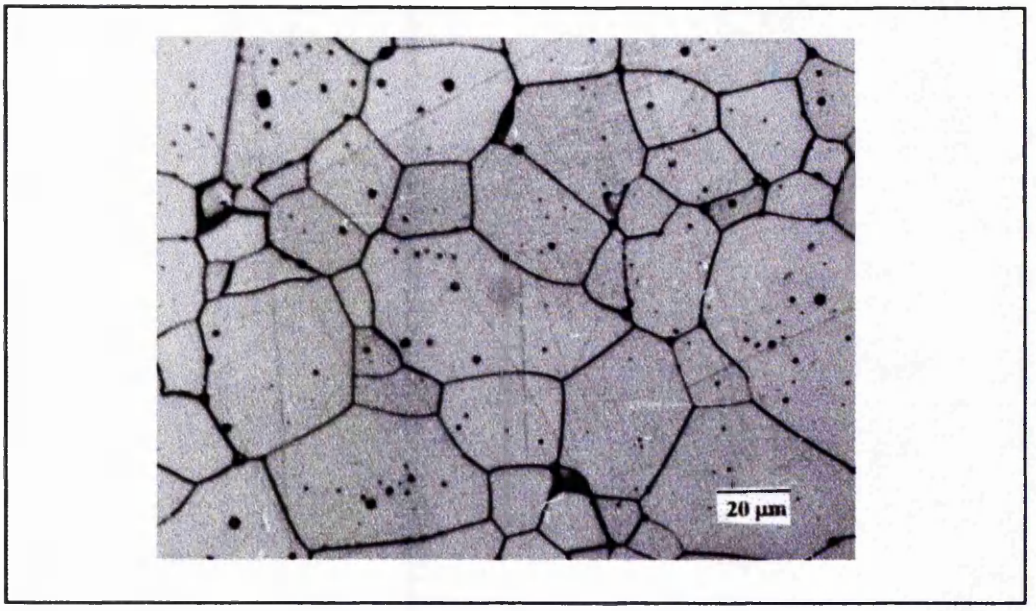

(b)

continued/

concluded/

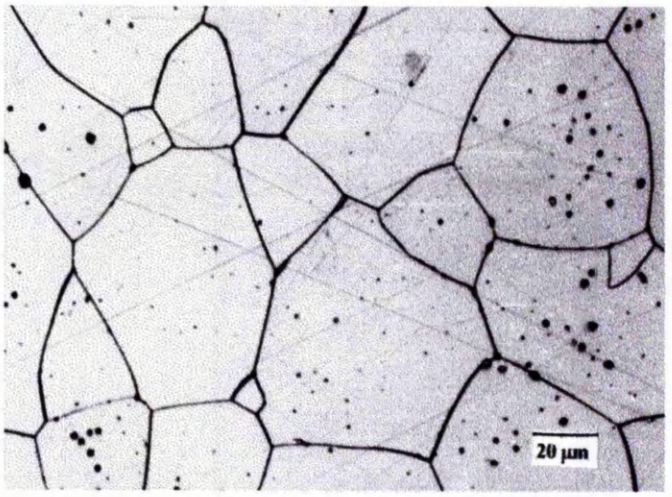

c)

Figure 4.13. Optical micrographs of Mn-Zn ferrite with 0.4 wt% HfO_2 in combination with 0.04 wt% CaO additions (a) sample prepared by citrate gel processing, (b) sample prepared by mixed oxides method (route 1) and (c) sample prepared by mixed oxides processing method (route 2).

liquid film, which promotes discontinuous grain growth forms around the grains. The liquid film changes the surface energy of the grain boundary and in matrix of small grains at a certain temperature the grain boundaries will sweep over the pores giving large grains with intragranular pores.

In the case where both impurities were present the grain size reduced significantly and became more uniform relative to that observed when both titania or hafnia and silica were added. The implication is that *CaO* segregates on the grain boundaries and prevents the exaggerated grain growth caused by combined effect of TiO_2 (*figure 4.16*) or HfO_2 and silica (*figures 4.17a, b* and *c*). The most notable improvement was seen for samples prepared by the mixed oxides method. Significant grain size reductions were observed for the sample prepared by route 2, however similar reductions were also observed for other samples prepared by the both citrate gel and mixed oxides route 1.

Composition	*Grain Size (μm)*		
	Gel Processing Method	*Mixed Oxide Processing Method*	
		Route 1, Additives introduced after calcination	*Route 2, Additives introduced before calcination*
Mn-Zn ferrite with 0.4 wt% HfO_2	*10±0.6*	*27±3*	*45±18*
Mn-Zn ferrite with 0.4 wt% HfO_2 and 0.04 wt% CaO	*8.4±0.5*	*18±1*	*25±12*
Mn-Zn ferrite with 0.4 wt% HfO_2 and 0.02 wt% SiO_2	*16.7±0.6*	*85±25*	*D.G.G**
Mn-Zn ferrite with 0.4 wt% HfO_2, 0.04 wt% CaO and 0.02 wt% SiO_2	*12.5±0.5*	*40±3*	*50±4*

D.G.G.* Discontinues Grain Growth

Table 4.9. Grain size dependence on HfO_2, CaO and/or SiO_2 additions

Franken[24] reported that at the grain boundary of *Ti*-substituted Mn-Zn ferrite a *Ca/Si* and *Ti* containing phase been found, and apart from this layer a large content of titania was also found in the matrix, that indicates the titania mostly dissolves in the matrix. It was also reported that discontinuous grain growth during the sintering of Mn-Zn ferrite was caused by the simultaneous addition of *CaO* and SiO_2 and was explained by liquid phase sintering. *Bando et. al.*[42] reported that the proportion of large grains increases with an increasing amount of simultaneous CaO/SiO_2 additions because of the formation of liquid phase, above 1100 ^{0}C, and the rate of grain growth is accelerated in the presence of the liquid, while it is small in the absence of the liquid. It was also recognised that the liquidus temperature in the silica rich region of the phase diagram was lower than that of *CaO* rich region.

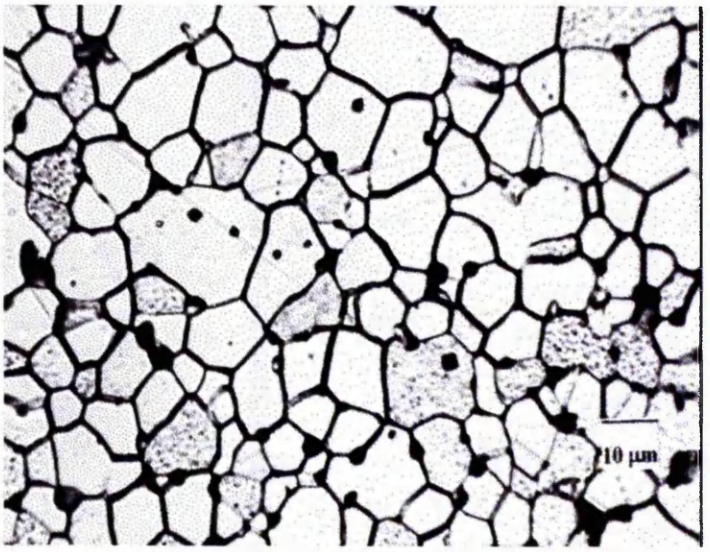

Figure 4.14. Optical micrograph of Mn-Zn ferrite with 0.4 wt% TiO_2 additions prepared gel processing method in combination with 0.02 wt% SiO_2.

According to *Jain et. al*[149], assuming that the liquid phase is not uniformly distributed, discontinuous grain growth is likely. Conversely if the liquid phase is uniformly distributed, grain growth impediment can occur. Hence, discontinuous grain growth is likely to occur in the lower range of CaO/SiO_2 additions, and is most probably caused by the liquid phase not being uniformly distributed. This is particularly likely when it is considered that the liquid phase at lower mole ratio of the additives is more viscous than at higher mole ratio[150]. The more viscous the liquid phase, the more difficult it is to distribute it uniformly and therefore discontinuous grain growth tends to occur[151]. *Kono*[26] assumed that on the simultaneous addition of CaO and SiO_2 the iron ions located at the grain boundaries will be strongly pushed out of the liquid phase and the liquid phase will be rich in the *Ca-Si* containing phase. *Otsuka et. al.*[6] found that the optimum amount of CaO/SiO_2 additions into the Mn-Zn ferrites with conjunction to TiO_2 or HfO_2 is 0.04 wt% and 0.02 wt% respectively.

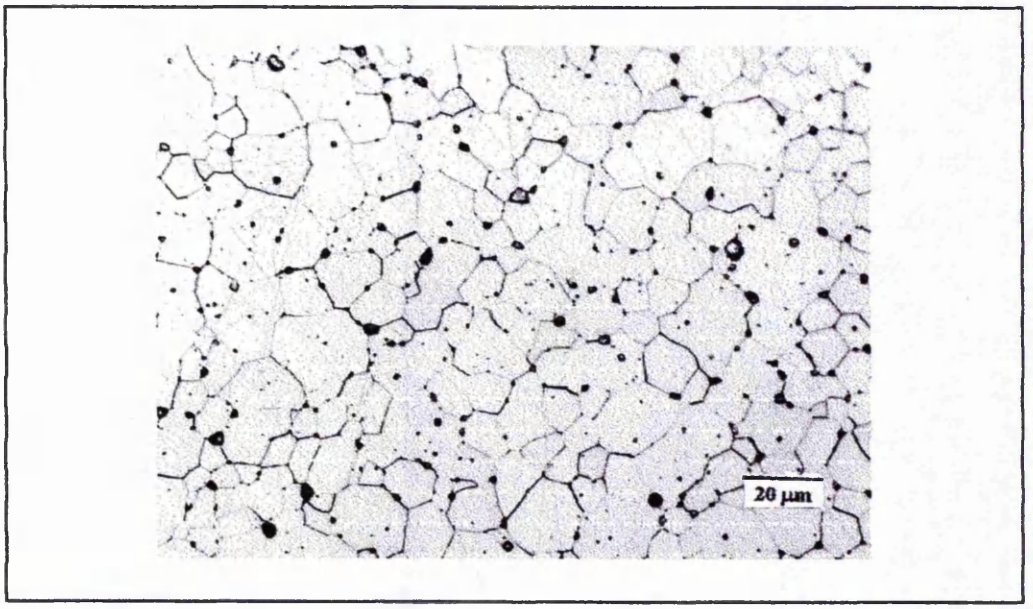

(a)

(b)

continued/

Concluded/

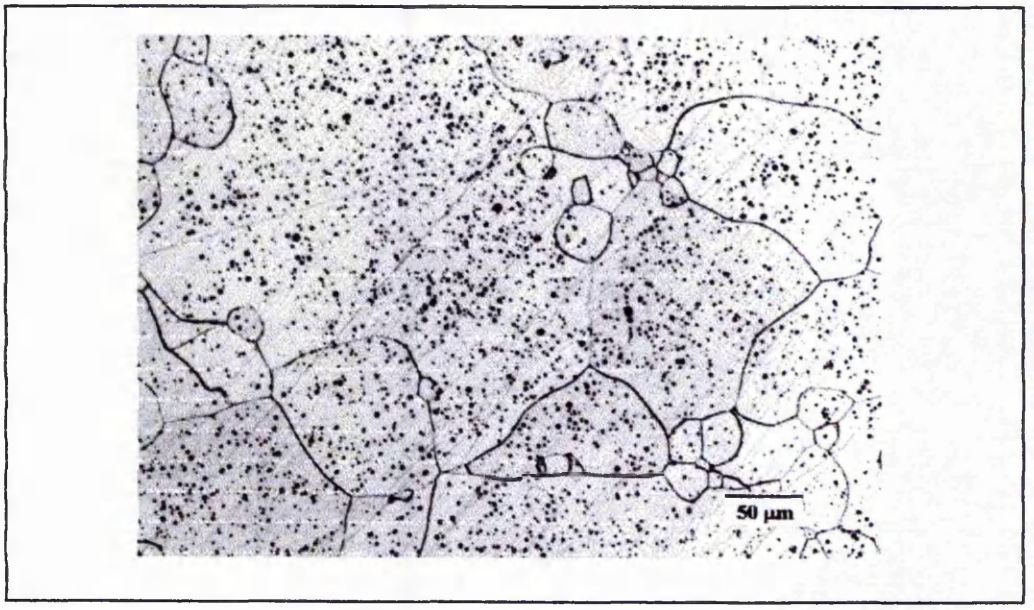

(c)

Figure 4.15 Optical micrograph of Mn-Zn ferrite with 0.4 wt% HfO_2 in combination with 0.02 wt% SiO_2 additions, (a) sample prepared by gel processing, (b) sample prepared by mixed oxides method (route 1), and (c) sample prepared by mixed oxides method (route 2).

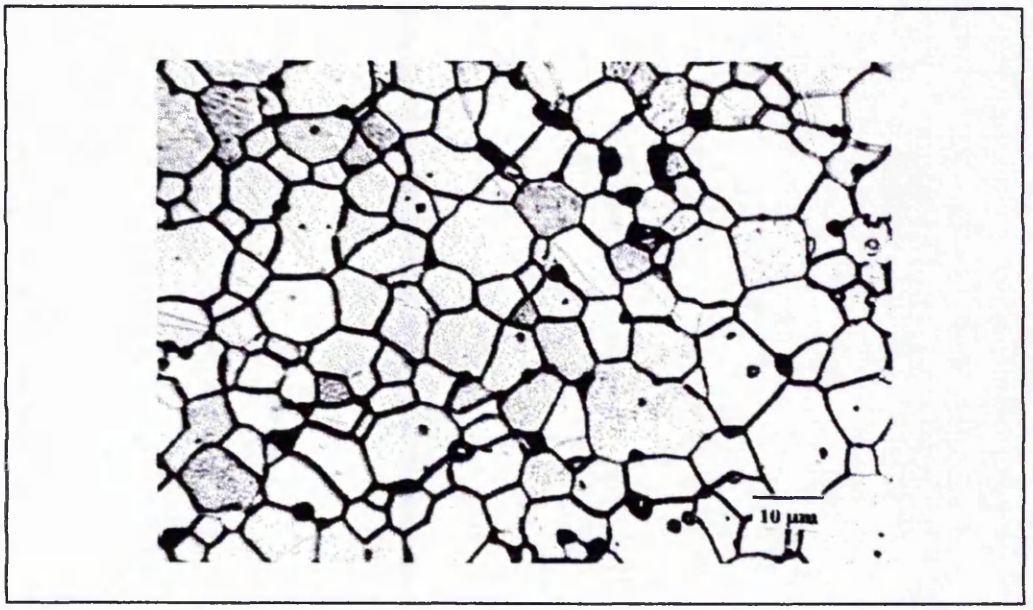

Figure 4.16. Optical micrograph of Mn-Zn ferrite with 0.4 wt% TiO_2 additions prepared by gel processing method with both CaO and SiO_2.

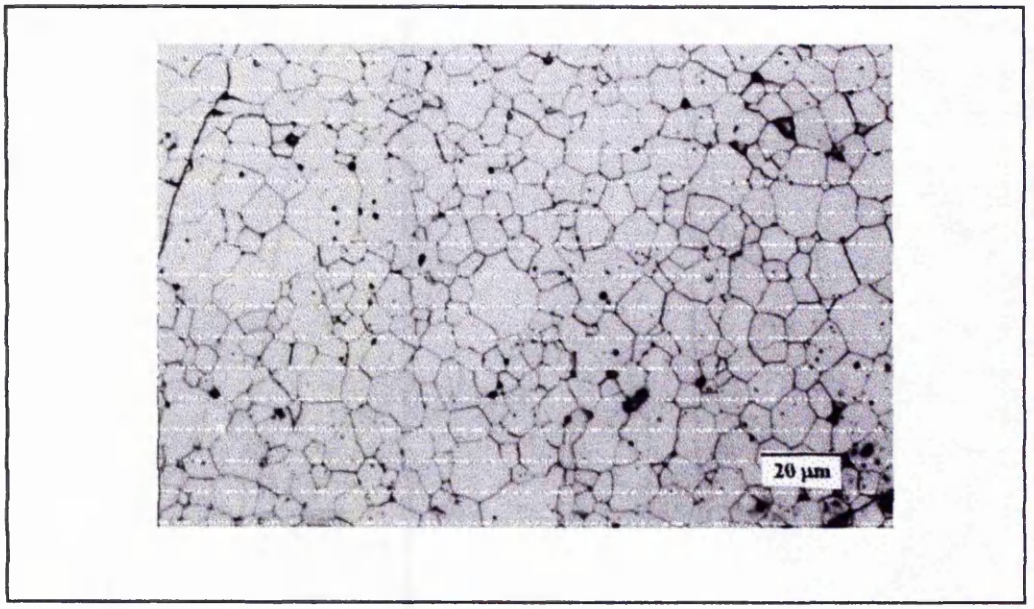

(a)

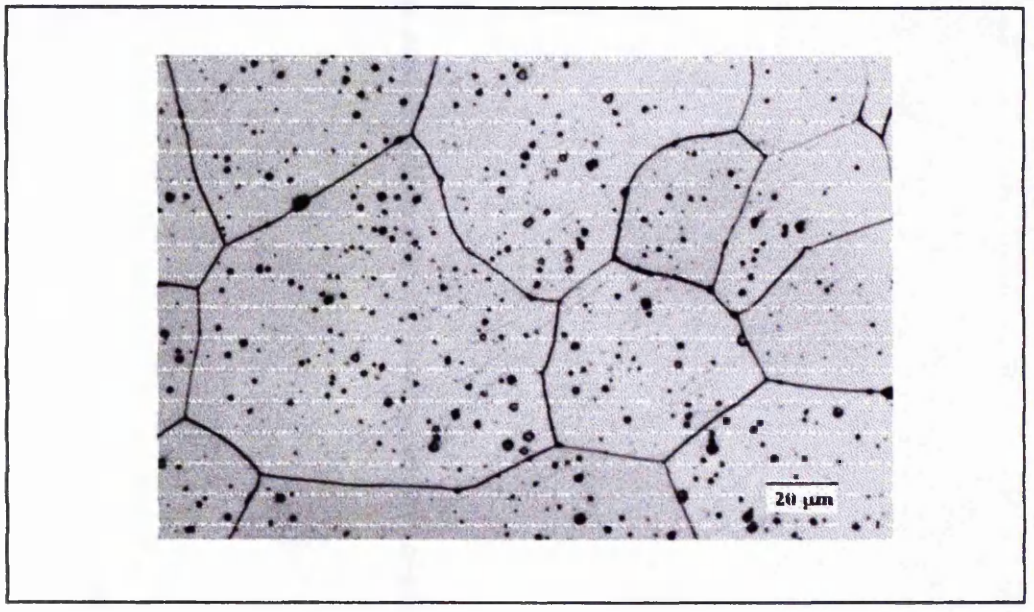

(b)

Continued/

Concluded/

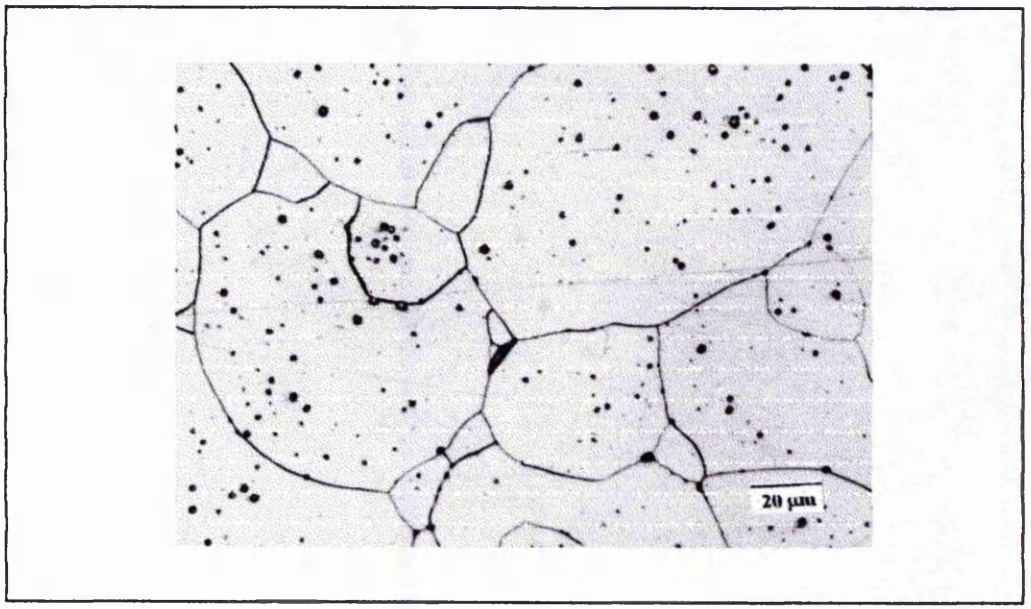

(c)

Figure 4.17. Optical micrograph of Mn-Zn ferrite with 0.4 wt% HfO_2 combination with CaO and SiO_2.(a) sample prepared by gel processing method, (b) sample prepared by mixed oxides method (route 1), and(c) sample prepared by mixed oxides method (route 2).

Results appear to indicate that microstructure observations obtained in this study are in good agreement with the work of many authors[5,6,24,26]. For instance, the addition of calcia on its can to the ferrite samples results in small grain size microstructures. Conversely, microstructure observations of samples containing silica on its own shows that grain growth has occured as a result of the formation of a liquid phase that promote the mobility of grain boundaries. However, the degree of grain growth varies as it also depends on other additives such as titania, hafnia and/or calcia and the method of powder preparation. The exaggerated grain growth observed in ferrite samples prepared by mixed oxides processing and containing both silica and hafnia (*figures 4.15b and c*) was as a result of the double effect of both hafnia and silica as they are both classified as grain growth promoters and only a fraction of a weight percent is needed to induce grain growth. However, samples prepared by the gel processing method containing the same

additive have also showed grain growth but to a much lower extent than samples prepared by mixed oxides processing (*figure 4.15a*). As indicated earlier, significant grain growth prevention occurred when calcia was added to the ferrite samples along with other additives. This observation was also reported by other workers[5,6,149,151].

4.4 *Transmission Electron Microscopy Analysis of Mn-Zn ferrites*

Results obtained from selected samples with HfO_2, TiO_2 and CaO/SiO_2 are presented in the following section. The chemical analyses of the Mn-Zn ferrite with 0.4 wt% HfO_2 are shown in *table 4.10. Figure 4.19* shows a HfO_2 rich second phase located on the grain boundary of the ferrite. This observation is in strong confirmation of the work of *Otsuka et. al.*[6] who reported that HfO_2, among other elements such as Ta_2O_5, exclusively segregates on the grain boundaries and triple points. Point analyses on random areas of the Mn-Zn ferrite grains showed no detectable traces of HfO_2 presence, and gave only the major constituent oxides in accordance with the original mixing levels of Fe_2O_3=75.5 *wt%*, *MnO*=14.98 *wt%* and *ZnO*=9.53 *wt%*.

Oxide	*Grain Region*	*Grain Boundary Region*
Fe_2O_3	*75.6 wt%*	*31.24 wt%*
MnO	*16.26 wt%*	*6.4 wt%*
ZnO	*8.14 wt%*	*3.08 wt%*
HfO_2	-	*59.28 wt%*

Table 4.10. Chemical Micro analysis of Mn-Zn ferrite with 0.4wt% HfO_2.

Any slight deviations in the major composition values compared with the base composition could be as a result of local inhomogeneities, however the deviation detected by EDAX is very small and within experimental uncertainty. The detection of HfO_2 as a precipitate at the grain boundary indicates that hafnia does not dissolve in the

Mn-Zn ferrite lattice, a behaviour which according to the work of *Otsuka et. al.*[6], is exacerbated by the presence of SiO_2 and *CaO*.

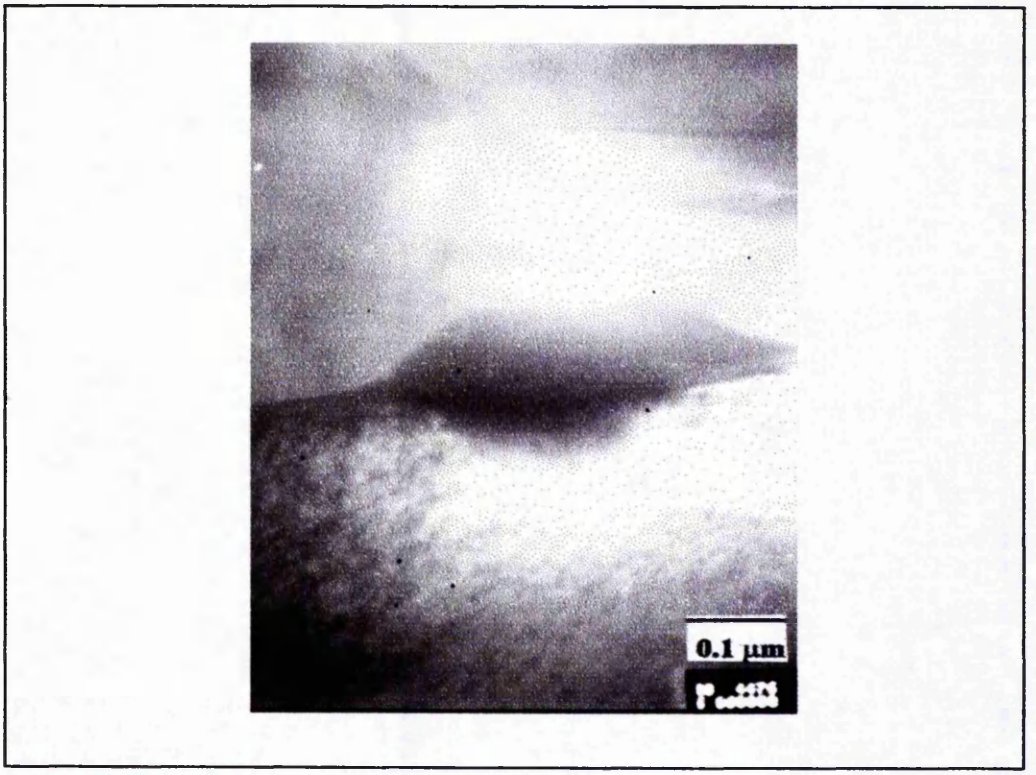

Figure 4.19. TEM photomicrograph of Mn-Zn ferrite with 0.4 wt% HfO_2

In order to clarify whether any hafnia-silica interaction exists, a Mn-Zn ferrite with 0.4 wt% HfO_2 and 0.04 wt% SiO_2, was prepared for analysis by TEM for this purpose. *Table 4.11.*shows the EDAX analysis of this ferrite. In this case, a second phase, rich in HfO_2-SiO_2, was found to be present at the grain boundary of the ferrite, *figure 4.20*. The second phase was found to vary slightly in composition form position to position, but it was always rich in both hafnia and silica. It is interesting to find a small amount of *CaO* present in the phase even though no *CaO* had been added intentionally to the composition of the ferrite. The presence of the *CaO* indicates that it was contaminated as impurity in the raw materials used for the main chemical constituents. The major finding, however, is the confirmation of the tendency of the hafnia and silica to form a chemical compound that mainly precipitates at the grain boundaries. Generally it is known that silica[42] reduces the melting point of other additives and also often lowers surface tension of the melted second phase. The behaviour of hafnia and silica

interactions may be generally explained as the HfO_2 segregates into grain boundary through a melting glassy phase that has high wettability during sintering process, the Si^4 ions remain inside the glassy phase at the grain boundary, and serve to lower the melting point of the hafnia-silica secondary phase[5].

The diffusion of additives towards or from the grain boundary can be classified into equilibrium and non-equilibrium conditions. The non-equilibrium condition in most cases depends on oxygen partial pressure and/or sintering temperature. The equilibrium condition in mostly caused by deformation energy associated with inserting an ion in the host lattice, changes in grain boundary surface energy, and space change regions next to grain boundaries. In addition to these factors there are stress fields associated with grain boundaries that effects the solute distribution.

The formation of a secondary liquid phase at the grain boundaries, as the case of silica in the ferrites, mostly depends on both thermodynamic and kinetics effects. During cooling stage substantial stresses are induces at the grain boundaries. For the same reasons that the lowered strain energy induces solute segregation at the grain boundary, there is a tendency for solute segregation in the associated stress field during cooling. This effect could be responsible for the influence of silica precipitates in the ferrite in enhancing the boundary segregation of hafnia or calcia.

Analyses of grains and grain boundary phases in Mn-Zn ferrite with 0.4 wt% HfO_2 and both 0.04 wt% CaO and 0.02 wt% SiO_2 additives are given in *table 4.12.* As was the case with previous samples, there is no evidence of the additives within the grains. The nano-probe chemical characterisation shows that grains consist only of the main elements of the Mn-Zn ferrite. Analysis of the second phase at the grain boundaries, *figure 4.21,* shows a high presence of HfO_2-SiO_2-CaO in the secondary phase. SiO_2 and HfO_2 were been determined as the major involved in the second phase which suggested again that hafnia and silica tend to form a chemical compound which exists exclusively at the grain boundaries. The relatively small amount of CaO is generally varied and the second phase did always contain CaO. Where CaO was present,

it always occurred in a smaller amount than silica. The only explanation of the lower presence CaO than SiO_2 is that some of CaO could dissolved in ferrite lattice at high sintering temperatures. *Otsuka et. al.*[6] reported that HfO_2 presence with CaO and SiO_2 in Mn-Zn ferrites always tend to form CaO-HfO_2 compound that precipitate mostly in the triple point and grain boundaries. However, *Mochizuki*[5] hinted that hafnia precipitated at the grain boundaries along side both silica and calcia.

Oxides wt%	*Secondary Phase*	
	Location A	*Location B*
Fe_2O_3	*9.37 wt%*	*29.7 wt%*
MnO	*1.87 wt%*	*7.06 wt%*
ZnO	*0.78 wt%*	*4.2 wt%*
HfO_2	*61.3 wt%*	*46 wt%*
CaO	*0.29 wt%*	*0.14 wt%*
SiO_2	*26.39 wt%*	*12.9 wt%*

Table 4.11. Chemical Micro analysis of Mn-Zn ferrite with HfO_2 and SiO_2

Oxides wt%	*Grain*	*Grain Boundary Region*
Fe_2O_3	*72.8 wt%*	*22.79 wt%*
MnO	*16.41 wt%*	*5.35 wt%*
ZnO	*10.79 wt%*	*2.28 wt%*
HfO_2	-	*29.77 wt%*
CaO	-	*8.68 wt%*
SiO_2	-	*31.13 wt%*

Table 4.12. Chemical micro-analysis of Mn-Zn ferrite with HfO_2, CaO and SiO_2

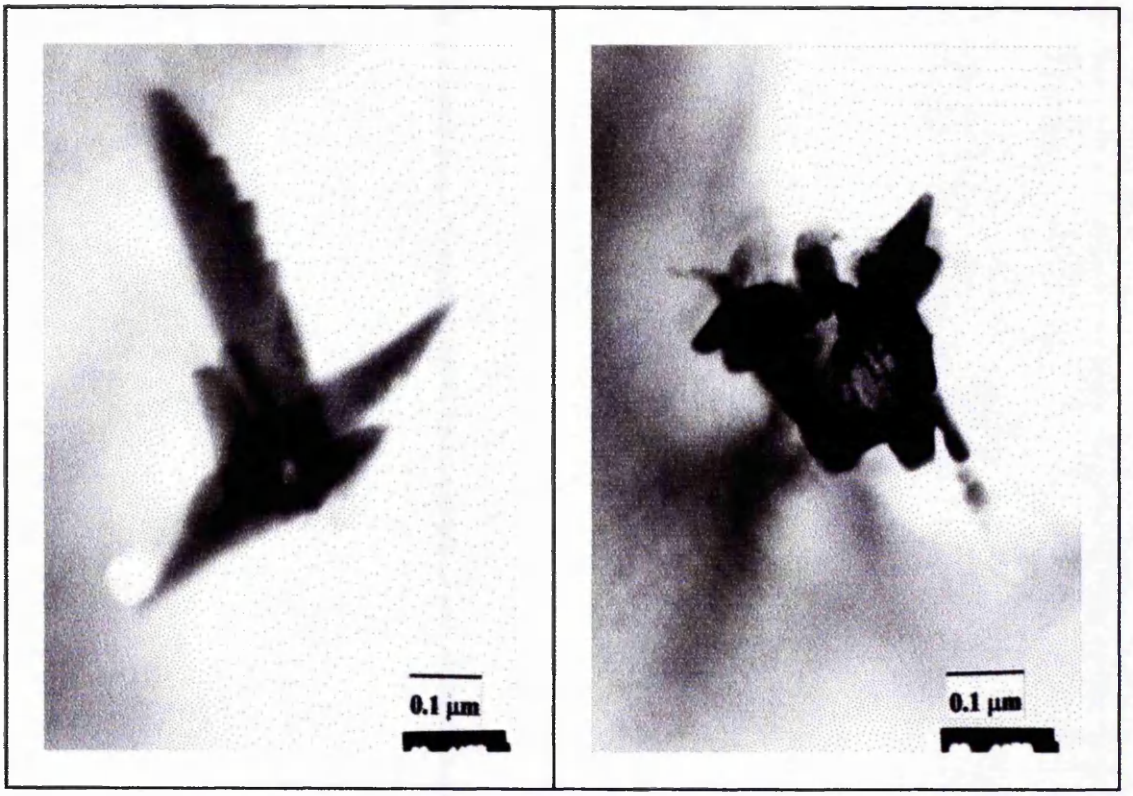

(a) *(b)*

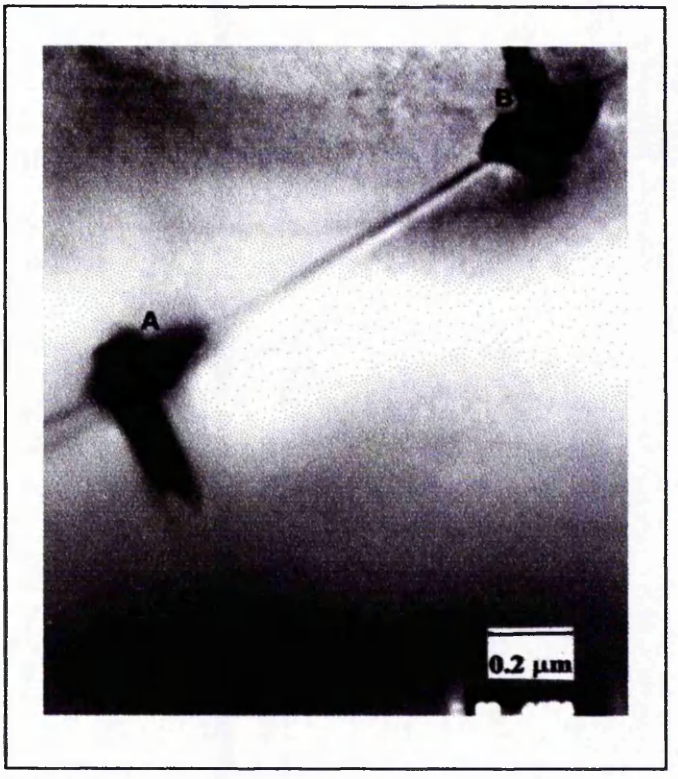

Figure 4.20. TEM photomicrograph of Mn-Zn ferrite with 0.4 wt% HfO_2 and 0.04 wt% SiO_2

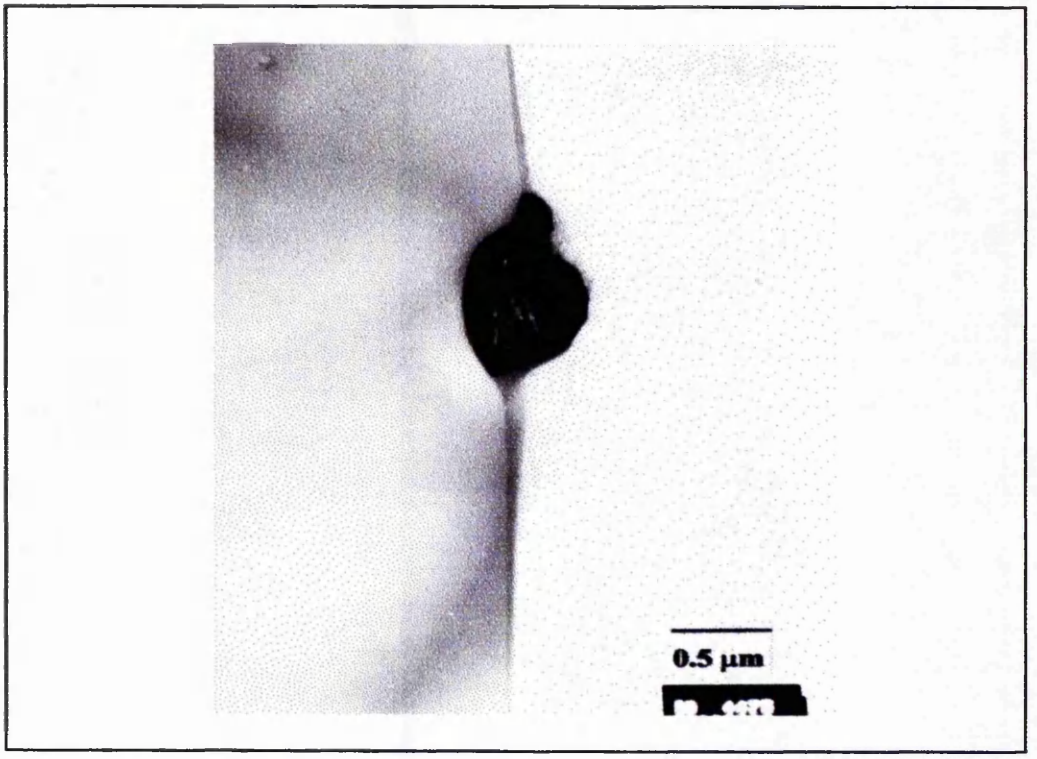

Figure 4.21. TEM photomicrograph of Mn-Zn ferrite with 0.4 wt% HfO_2,CaO and SiO_2

Results obtained from sample containing *TiO_2, SiO_2* and *CaO*, which had been prepared by the gel processing method, are presented in *table 4.13.* Chemical characterisation of the ferrite of composition 0.6 wt% *TiO_2, 0.02 wt% SiO_2* and *0.04 wt% CaO*, showed titania presence inside the grains, location A *figure 4.22,* alongside with the major constituents of Mn-Zn ferrites, but no traces of *CaO* and *SiO_2* were detected. Point analysis of the matrix next to the grain boundaries revealed a *CaO* and *SiO_2* presence alongside titania and the other Mn-Zn ferrite major components, location B *figure 4.22,*and, *table 4.13.* There is some deviation from the original chemical composition in the elements detected in the area next to the grain boundaries. The amount of *CaO* has increased by 50% while the amount of *SiO_2* has doubled compared with the original addition level of 0.02 wt% which confirmed that *CaO* and *SiO_2* tend to precipitated on or next to the grain boundaries[24]. However, the presence of *TiO_2* still unchanged, which suggested that titania was homogeneously distributed throughout the ferrite matrix.

Oxides wt%	*Grain Location A*	*Matrix Next to the Grain Boundaries Location B*
Fe_2O_3	*72.58 wt%*	*71.52 wt%*
MnO	*16.94 wt%*	*16.93 wt%*
ZnO	*10.79 wt%*	*10.77 wt%*
TiO_2	*0.69 wt%*	*0.68 wt%*
CaO	-	*0.06 wt%*
SiO_2	-	*0.04 wt%*

Table 4.13. Chemical micro-analysis of Mn-Zn ferrite with 0.6 wt% TiO_2, CaO and SiO_2

Chemical characterisations of grain boundaries and triple points in the Mn-Zn ferrite with TiO_2, *CaO* and SiO_2 addition is given in *table 4.14*, where is evident that a $SiO_2/CaO/TiO_2$ grain boundary layer has been formed in the grain boundaries and triple points. Surprisingly is to find high titania presence of 0.65 wt% at the grain boundary region. This observation defer to the finding by other workers who suggested that the titania mostly dissolves in the ferrite lattice[4,9,24]. The segregation of Ti^{4+} ions at the grain boundaries could be promoted by supersaturation of titanium ions in the ferrite bulk. Any excess ions tend to migrate toward the grain boundary regions during cooling stage, which confirm the suggestion that given in the previous section regarding the solubility limit of titania in the ferrite. Furthermore, analysis of triple point shows that there still around 1.1 wt% TiO_2 presence. However, the amount of calcia and silica additives was higher in the triple point than in the grain boundary layer. It is evident from the presented results that the amount of SiO_2 is much higher than the amount of *CaO* in both grain boundary and triple point regions. A possible explanation of higher presence of both additives in the triple point is because the melted CaO-SiO_2 phase always tend fills the multiple-grain junction during the generation of a liquid phase[5]. The free energy associated with the formation of a glassy second phase consists of three terms.

Oxides wt%	*Grain Boundaries Location C*	*Multiple-Grain Junction Location D*
Fe_2O_3	*69.43wt%*	*67.77 wt%*
MnO	*17.13 wt%*	*16.46 wt%*
ZnO	*11.04 wt%*	*9.19 wt%*
TiO_2	*0.65 wt%*	*1.09 wt%*
CaO	*0.29 wt%*	*1.82 wt%*
SiO_2	*1.46 wt%*	*3.67 wt%*

Table 4.14. Chemical micro-analysis of Mn-Zn ferrite with 0.6 wt% TiO_2, CaO and SiO_2

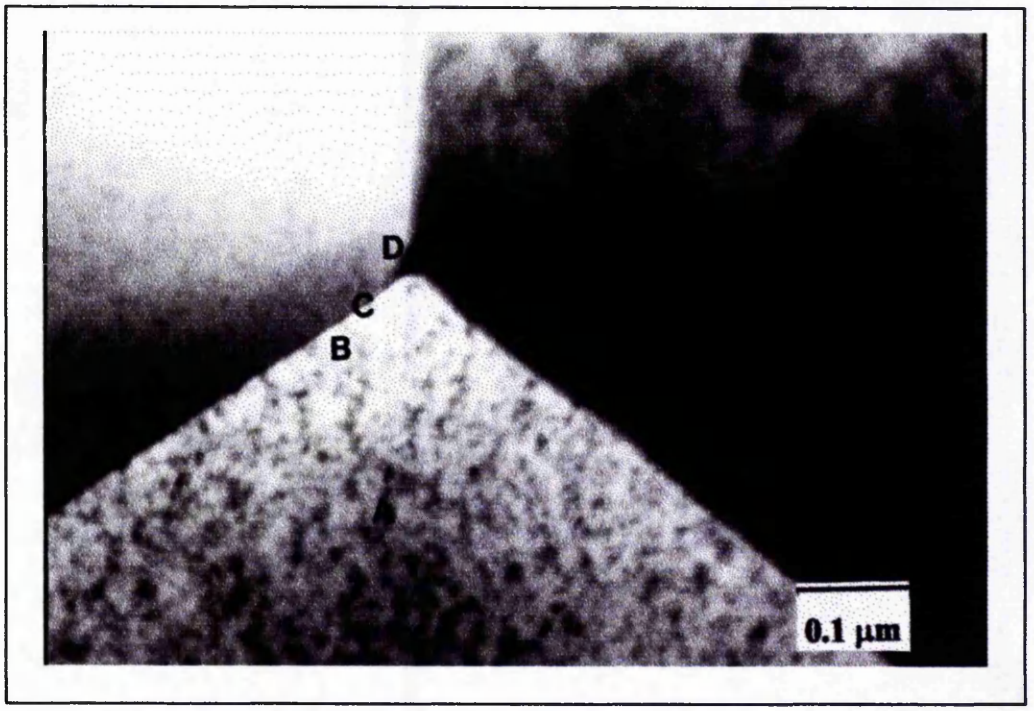

Figure 4.22. TEM photomicrograph of Mn-Zn ferrite with 0.6 wt% TiO_2, 0.04 wt% CaO and 0.02 wt% SiO_2

There is significant evidence in the literature to support the segregation of minor additions of additives at the grain boundaries and triple points of Mn-Zn ferrites[5,6,24,42]. *Franken*[24] reported the existence of a *Ca, Si* and *Ti*-containing layer, of 2 nm thickness, of the grain boundaries of a Mn-Zn ferrite. *Franken and Stacy*[45] reported the presence of amorphous phases at triple points of a Mn-Zn ferrite, but noted in addition, a crystalline phase described as a garnet $(Mn,Ca)_3Fe_2Si_3O_{12}$. They also discussed the presence of an enriched grain boundary layer, consistent with earlier finding by *Franken and van Doveren*[44] and found that the maximum thickness of the layer is about 2 nm.

Baumgartner et. al.[7] have found that in Mn-Zn ferrites with a higher level of CaO/SiO_2 addition there is an amorphous phase in the triple point which extends to the grain boundaries. *Otsuka et. al.*[6] reported that there are no traces of TiO_2 in the grain boundaries or triple point when they analysed Mn-Zn ferrite samples containing TiO_2, SiO_2 and CaO, which is contrary to the results, obtained in this study. That could be due to the low titania level, 0.1 wt%, added to their sample compared with 0.6 wt% TiO_2 in the sample analysed in this study. *Kingery*[112] hinted that some additives such as titania and zirconia can effectively reduce the interfacial energy by their strong chemical attraction to the calcia and/or silica and enhances wetting behaviour. *Otsuki*[151] related the segregation of CaO and SiO_2 in the grain boundaries to the sintering conditions of Mn-Zn ferrites. He reported that both additives, CaO and SiO_2, tend to segregate at grain boundaries as oxygen partial pressure at the sintering atmosphere increases.

Chapter 5

5. Results and Discussion II

5.1. Magnetic Properties of Mn-Zn Ferrites

5.1.1. Effect of Titania Additions on the Initial Permeability of Mn-Zn Ferrites

The room temperature initial permeability values obtained from Mn-Zn ferrite toroids produced under two different heat treatments are shown in *table 5.1.*

Composition	***Room Temperature Initial Permeability***	
	1300 ^{0}C for 2 hours cooled in nitrogen	***1330 ^{0}C for 3 hours cooled in nitrogen***
Base Mn-Zn ferrite	*735*	*1578*
3C21 Mn-Zn ferrite with 0.6 wt% TiO_2	*1150*	*1964*
3C22 Mn-Zn ferrite with 0.6 wt% TiO_2	*1423*	*2210*

Table 5.1. The effect of sintering time and temperature the initial permeability of Mn-Zn ferrites at 100 kHz

The room temperature initial permeability increases with the higher sintering temperature, *table 5.1*, because of the lower porosity and larger grain sizes achieved as further TiO_2 increased. Hence, it is clear that the microstructural and compositional properties obtained relative to the base composition by the substitution of TiO_2 gave a marked improvement in the initial permeability.

The permeability arises as a result of reversible displacements of the magnetic domain walls within the Mn-Zn ferrite. If the magnetocrystalline anisotropy is relatively high then the rotations of spins within the domains contribute a little to the permeability. The pores in the microstructure can act as barriers that prevent or obstruct the movements of domain walls and they may also give rise to a local demagnetising field[111]. Consequently, as there is a significant relationship between the density and higher sintering temperature and longer sintering time, the improvements in initial permeability that result that are related to both the decrease in porosity and the grain growth that occurs because of the higher temperature and longer sintering time. *Roess*[12] reported that if the ferrite preparation conditions are equal, the permeability generally increases with the increases of grain size. *Drofenik et. al*[152] have suggested that the initial permeability depends on the shortest distance between pores or grain boundaries that could potentially pin the domain walls and therefore reduce the permeability.

The effect the introduction of the nitrogen at 700 ^{0}C during the heating process during sintering on the initial permeability of Mn-Zn ferrites are shown in *figure 5.1.* and *table 5.2.* As *table 5.2* shows the initial permeability increases significantly with the introduction of nitrogen in the sintering atmosphere at 700 ^{0}C in heating. It is interesting to notice that the most improved composition was the base Mn-Zn ferrite composition by 11.8%, followed by the Mn-Zn ferrite with 0.6 wt% TiO_2 which improved by 11.2%. All these increases in permeability corresponded to the improvements in sintered density and microstructural homogeneity. For the other two samples, 0.2 and 0.4 wt% TiO_2, the initial permeability has also improved by 7.6% and 7.4% respectively.

The effect of controlled oxygen partial pressure on room temperature initial permeability have been examined by many authors[141,153,154,155]. *Rosales et al*[141] studied the effect of sintering atmosphere on the magnetic properties of Mn-Zn ferrites. Their results showed that samples sintered in nitrogen gave better results than those sintered in air, which agrees with the results obtained in this study as shown in *figure 5.1.* *Rikukawa*[153] reported that at higher sintering temperature the oxygen partial

pressure will, beside controlling the Fe^{2+} and cation vacancy concentrations and influence the achievement of high density and grain growth. *Ochiaki et al*[154] noticed that control of the sintering temperature and the oxygen partial pressure in the sintering atmosphere suppresses grain growth in the initial stages of sintering. Additionally, it was thought that the heating rate should be low to allow the grain growth in the subsequent firing to be uniform. *Sainamthip et al*[155] reported that at high temperature and low oxygen partial pressure the ferrite near the grain boundaries is reduced which results in a local high oxygen vacancy concentration that promotes diffusion across the grain boundaries. Conversely, at high oxygen partial pressure the Fe^{2+} cations near grain boundaries are oxidised forming Fe^{3+}. The decrease in Fe^{2+} concentration at the surface of the bulk increases the diffusion of Fe^{2+} from the bulk to the surface where they are oxidised forming Fe^{3+} and cation vacancies. At the surface of the grains the concentration of various cations and vacancies should attain their equilibrium values as dictated by the value of respective *Gibbs' free energy*. As a result a counter diffusion process "toward the grain interior" of Fe^{3+} and cation vacancies occurs to keep the number of lattice sites in the grain interiors constant. Consequently in an oxidised ferrite, the concentrations of oxygen vacancies are low and diffusion become very slow.

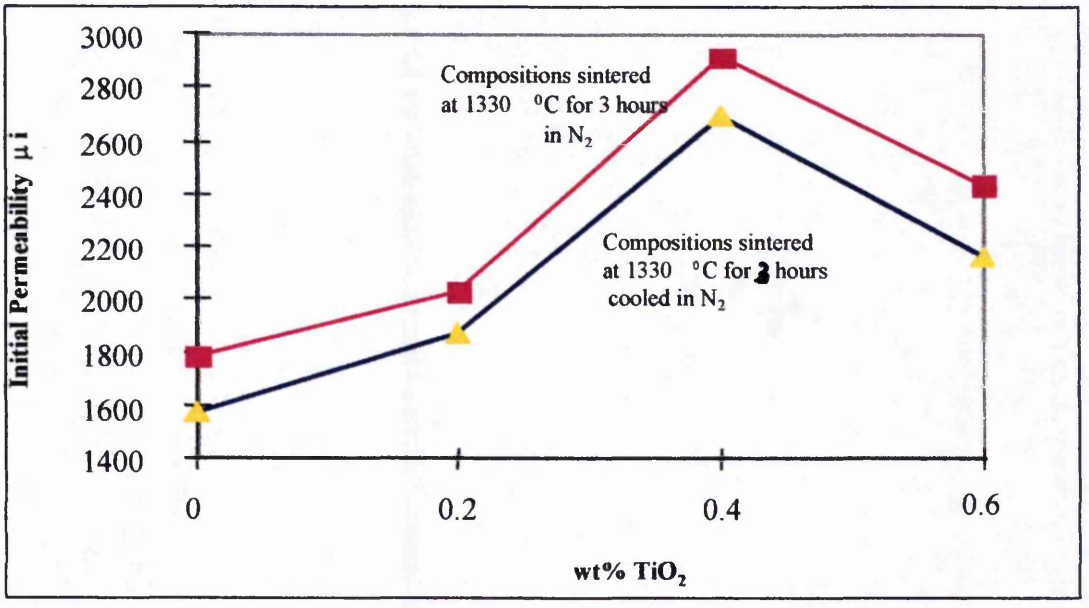

Figure 5.1. Effect of sintering conditions and TiO_2 additions on the initial permeability of Mn-Zn ferrites at 100 kHz

wt % TiO_2	*Room Temperature Initial Permeability*	
	1330 ^{0}C for 3 hours and cooled in nitrogen atmosphere	*1330 ^{0}C for 3 hours in nitrogen atmosphere from 700 ^{0}C in heating stages*
0	*1578*	*1788*
0.2	*1870*	*2024*
0.4	*2695*	*2917*
0.6	*2155*	*2427*

Table 5.2. The Initial permeability as a function of TiO_2 addition in Mn-Zn ferrites at 100 kHz

The effect of TiO_2 substitutions on the room temperature initial permeability are also shown in *table 5.2.* The required conditions for ferrites with better magnetic properties are high density and homogenous microstructure. Values of initial permeability are higher for the Ti^{4+} ion substituted compositions than for the base Mn-Zn composition because of the increases of density and microstructural homogeneity. The given results indicate that TiO_2 substitutions not only increase the density but also allow increase domain walls movements in the ferrites because of the significant increases of grain size. As discussed in *Chapter 4, section 4.3*, grain growth kinetics depend very strongly on the addition levels. A minor dopant, such as TiO_2, can effectively change the nature and concentration of defects in the matrix, affecting grain boundary mobility, pore transportability and pore elimination[25].

With the increases of TiO_2 substitutions the room temperature initial permeability increases significantly. The highest value of initial permeability for samples cooled in nitrogen was 2695 for the composition with 0.4 wt% TiO_2 when cooled in nitrogen atmosphere. However, the initial permeability notably improved by 10% with the introduction of nitrogen at 700 ^{0}C in the heating stage. This improvement has also been noticed for all other compositions. Distinctive differences are observed between the room temperature initial permeability values of the ferrite with Ti^{4+} substitutions compared to the base composition. Additions of 0.2 wt% TiO_2 gave initial permeability values of 2024 at 100 kHz and the initial permeability increased further with the increases of TiO_2. The 0.4 wt% TiO_2 substitution composition showed significant increases in the initial permeability to 2917 at 100 kHz. However, the 0.6 wt% TiO_2 substitution composition showed decreases of around 17% to compared with that of the 0.4 wt% TiO_2 substitution measured at 100 kHz.

The variations in initial permeability are thus a reflection of the effect of TiO_2 content on the Mn-Zn ferrite microstructure. The initial permeability improvements were due to the beneficial effect of titanium upon the grain growth, higher densification and Fe^{3+}-Fe^{2+} cation distribution. The grain boundaries have a decisive impact on initial permeability because they are discontinuities within the ferrite. They act as barriers to the domain walls movement and hence should be decreased, which means a large grain size is desirable to obtain high initial permeability. Since the high density and homogenous microstructures are also requirements for improved permeability, the compositions that have high density have also been shown to have high permeability values.

The effect of TiO_2 on magnetic properties have reported by many workers[4,7,8,9]. Many workers have indicated that the substitution of $2Fe^{3+}$ ions by Ti^{4+} + Fe^{2+} ions on the octahedral site in the spinel lattice yields strongly positive contribution to the magnetic anisotropy. The combination of the substitution of Fe^{3+} by Ti^{4+} + Fe^{2+} with that of Ti^{4+} + Mn^{2+} results in improvement in the magnetic properties of the base Mn-Zn ferrite composition of this study. The values of initial permeability are closely related to the values of saturation magnetisation and the magnetic anisotropy that are

usually dominated by the first order cubic constant. The magnetisation process depends on domain wall displacements and usually finds a qualitatively similar dependency on saturation magnetisation and the first order cubic constant. The saturation magnetisation can be controlled by Mn^{2+} substitution, while the effect of the first order cubic constant can be minimised by the substitution of suitable ions. Ti^{4+} ions are known to have large positive contributions to the first order cubic constant. As a result Ti^{4+} ions cancels the negative first order cubic constant due to substitutions of Fe^{3+} to Fe^{2+} ions on the octahedral sites in the spinel lattice. The magnetic properties of Mn-Zn ferrites are strongly associated with the Fe^{3+}-Fe^{2+} cation distributions among the octahedral and tetrahedral sublattice of the spinel structure. If the titanium is substituted into the base composition of Mn-Zn ferrites, the Ti^{4+} ions will be exclusively located on the octahedral site, and simultaneously an equal number of Fe^{3+} ions have to change into Fe^{2+} to preserve the electron-neutrality[9]. In contrast, *Shambalev et. al.*[11] suggested that the increase of initial permeability with the Ti^{4+} ion substitutions is simply due to anomalous grain growth as a result of secondary recrystallisation of the ferrite grains in the presence of Ti^{4+} ions.

The effect of CaO and/or SiO_2 additions to the Mn-Zn ferrites, in the presence of titanium oxide substitution, on the initial permeability obtained in samples sintered at 1330 ^{0}C for 3 hours in nitrogen from 700 ^{0}C in the heating stage, are shown in *table 5.3*.and *figure 5.2.* It is evident that the addition of CaO decreases the initial permeability of all compositions, but to various levels. Microstructurally, the most affected Mn-Zn ferrite was the base composition which had the smallest grain size, while the smallest reduction in the initial permeability was found for the 0.4 wt% TiO_2 ion substituted composition which had the most improved microstructure compared to the other compositions. The other two compositions were also influenced by the addition of CaO but to a lesser effect than the base composition. The obtained initial permeability results correspond fully with the microstructure analysed in *Chapter 4*. Compositions with homogeneous microstructures and higher density were shown to have much improved initial permeability.

wt% TiO_2	*Room temperature initial permeability*		
	0.04 wt% CaO	*0.02 wt% SiO_2*	*0.4 wt% CaO & 0.02 wt% SiO_2*
0	*946*	*1820*	*1024*
0.2	*1520*	*2144*	*1877*
0.4	*2746*	*3050*	*2797*
0.6	*1670*	*2566*	*2077*

Table 5.3. Room temperature initial permeability as a function of TiO_2, CaO and SiO_2 additions at 100 kHz

CaO typically is found to be segregated at the grain boundaries and its presence affects the grain growth. All the compositions with *CaO* additions were found to have small grain size and high levels of porosity, which gave, rise to the lower initial permeability values. In contrast, SiO_2, was found to increase the permeability of all compositions which corresponded to improvements of grain size and density.

According to *figure 5.2.* the best initial permeability results were obtained for Mn-Zn ferrite compositions with Ti^{4+} ion substitutions and SiO_2 addition, while again the least affected composition was the base composition with 0.02 wt% silica addition. The combined TiO_2 and SiO_2 effect on grain growth has been shown to yeild improved initial permeability values. *Akashi*[34] suggested that SiO_2 additions to the ferrites increases the initial permeability because they enhance grain growth. However, it has been reported elsewhere that SiO_2 additions may give ferrites with duplex structures which lower the magnetic properties[39,41].

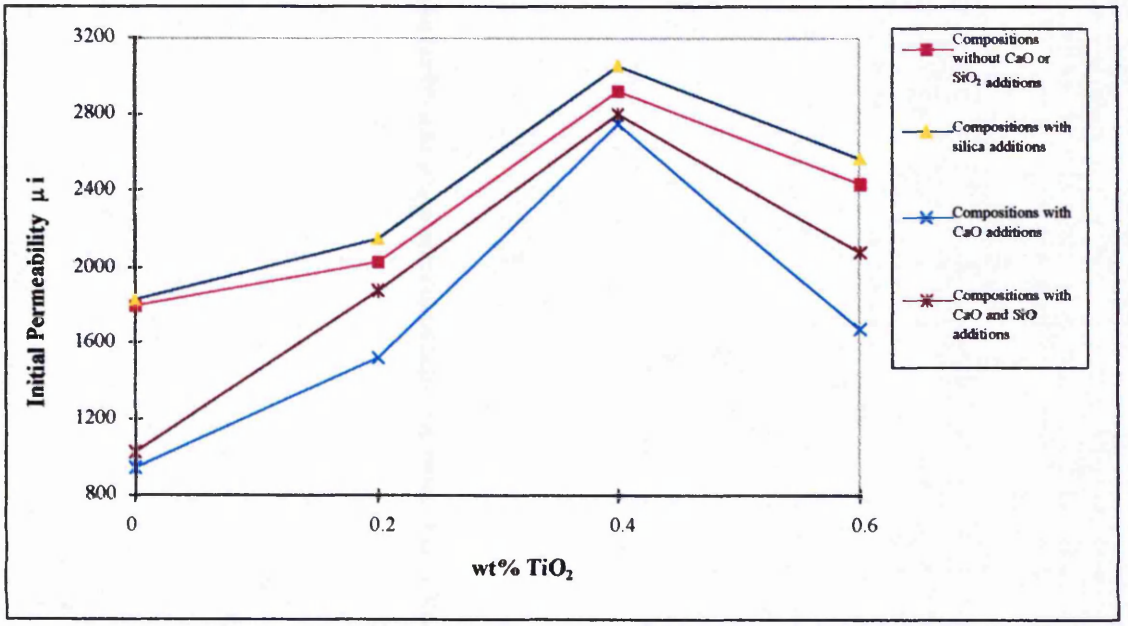

Figure 5.2. Effect of CaO and/or SiO_2 on the initial permeability of Mn-Zn ferrites at 100 kHz

In addition to the effect on grain growth and densification the addition of *CaO* and SiO_2 to the ferrites usually form a non-magnetic insulating glassy phase located primarily on the grain boundaries which eventually result in decrease of initial permeability values as shown in *table 5.3.* Such a secondary phase has been found in samples analysed by the transmission electron microscopy carried out in this study, *Chapter 4, section 4.4.*, where a rich SiO_2-*CaO* secondary phase was found on the grain boundaries and at triple points. All compositions showed that the combined additions of *CaO* and SiO_2 resulted in reduction of initial permeability compared with the same composition without impurity additions. *Mishra*[156] found that the glassy phase introduces residual stress in the ferrite, which could reduce the initial permeability. *Mochizuki*[5] also suggested that an increase of the second phase at the grain boundaries may lead to increases of internal stresses that are potentially detrimental to the magnetic properties. The results obtained here show undoubtedly that beside effects resulting from the Ti^{4+} ion substitutions, the initial permeability of Mn-Zn ferrites also depends on the microstructure and the presence of impurities in the ferrite.

5.1.2. Effect of Hafnia Additions on the Initial Permeability of Mn-Zn Ferrites

At the present time it is well known that in order to improve the magnetic properties of Mn-Zn ferrites, a small amount of additives may be used. Amongst these additives are two of the titanium group elements. TiO_2 is reported to be beneficial in achieving good initial permeability[8,9], while ZrO_2 appears to have an opposite effect[29]. However, no work has been published to date on the effect of HfO_2 on the initial permeability of Mn-Zn ferrites. Accordingly, this part of the study will focus primarily on the influence of Hf^{4+} ion substitutions on the initial permeability of Mn-Zn ferrites prepared by both citrate gel processing and conventional mixed oxide methods. In order further to examine the effect of the addition stage of impurities on initial permeability, compositions with hafnium were prepared by the conventional mixed oxides method where the additions were made before and after the calcination process.

Table 5.4. and *figure 5.3.* show the effect of hafnium ion substitutions on the initial permeability of Mn-Zn ferrites prepared by both methods utilised in this study. It can be seen that the additions of hafnium result in an increase in initial permeability, for samples prepared by gel processing , while a small or no improvement in initial permeability occurred in the samples prepared by both mixed oxides processing routes. These differences in initial permeability may be attributed to the more homogeneous microstructures obtained by gel processing having more homogeneous microstructures, while the samples prepared by the mixed oxides routes showed a much wider deviation in grain size distribution. Although, one of the requirements for high permeability is a large grain size[12], which was the main characteristic of the ferrites prepared by the mixed oxides methods, the samples prepared by the gel processing method showed higher initial permeability values, even though they have smaller grains. *Sale et. al.*[138] concluded that gel processing of Mn-Zn ferrite offers many improvements relative to mixed oxides processing, particularly in magnetic properties that are associated with the chemical homogeneity and more uniform fine-grained microstructures. Furthermore, reference should be made to the benefits of laboratory prepared samples relative to the commercially produced base composition because of their improved initial

permeability. A comparison of the initial permeability of the base composition of the Mn-Zn ferrite produced commercially with that of the same chemical composition, with and without HfO_2 additions produced by the gel and mixed oxide routes is made in *table 5.4* and shown on figure *5.3* as a point value (★).

Chemical Composition	***Initial Permeability(μ_I)***
Base composition prepared by Gel processing	*1788*
Commercially produced base composition by conventional mixed oxide processing	*900**
Base composition prepared by Mixed Oxides processing	*1338*
3C22 with 0.4 wt% HfO_2 composition prepared by Gel processing	*1802*
3C22 with 0.4 wt% HfO_2 composition prepared by Mixed Oxides processing, route 1	*1343*
3C22 with 0.4 wt% HfO_2 composition prepared by Mixed Oxides processing, route 2	*1323*

- At 10 kHz[138]

Table 5.4. Effect of HfO_2 additions on initial permeability of Mn-Zn ferrites at 100 kHz

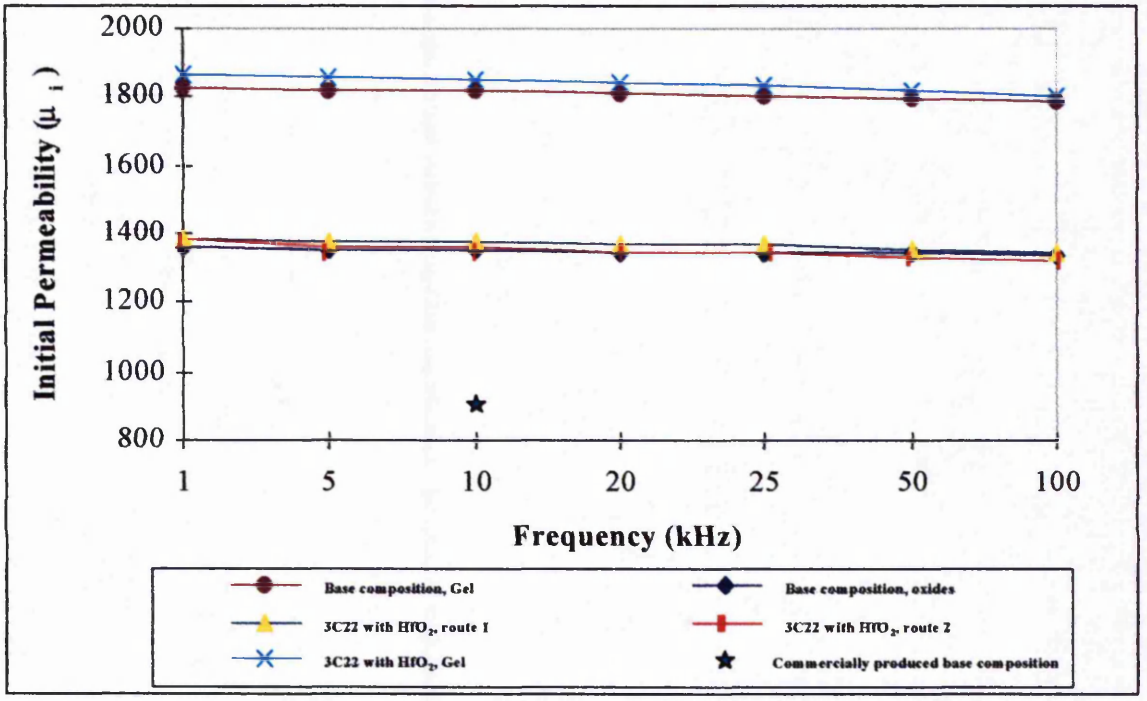

Figure 5.3. Initial permeability measurements of Mn-Zn ferrites in function of frequency

It is evident that whilst the mixed oxides, laboratory prepared, base samples have an initial permeability almost 50% higher compared to the base composition produced commercially, the initial permeability of the same composition prepared by gel processing increased by 100%. This notable improvement for samples prepared by mixed oxides processing relative to the commercial sample could be related to either, or both, the higher sintering temperature used and the controlled oxygen partial pressure, both of which may resulting in ferrites with higher density and more uniform microstructures. The fact that the composition with 0.4 wt% HfO_2, prepared by first route, where the additives were introduced after the calcination process, have much improved initial permeability relative to the same composition prepared by the second route where the additives were introduced before calcination, could be due to better impurity distribution which will be more evident in the cases of CaO and/or SiO_2 additions. As seen in *Chapter 4, section 4.5.* the grain size distributions of samples with additives introduced after calcination are better than those of samples with additives introduced before calcination. This could be a clear indication that the homogenous

distributions of impurities have an important effect on the initial permeability of Mn-Zn ferrites.

The effect of other additives, *CaO* and/or SiO_2, in combination with HfO_2 on the room temperature initial permeability is shown in *table5.5.* and *figure 5.4.* Once again the presence of SiO_2 and/or *CaO* are shown to have great influence on the initial permeability, but the extent of their effects are dependent on the preparation method and the introduction stage of impurities.

Values of initial permeability are higher for the all the Mn-Zn ferrites containing SiO_2 and 0.4 wt% HfO_2 regardless of their preparation method. Silica is well known to enhance the density as well as the grain growth. It can be seen from *figure 5.4.*that the initial permeability increased with silica additions. Requirements for high initial permeability are high density, chemical homogeneity, and most of all a single phase microstructure[53]. The increase of initial permeability corresponds to increases of grain size due to the additions of SiO_2 along with HfO_2, and with the relatively high proportions of intragranular porosity which have a secondary effect on the domain wall movements. A rich HfO_2-SiO_2 secondary phase was found using transmission electron microscopy on the grain boundaries in samples containing both additives, *Chapter 4., section 4.6.*, which confirms the hypotheses of the tendency of both additives to make a compound that enhances the grain growth in Mn-Zn ferrites. Once more, the samples prepared by gel processing show the highest initial permeability values, while samples prepared by the mixed oxides method with additives introduced after calcination have also higher permeability values than samples with additives introduced before calcination. This may be again attributed to the uniform distribution of additives on grain boundaries as well as to better grain size distribution.

The addition of *CaO* on its own to the Mn-Zn ferrites containing 0.4 wt% HfO_2, results in a significant decrease in initial permeability. The role of *CaO* is well known as a grain growth inhibitor and therefore may be expected to decrease the grain sizes of ferrites[35]. The data given in *Chapter 4, section 4.5.* confirm that this observation occurred in all samples where *CaO* was present. Microstructural analysis *figures 4.14.*

a, b and *c*, showed that samples contains HfO_2 and *CaO* have smaller grain sizes than the samples without *CaO* addition. The decreases in initial permeability in the presence of *CaO* have been attributed to the interaction between hafnia and *CaO* that results in a second phase at the grain boundaries[5] and smaller and non-uniform grains compared to the composition that contains Hf^{4+} ions only. Such a second phase hampers the domain wall movements, which results in decreases in initial permeability. The data given in *table 5.5.* and *figure 5.4.* shows that the samples containing *CaO* and HfO_2 analysed in this study have much lower initial permeability than samples containing HfO_2 alone. The most affected sample is the Mn-Zn ferrite prepared by the conventional mixed oxides, second route, which yields the lowest value of initial permeability. Meanwhile the same composition prepared by the same basic method, but with the additives being introduced after the calcination stage, have slightly better initial permeability values. Again, the samples prepared by gel processing have the highest initial permeability value. From the microstructural analysis and sintering density results it is obvious that the samples having uniform microstructures and higher sintered densities also have better initial permeability values. Consequently in summary, it is evident that the addition of a small amount of *CaO* on its own to Mn-Zn ferrites results in significant decreases of initial permeability, which is very much in agreement with the finding of other workers[21,22,23,42].

Observation of the effect of both SiO_2 and *CaO* additions combined with HfO_2 on the initial permeability, show that the initial permeability improves significantly in comparison with compositions containing *CaO* alone. However, the permeability values were reduced relative to the base material even though the samples containing both *CaO* and SiO_2 had larger grain sizes. The benefit of *CaO* and SiO_2 additions to the ferrite seems to be that the silica increases the sintered density while *CaO* prevents exaggerated grain growth[51]. Nevertheless, the combined effect is not beneficial for the initial permeability values obtained in this study. From *table 5.5.* it is evident that the effects of microstructure, the stage of introduction of the additives as well as the formation of a SiO_2-*CaO*-HfO_2 containing secondary phase on the grain boundaries all have a significant effect on the initial permeability values. As indicated earlier, the formation of secondary glassy phase on the grain boundaries has been recognised to

produce an insulating barriers which prevent the domain walls free movement and hence decrease the initial permeability of all studied compositions[3,18]. The transmission electron microscopy carried out in this study, *Chapter 4., section 4.6.*, revealed a rich secondary, HfO_2-SiO_2-CaO precipitation phase on the grain boundaries and the surrounding area. The most affected samples by the additions of both CaO and SiO_2 are once more, the mixed oxides prepared samples with additives introduced before calcination where the initial permeability has decreased by 25% relative to samples containing HfO_2 only. Whilst, samples prepared by the same method but with the additives introduced after calcination has shown a decrease of around 23% relative to the samples containing HfO_2 alone. The same composition prepared by gel processing showed a reduction in initial permeability values of only 12% relative to that of the sample containing HfO_2 also was prepared by the same method.

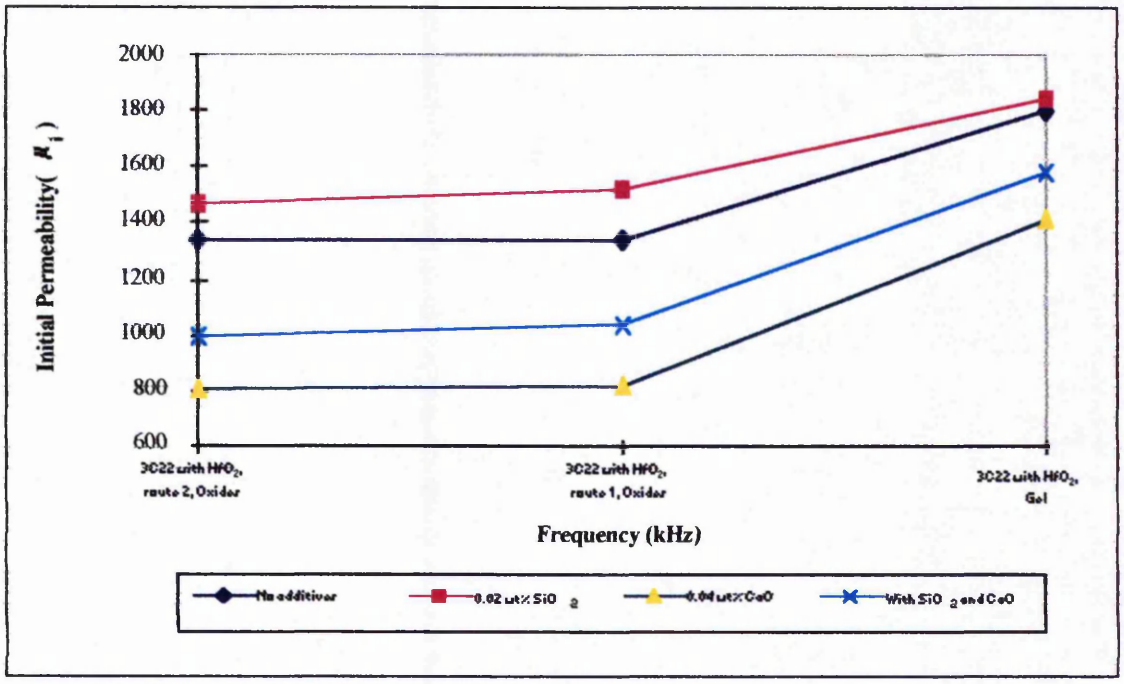

Figure 5.4. Comparison between initial permeability versus chemical compositions of a conventional mixed oxides and gel processing methods, at 100 kHz.

Chemical Composition	*Initial Permeability μ_I*		
	Mixed Oxides Method		*Citrate Gel Method*
	Additives Introduced After Calcination, Route 1	*Additives Introduced Before Calcination, Route 2*	
Mn-Zn with 0.4 wt% HfO_2	*1343*	*1323*	*1802*
Mn-Zn with 0.4 wt% HfO_2 and 0.02 wt% SiO_2	*1516*	*1470*	*1819*
Mn-Zn with 0.4 wt% HfO_2 and 0.04 wt% CaO	*815*	*806*	*1413*
Mn-Zn with 0.4 wt% HfO_2 and 0.02 wt% SiO_2 and 0.04 wt% CaO	*1039*	*992*	*1580*

Table 5.5. Initial permeability values of Mn-Zn ferrites with 0.4 wt% HfO_2, 0.04 wt% CaO and 0.02 wt% SiO_2, at 100 kHz.

From foregoing presented results it is very clear that the introduction stage of oxide additions, on their own or in combination, have a notable influence on the microstructure and hence upon the initial permeability. The addition of additives to the precalcined powders during ball milling results in a more effective distribution of these oxides which correspond to better initial permeability values and microstructural homogeneity. Furthermore, it has been shown that the utilisation of gel processing method for the production of the Mn-Zn ferrite powders has given more homogenous materials with improved physical and initial permeability values.

5.2. Power Loss Analysis of Mn-Zn Ferrite Samples

5.2.1. Power Loss Analysis of the Base Composition Samples

One of the important properties of ferrites is the power loss because it leads to a temperature rise in operating components and therefore, should be reduced as much as possible. As indicated in the literature review, the power loss of Mn-Zn ferrites consists of hysteresis loss, eddy current loss and residual loss, the latter two of which are more of a problem high frequency working environments. *Figure 5.5.* show a comparison of the power losses of the base composition samples which were prepared by sol-gel and mixed oxides processing methods as a function of frequency. It is evident that the power loss of the Mn-Zn ferrites is drastically reduced for the samples prepared by gel processing with, average grain size of 4 μm shown in *figure 4.8.b* compared with the equivalent mixed oxides composition, with an average grain size of 20 μm shown in *figure 4.8c.* The losses of the mixed oxides sample increased sharply as the frequency increased and reached a value of 1394 mW/cm^3 at 128 kHz, whereas the gel produced sample also increased as a function of frequency but to a lesser extent than the mixed oxides sample. The value of the total power loss of the gel produced sample at 128 kHz was 1010 mW/cm^3. These results showed that a reduction of 30% in the power loss can be achieved with the gel produced sample analysed in this study. A similar tendency in the improvement of electrical resistivity values for the gel produced sample was also observed. The sample prepared by gel processing showed resistivity values of 1.1 Ω.m, while the sample prepared by mixed oxides had only 0.35 Ω.m.

At low frequencies the predominant loss should be the hysteresis loss. The hysteresis loss is shown to be a mostly microstructurally dependent factor, i.e. governed by the amount of pores or inclusions, average grain size and sintered density, as well as the control that is obtained by the chemical composition. To minimise the hysteresis loss, the inner parts of the grains should be homogeneous and free of pores or other defects and the grain size should be as large as possible to reduce the domain pinning centres. It is well known that coericivity increases as the average grain size decreases[14], thus the hysteresis loss increase and expected to take major part at low frequencies and relatively high flux density (50 mT). Optical microscopy

observations of the base composition prepared by both gel processing and mixed oxides methods, *figures 4.8b* and *4.8c*, revealed that samples prepared by the mixed oxides route have larger grain sizes and non-homogeneous grain size distributions. Conversely, samples prepared by the gel processing method have smaller grain sizes with homogenous size distributions and a higher sintered density.

The average grain size has a major effect on the power loss at higher frequencies. High omic layers, the grain boundaries, which can effectively block the electric current, separate ferrite matrix. As the electric field passes through the ferrite, the grain boundaries will lie perpendicular and parallel to the direction of its path. The proportions of grain boundary concentration located on the path of electric field of ferrite with large grains are much lower than those of ferrite with smaller grains. In the case of small grained ferrite matrix, the grain boundaries can effectively block the electric current, thus increasing the ferrite resistivity

The eddy current loss is due to electrical resistance losses within the ferrite caused by the alternating electric field. Since the eddy current loss increase is proportional to frequency (*equation 2.18*), it is an important factor at high frequencies. It is well known that electrical resistivity is also microstructurally dependent and its increase is related to the reduction of grain size because grain boundaries are regions of high resistivity. Since the eddy current loss is proportional to the reciprocal of resistivity it can be decreased by increasing the resistivity[142]. It is notable from the results presented in *(figure 5.5)* that the losses at 128 kHz decreased to lesser degree than the resistivity increases i.e. for a resistivity increase of 3 folds, from 0.35 to 1.1 Ω.m, the power losses decreased by just 30%, from 1394 to 1010 mW/cm^3. *Figure 5.5* shows that the power loss of sample prepared by mixed oxides processing have increased sharply as the frequency increased. However, samples prepared by the gel processing method show a steady increase in power losses. Gel processing sample should have a uniform microstructure and chemical homogeneity. As indicated earlier in this study, microstructural observations of samples prepared by gel processing have a uniform microstructure with higher density compared to samples prepared by mixed oxides processing. *Chien*[30] reported that dilatometery results of ferrite samples

prepared by mixed oxide processing shrank sharply at high temperature compared to samples prepared by gel processing. The high rate of shrinkage could cause high internal stress, which could affect the final power loss of ferrite samples. In addition to the shrinkage effect, the loss of zinc during processing of powders prepared by mixed oxides route would also introduce additional internal stress as zinc could lower magnetostriction, and anistropy as has been reported by *Goldman*[57].

Mn-Zn ferrites have the disadvantage of a relatively low electrical resistivity that affects the eddy current losses as they are playing significant roles in overall power losses. As indicated above, the resistivity of polycrystalline Mn-Zn ferrite may be increased by grain boundary resistivity, i.e. by reducing grain size and thus increasing the number of grain boundaries in the bulk[157]. However, another way to increase the resistivity within the grains is to substitute Ti^{4+} ions in the spinel lattice of the Mn-Zn ferrites. These may form pairs with Fe^{2+} ions which are responsible for the resistivity reduction and thus reduce the electron hopping effect[9]

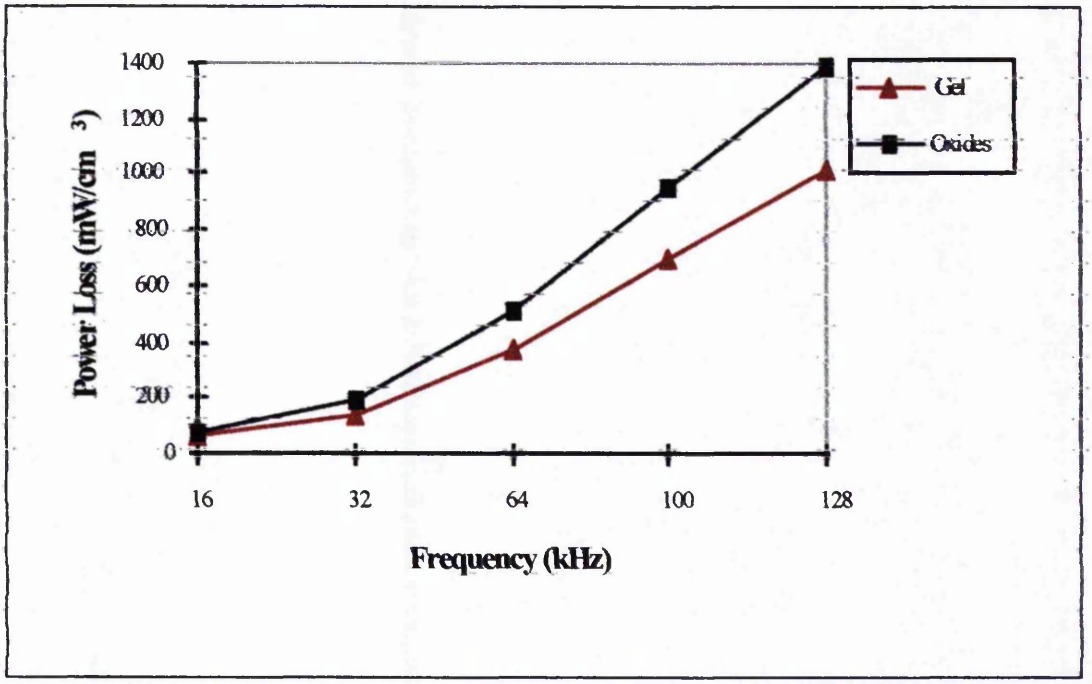

Figure 5.5. Power loss analysis of base composition prepared by gel processing and mixed oxides methods at 100 mT.

5.2.2. *Effect of Titania additions on the Power Losses of Mn-Zn Ferrites*

The relations between power loss and frequency for various amounts of Ti^{4+} ion substitution in the base Mn-Zn ferrite are shown in (*figure 5.6).* Evidently the presence of TiO_2 in the ferrites causes reduction in power losses at all substituted levels. The 0.2 wt%TiO_2 addition to the base composition leads to a notable reduction in power loss compared to the base composition prepared and processed in the same conditions. Increasing the titania additions to 0.4 wt% and 0.6 wt% give further power loss reduction with 0.6 wt% giving the lowest power loss values that have been measured in the study. Clearly Ti^{4+} ion substitutions into Mn-Zn ferrite samples are beneficial in the reduction of power losses of Mn-Zn ferrite.

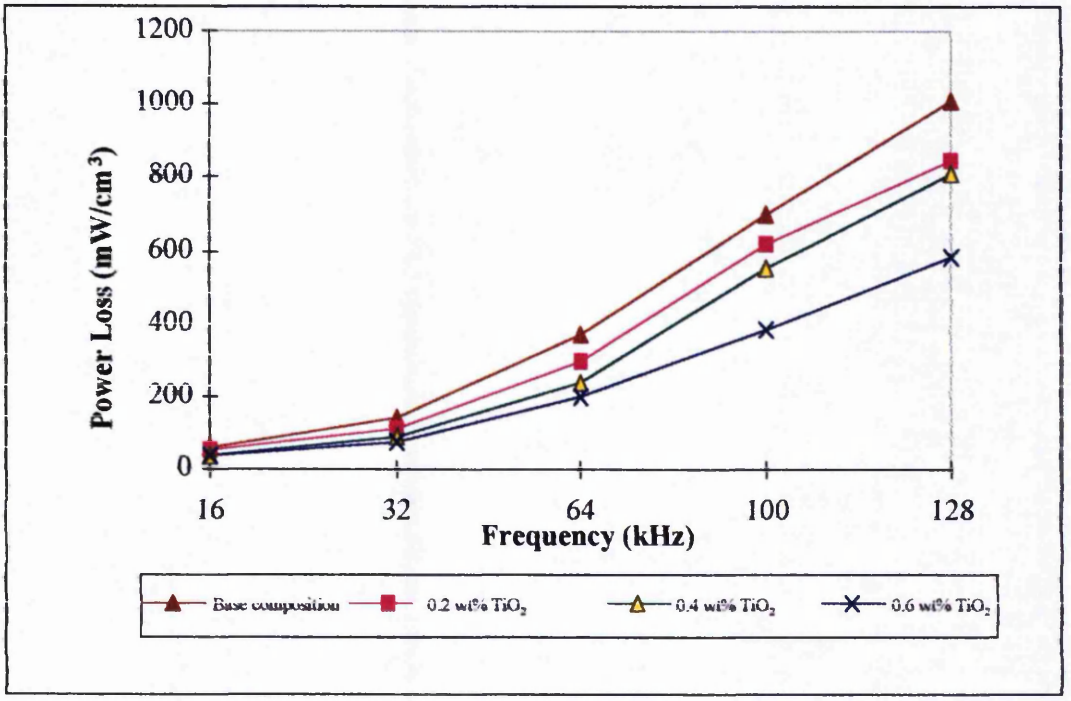

Figure 5.6. Power losses of titania added samples

wt% TiO_2	*Resistivity (Ωm)*
Mn-Zn ferrite with 0.2 wt% TiO_2	*2.4*
Mn-Zn ferrite with 0.4 wt% TiO_2	*3.1*
Mn-Zn ferrite with 0.6 wt% TiO_2	*5.8*

Table 5.7. Dc resistivity values of TiO_2 added Mn-Zn ferrite samples

To explain the effect of TiO_2 substitution the microstructural parameters, which influence the power loss of the Mn-Zn ferrites, should be addressed. Optical microscopy revealed that the average pore percentage reduced significantly as the titania was introduced into the Mn-Zn ferrite. Consequently, the final sintered density was increased with increases of TiO_2 additions, as shown in *chapter 4, sections 4.1.4.* and *4.3.* In addition, the grain sizes of the ferrites were increased with increase in TiO_2 addition. It is noticeable therefore that the core loss of 0.2 wt% TiO_2 sample is higher than those of samples with 0.4 and 0.6 wt% TiO_2 in spite of its small grain size microstructure. The 0.4 wt% TiO_2 sample was shown to have a higher power loss than sample containing 0.6 wt% TiO_2, however, the average grain size of 0.4 wt% TiO_2 sample was larger than that of 0.6 wt% TiO_2 sample. Also, the final sintered density of the 0.4 wt% TiO_2 sample was higher than that of the 0.6 wt% TiO_2 sample by 0.3%.

The electrical resistivity results are given in *table 5.7.* The additions of 0.2 wt% TiO_2 gave notable increases in electrical resistivity of more than 100% compared to the base composition. Further increases of TiO_2 to 0.4 wt% result in more improvements in the final resistivity of Mn-Zn ferrites. The extent of the resistivity improvement of the sample containing 0.6 wt% TiO_2 is evident that it is increased by a fraction of almost six times compared to the base composition sample. The improvement in the resistivity results is very likely to be related to the power losses of measured for the samples. The most significant reduction has been measured for the sample containing 0.6 wt% TiO_2 as the power losses are reduced by almost 56% compared to the base composition sample. While the power losses of samples containing 0.2 and 0.4 wt% TiO_2 been reduced by 15 and 20% respectively. Apart of sample containing 0.6 wt% TiO_2 which shows a steadily increase in power

losses, the other two samples, 0.2 and 0.4 wt% TiO_2, showed similar tendency in power losses behaviour as the base composition sample.

Mn-Zn ferrites have a low electrical resistivity caused by the hopping effect of Fe^{2+} to Fe^{3+}. The high valency of Ti^{4} ions would act as an electrostatic trap by pining the electrons at Fe^{2+} sites and therefore increasing the resistivity of grains[9], as the titanium mostly dissolves into the ferrite lattice. TEM analysis, *chapter 4. section 4.4.*, has confirmed that the titanium mostly dissolves in the ferrite lattice. The so called hopping effect can be explained as additives, especially Ti^{4+}, which usually occupy the octahedral '*B*' sites next to the Fe^{2+} ions preventing the electron movements from Fe^{3+} to Fe^{2+}. The Ti^{4+} ions at the octahedral sites form a complex with the Fe^{2+} ions in the spinel lattice resulting in Ti^{4+}-Fe^{2+} complex formation. These electrons will be located at the octahedral sites, which prevent the hopping effect, and as a result the Mn-Zn ferrite resistivity improves significantly. A similar mechanism may occurs when manganese ions been substituted into ferrites. *Van Uiert*[159] reported a small amount of manganese ions additions to the ferrites gives a substantial increase in the electrical resistivities. In the present study, the dc resistivities of samples containing addition of titania to substitute for manganese ions were measured. The resultant values are very much improved compared with base composition.

At high induction level in Mn-Zn ferrites, domain walls displacement mainly occurs. Obstructions to these displacements may give a rise to a hysteresis losses. As indicated earlier, one of the main factors, which govern the hysteresis loss, is the microstructure of the ferrite. The microstructural homogeneity, grain boundaries density and density mostly govern the hysteresis loss, thus samples with TiO_2 are expected to have low hysteresis losses. This result suggests those Mn-Zn ferrites with high density, homogenous microstructure and high resistivity can be affect by eddy current loss at higher frequencies to great extent.

The results obtained in this study are in agreement with the results of other authors. *Stijntjes et. al.*[9] shown that Ti^{4+} substitution is a good way for adjusting the magnetocrystalline anisotropy and increasing the resistivity of Mn-Zn ferrite.

Lebourgeois et. al.[51] reported that the Ti^{4+} substitutions into Mn-Zn ferrites results in low hysteresis and eddy current losses due to the increases of electrical resistivity as well as the microstructure homogeneity and the optimum grain size.

5.2.3. Effect of Hafnia Additions on the Power Losses of Mn-Zn Ferrites

HfO_2 addition reported to be remarkably effective in increasing the resistivity and therefore reduces the power loss as it segregates at the grain boundaries and triple points[5,6].The effect of 0.4 wt% HfO_2 additions on the magnetic properties of Mn-Zn ferrite prepared by both gel processing and mixed oxides have been analysed in this study. Power loss analysis of samples containing hafnia prepared by both gel and mixed oxides processing are shown in *figure 5.7.*

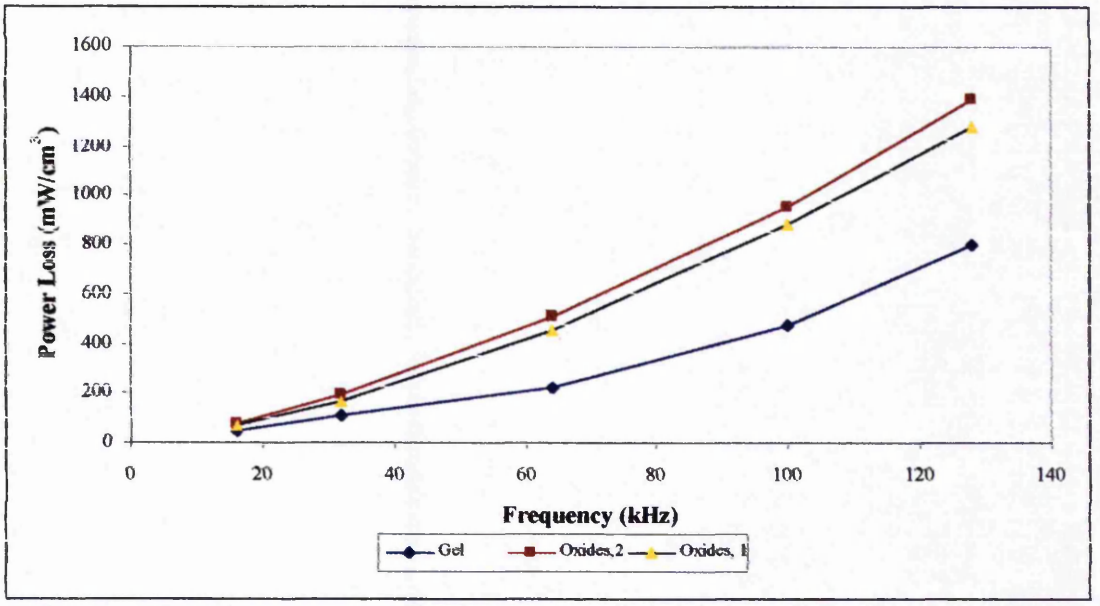

Figure 5.7. Power loss analysis of samples contains hafnia prepared by both gel and oxide processing tested at 128 kHz and 100 mT.

The introduction of HfO_2 to the ferrite is shown to give a significant benefit in power loss reduction, as well as resistivity improvements as given in *table 5.8.* The power loss of sample containing 0.4 wt% HfO_2 has been reduced by almost 21% compared to the base composition sample, even though there was grain growth as a result of the hafnia addition as discussed in *Chapter 4, section 4.3, figure 4.11a.* The dc resistivity of the sample containing 0.4 wt% HfO_2 prepared by the gel processing method has increased significantly by 200% compared with the base composition sample prepared by the same processing method.

The increase in grain size seen as a result of the hafnia addition may be expected to reduce the hysteresis loss, for the reasons mentioned elsewhere in this theses, namely that there will a reduction in domain wall pinning as the grain boundary area is reduced. However, the hafnia addition also clearly increases resistivity and as discussed elsewhere such resistivity increases will decrease the eddy current loss contribution.

It is evident that the hafnia is playing this dual role in the reduction of both components to the total power loss, as indicated in *figure 5.7.* The increase in resistivity would appear to be occurred by precipitation of grain boundaries, as confirmed by TEM analysis, *Chapter 4, section 4.4.1., figure 4.19*, where HfO_2 containing precipitates are shown to exist on the grain boundaries and at triple point in the sample. These observations indicate that little, or no, hafnia is dissolved within the spinel lattice during the production process.

In order to examine the effect of processing method on the power loss and resistivity two variants of the conventional mixed oxides ceramic processing routes had been used for sample preparation as indicated in *Chapter 3, figures 3.3* and *3.4.* In the first processing route hafnia were added to the precalcined powder during ball milling (this will be referred to as route 1), while in the second processing route hafnia was introduced from the start of the preparation stages (this will be referred to as route 2). The addition of HfO_2 by route 1 (additives introduced after calcination) has increased the resistivity by 40%, and the power loss decreased by 12%.

Meanwhile the sample prepared by the second route *figure 5.7.*, where additives were introduced from the start of processing, showed resistivity increases of 22% and a power loss reduction of 8%, compared to the base composition sample prepared by

Processing Method	***Ferrite composition***		***Resistivity (Ωm)***
Gel processing method	*Mn-Zn ferrite with 0.4 wt% HfO_2*		*2.23*
Mixed oxides processing method	*Route 1, additives introduced after calcination*	*Mn-Zn ferrite with 0.4 wt% HfO_2*	*0.49*
	Route 2, additives introduced before calcination	*Mn-Zn ferrite with 0.4 wt% HfO_2*	*0.43*

Table 5.8. Dc resistivity values of hafnia added Mn-Zn ferrite samples prepared by both gel and mixed oxides processing

the same method and analysed under the same conditions. Microstructure analysis shows that more uniform microstructure can be obtained by introducing HfO_2 into Mn-Zn ferrite after the calcination process than at the start of preparation process. This is an interesting observation because this type of addition gives less time at elevated temperature for the hafnia to potentially diffuse into the spinel. As indicated earlier, a uniform distribution of hafnia on the grain boundaries of Mn-Zn ferrites may be expected to be more beneficial for the reduction of power losses of the final product because such distribution can increase the resistivity by providing the ferrite

grains with electrically insulating grain boundaries. It seems, therefore, that route 1 is beneficial for this reason. With gel processing we may expect more dissolution of hafnia within the ferrite spinel (i.e. goes into spinel as the ferrite lattice is crystallised from the gel), however, TEM analysis shows that hafnia is mostly precipitated on the grain boundaries. This behaviour can be explained as gel decomposed hafnia would precipitate separately coating the ferrite grains where its uniformly distributed on the grain boundaries in a similar fashion to that of samples prepared by mixed oxide processing, route 1.

The production of such insulating layer at grain boundaries is well documented and so for this purpose, dopands such as CaO and SiO_2 may also be added in small quantities. These dopands diffuse toward grain boundaries during the cooling part of the sintering process to create the electrically insulating layer[45].

5.2.4. Effect of CaO and/or SiO_2 on the Power Losses of Mn-Zn Ferrites

5.2.4.1. Effect of CaO and/or SiO_2 Additions on the Base Composition Samples

As mentioned above, it is well known that the resistivity of ferrites can be increased by adding small quantities of CaO and SiO_2, and the power losses are consequently reduced[5,6,34]. Adding 0.04 wt% CaO and 0.02 wt% SiO_2 to Mn-Zn ferrites has been reported to increase the resistivity and therefore reduce the power loss significantly[6]. In order to elucidate this effect the same amount of impurities were utilised in this study and the impurities were added individually or together to the gel produced sample as a precursor series of experiments to ones in which both transition metal oxide additives and these impurity oxides were to be added to the ferrite.

Figure 5.8. shows the relationship between total power losses (P_L) and frequency at 100 mT of the base composition prepared by gel processing with CaO and/or SiO_2 additions. The results show that the addition of 0.04 wt% CaO improved the power loss slightly in comparison with undoped sample. Conversely, the sample doped with 0.02 wt% SiO_2 showed a significant increase in power loss. The best results

were obtained for the sample containing both *CaO* and SiO_2 additions where the combined additions gave a significant reduction in power losses compared to the undoped sample.

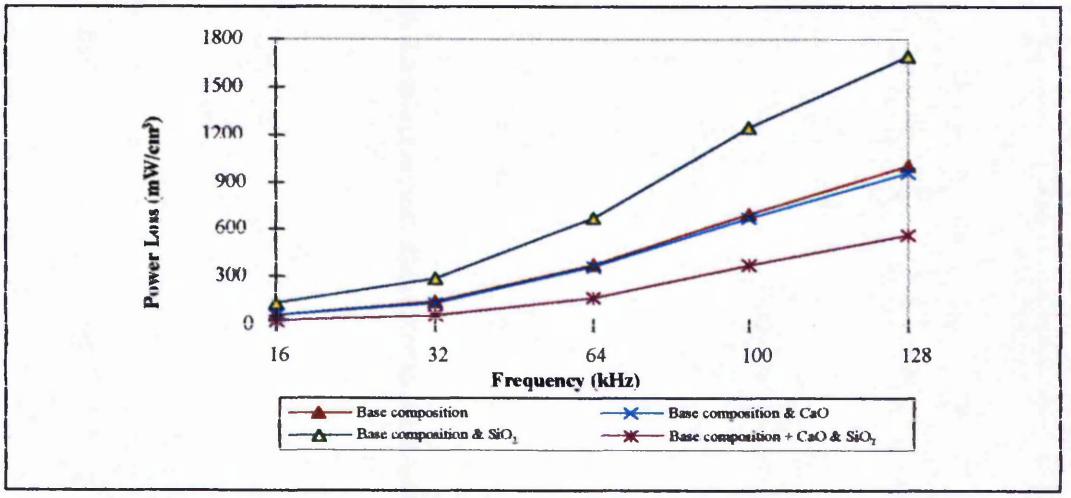

Figure 5.8. Frequency dependence of power loss of base composition samples with CaO and/or SiO_2 additions at 100 mT.

Again a correlation can be made between power losses and the resistivity of the analysed compositions. The dc electrical resistivity and power losses, measured at 128 kHz, 100 mT and at 25 ^{0}C, are given in *table 5.9*. Increasing the amount of grain boundary as a result of reducing the grain size increases the resistivity of the Mn-Zn ferrite. Samples containing *CaO* were shown to have smaller average grain size in comparison to the base composition sample and obtained a slightly lower total power loss with a significantly increased resistivity. Furthermore, the latter mentioned sample has slightly higher total porosity which can create a demagnetisation field which increases the magnetic flux density that affects the total power loss, by increasing the hysteresis loss. These additions, however, can cause an increase in hysteresis losses, since the nonmagnetic calcium rich layer insulates each grain and the grain boundaries, and act as pinning points for domain walls whilst reducing the eddy current loss[158]. Since the calcium-rich phase at the grain boundaries is nonmagnetic, the domains may be formed inside each grain the domain wall motion may be limited. As discussed in *Chapter 2*, in Mn-Zn ferrites the easy direction of magnetisation of each grain is randomly distributed but the anisotropy energy is small so that the direction of

magnetisation may be nearly lined up in order to relax magnetostatic energy. In the case when a magnetising force is applied then a number of domain walls nucleate, move and eliminate each other. This process could happen within a single grain or in a complex of grains. The hysteresis loss, if this case occurs, is always due to the combined effect of both irreversible domain wall motion and the extinction of walls during the application of magnetic flux.

Sample	***Resistivity, ρ (Ωm)***	***Total power loss, P_L (mW/cm^3)***
Base composition	*1.1*	*1010*
Base composition with 0.04 wt% CaO	*1.9*	*960*
Base composition with 0.02 wt% SiO_2	*0.9*	*1687*
Base composition with 0.04 wt% CaO and 0.02 wt% SiO_2	*2.2*	*559*

Table 5.9. Dc resistivity, total power losses of Mn-Zn ferrite prepared by gel processing at 128 kHz, 100 mT.

The microstructural analysis of *CaO* added sample showed that it to have a smaller average grain size of 3.5 μm and a lower sintered density than the other samples. This microstructural feature would increase the grain resistivity and as a result lower the eddy current, but at the same time increases the hysteresis loss. TEM observations confirm that the *CaO* is mostly precipitated at the grain boundaries, as discussed in *Chapter 4, section 4.4*, with the result that an increase in the inherent grain boundary resistivity occurs because of the formation of a nonmagnetic *CaO* rich secondary phase. These two factors combined to have an influence on the reduction of

eddy current loss at low frequencies, but at the same time are likely to increase the hysteresis loss.

The Mn-Zn ferrite sample containing only SiO_2 exhibits larger average grain size and higher sintered density compared to the other samples. Electrical and magnetic characterisation however, showed that this addition of silica results in higher power loss and lower resistivity. The addition of silica to ferrites is generally made to enhance their sintered density and give increase in grain size, thereby reducing the hysteresis part of total power losses. In this study it has been confirmed that a significant increase in average grain size occurred, which lowers the grain boundary density in the bulk. However, the total power loss shows increases with the silica addition compared to the base and calcia added composition samples. Thus could be due to the effect of eddy current loss, especially for the losses, which occurred at high frequencies. The obtained result contradict the findings by *Jain et.al.*[149] who reported that the addition of a small amount of silica would increase the grain boundary resistivity as the silica precipitated on the grain boundaries and formed a nonmagnetic glassy phase[149]. Clearly, in the work of *Jain et.al.*[149] a significant grain size increase, with its commensurate decrease in high electrical resistivity grain boundary area, could not have occurred as a result of the addition of the silica.

The lowest power loss values were obtained for the sample containing both CaO and SiO_2 which had an average grain size that was larger than both the base composition and the CaO-containing samples. It has been reported[5,6,34] that the simultaneous addition of CaO and SiO_2 to a ferrite results in a nonmagnetic glassy film located on the grain boundaries that increases the resistivity and therefore reduces the total power losses. High fractions of these nonmagnetic boundaries can substantially decrease the eddy current paths in the ferrite. From the overall results obtained for power losses they are mostly dependent on frequency, resistivity and average grain size. Samples containing both additions and the sample containing only CaO show the best overall power loss values. The total power loss of the SiO_2 doped sample is the highest of the other samples.

5.2.4.2. Effect of CaO and/or SiO_2 Additions on Titania Added Samples

In addition to *Ti*-substitution, and indicated in the previous section the additions of small amounts of *CaO* and/or SiO_2 are believed to enhance the resistivity of Mn-Zn ferrites and therefore reduce the total power losses.

The power losses increased for all samples containing silica, *table 5.10* and *figure 5.9*, furthermore, the resistivities all decreased significantly. The sample containing 0.6 wt% TiO_2 and 0.02 wt% SiO_2 showed the best power loss values compared to the other two samples containing 0.2 and 0.4 wt% TiO_2. The power loss value of the 0.6 wt% TiO_2 increased from 580 to 794 mW/cm^3, at 128 kHz and flux density of 100 mT, on making the SiO_2 addition to the sample. The electrical resistivity decreased by 26% compared with the same sample without the silica addition. The other two samples, 0.2 and 0.4 wt% TiO_2, were also affected by the silica additions, comparatively by the same extent. The sample containing 0.2 wt% TiO_2 and 0.02 wt% SiO_2 had a dc resistivity of 1.8 Ω.m compared with 2.4 Ω.m for the sample without the silica addition. The reduction in the resistivity as well as the increases in grain size affected the power loss values. The power loss increased from 850 to 1027 mW/cm^3. The dc resistivity of the 0.4 wt% TiO_2 sample reduced by almost 15% and the power losses increased to 936 mW/cm^3 compared to 811 mW/cm^3 at 128 kHz and 100 mT, on making the silica addition to the sample. This may be explained by the fact that the additions of silica alongside titania in Mn-Zn ferrite will enhances the grain growth and therefore results in large grains microstructure. Based on the above observations, the increases in power losses of ferrite samples are very much microstructurally related. Microstructural observations of samples containing both silica and titania (*figure 4.14 and table 4.8*) showed an increase in grain sizes compared to samples with containing titania only. Consequently, the electrical resistivity has decreased significantly due to the reductions of the concentration of grain boundaries in the ferrite matrix. Moreover, the presence of silica has done more degradation in the loss properties contrary to some reports in which has been stated that the addition of silica has improved the power loss of ferrite[149,160]. The addition of silica was reported to enhance the grain boundary resistivity as it is often found at grain boundaries where it contributes to the non-

magnetic grain boundary[160]. *Jain et.al.*[149] also reported that additions of 0.02 wt% SiO_2 decreases the total power losses in Mn-Zn ferrites. However, results obtained in this study of Mn-Zn ferrite samples containing SiO_2, *table 5.10* and *figure 5.9.*, showed that they have lower resistivity than samples without silica and therefore higher power losses have been obtained.

Much improved Mn-Zn ferrite resistivity has been obtained by the addition of a small amount of *CaO*. The combined additions of *CaO* and TiO_2 to the Mn-Zn ferrite were shown to cause a considerable improvement of the resistivity and the reduction of power loss samples analysed in this study. The electrical resistivity of the *Ti*-substituted and *CaO* added Mn-Zn ferrite samples are given in *table 5.10,* where is shown that the resistivity increases as the amount of titania addition increases. All samples are shown to improve their resistivities by at least 150% compared to samples with titania additions only. The Mn-Zn ferrite sample containing 0.2 wt% TiO_2 and 0.04 wt% *CaO* has improved its resistivity by 180%, while the resistivity of sample with 0.4 wt% TiO_2 has increased by almost 250% by the addition of *CaO*. Correspondingly, the resistivity of Mn-Zn ferrite sample containing 0.6 wt% TiO_2 and calcia has risen by 130%. Consequently, as *figure 5.9.*, shows the addition of *CaO* to *Ti*-substituted Mn-Zn ferrite samples results in significant reduction in power losses. From the results it seems that the combined effect of titania and calcia, by increasing the resistivity in the grains and grain boundaries has a positive contribution to the reducing of power loss in Mn-Zn ferrite. TEM analysis carried out in this study, *Chapter 4, section 4.4,* showed that calcia has precipitated at the triple point, grain boundaries and in the area next to the grain boundaries. *Tsunekawa et. al*[161] have reported that *CaO* phase was found close to, and within the grain boundaries as well as at the triple point of Mn-Zn ferrites. This may be explained by the fact that Ca^{+2} ions does not readily dissolve into the ferrite lattice due to its large ion size, 0.99 Å, therefore the calcium ions segregate to grain boundaries in order to ease strain energy and at equilibrium produce precipitates at the grain boundary region. These precipitates are non-magnetic and also tend to generate stresses, which affect the domain wall motion that increases the resistivity, and thus reduce the power loss. Additionally, the titanium ion substitution in the Mn-Zn ferrites

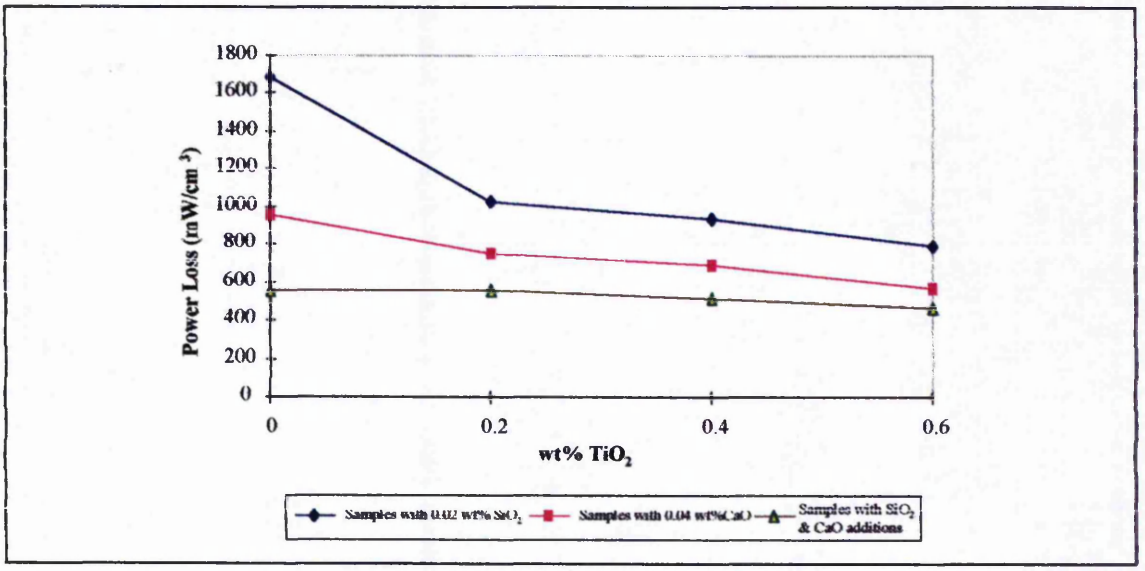

Figure 5.9. The effect of TiO_2, CaO and/or SiO_2 additions on Mn-Zn ferrite power loss at frequency 128 kHz and magnetic flux100 mT

wt% TiO_2 additions	*Resistivity (Ωm)*		
	0.04 wt% CaO additions	***0.02 wt% SiO_2 additions***	***0.04 wt% CaO & 0.02 wt% SiO_2 additions***
Mn-Zn ferrite with 0.2 wt% TiO_2	*4.3*	*1.8*	*6.7*
Mn-Zn ferrite with 0.4 wt% TiO_2	*7.7*	*2.7*	*10.6*
Mn-Zn ferrite with 0.6 wt% TiO_2	*8.2*	*3.9*	*13.8*

Table 5.10. Electrical resistivity values of Mn-Zn ferrite samples with TiO_2, CaO and/or SiO_2

prevents the Fe^{2+} hopping effect, and as a result increases the bulk resistivity. As a result of the double effects, the power loss has reduced substantially, as the resistivity increased. *Stijntjes et. al.*[9] reported that the presence of *CaO* in *Ti*-substituted Mn-Zn ferrite increased the resistivity and therefore decreased the power loss significantly. A much better effect in the reduction of power losses by simultaneous additions of small amount of SiO_2 and *CaO* to Mn-Zn ferrite containing TiO_2 has been reported by many authors[5,6,9,32.51].

It is well-known fact that *CaO* and SiO_2 will form a glassy non-magnetic phase mainly on the grain boundaries and triple point when they added to Mn-Zn ferrites[34]. The effect of glassy phase on the improvements of resistivity and the reduction of power losses of *Ti*-substituted Mn-Zn ferrite samples is evident as *figure 5.9.* and *table 5.10.* The results obtained in this study, *table 5.10*, and shows that the simultaneous addition of SiO_2 and *CaO* has a beneficial effect on the electrical resistivity of *Ti*-substituted Mn-Zn ferrite. The resistivities of 0.2 and 0.4 wt% TiO_2 samples with both *CaO* and SiO_2 have increased significantly by 2.6 and 3.4 times respectively, compared to Mn-Zn ferrite samples containing TiO_2 only. Likewise, the addition of both additives, *CaO* and SiO_2, has increased the electrical resistivity of the 0.6 wt% titania added sample by almost 250% compared to the sample containing titania only. TEM analysis of samples containing titania, silica and calcia detected the presence of a *Ca-Si-Ti* containing phase at the grain boundaries and triple point regions, *Chapter 4, section 4.4.* As shown in *figure 4.22.* and *table 4.13.*, there was no *CaO* or SiO_2 present inside the grains, however, the presence of 0.06 wt% *CaO* and 0.04 wt% SiO_2 were detectable by EDAX in the area next to grain boundaries. *Table 4.14.* shows that there was an increase in the presence of both additives, especially silica, at the grain boundaries and triple point been analysed. Rich *Si-Ca-Ti* containing phase been found in the triple points. The phases have a considerable effect in the increase of the resistivity as well as the reduction of power losses.

Power losses as a function of frequency of *Ti*-substituted Mn-Zn ferrite samples containing both *CaO* and SiO_2 are shown in *figure 5.10.* All samples show a considerable reduction in power losses compared to samples containing titania and *CaO* or SiO_2 alone. The power losses of 0.2 and 0.4 wt% TiO_2 with both *CaO* and SiO_2 addition samples been reduced by 35% and 37% respectively, compared to TiO_2 added samples. However, the reduction of 0.6 wt% TiO_2 and CaO/SiO_2 added sample shown a power loss reduction of 20%.

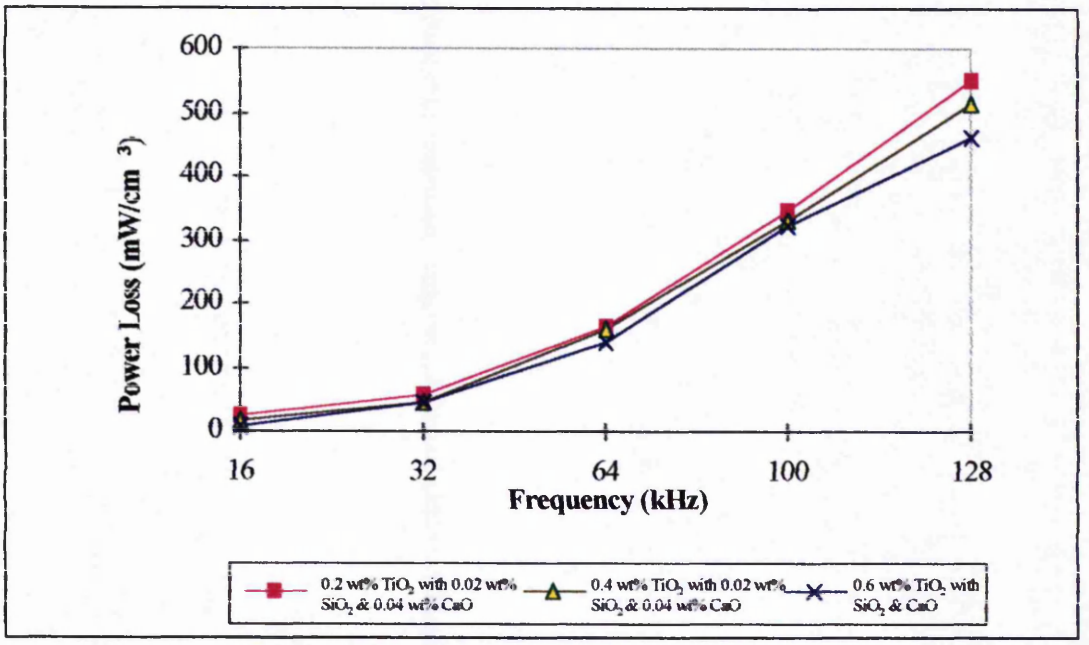

Figure 5.10. The effect of CaO and SiO_2 additions to TiO_2 containing samples on the power losses, at 25 ^{0}C and magnetic flux of 100 mT.

Otsuki[162] reported that the electromagnetic properties of Mn-Zn ferrites are strongly dependent on SiO_2/CaO additions amongst number of other factors, as they form a non-magnetic glassy phase on the grain boundaries that reduces the power losses by increasing the resistivity. *Lebourgeois et al*[51] have reported that the noticeable improvements of a lowering of the power losses by a factor of 20% were obtained by the additions of TiO_2, SiO_2 and *CaO* to Mn-Zn ferrites. Similarly, *Otsuka et. al.*[6] have reported that a remarkable improvement in the resistivity of Mn-Zn ferrite can be achieved by the additions of TiO_2, *CaO* and SiO_2 that results in extremely low power losses. All these reports substantiate the results obtained in the present study and

indicate that whilst the addition of transition metal oxides to a given ferrite may improve the magnetic properties, particularly the power losses, further improvements occur if impurities such as CaO and SiO_2 are present in small amounts such that added impurity-additive interaction may occur to produce desirable films and precipitates of grain boundaries.

5.2.4.3. Effect of CaO and/or SiO_2 Additions on Hafnia Added Samples

Table 5.11 shows the dc resistivity results obtained for Mn-Zn ferrite samples with HfO_2 and/or CaO and SiO_2 additions prepared by both mixed oxides and gel processing methods.

Processing Method	***Ferrite composition***		***Resistivity (Ωm)***
Gel processing method	*Mn-Zn ferrite with 0.4 wt% HfO_2 and 0.02 wt% SiO_2*		*1.51*
	Mn-Zn ferrite with 0.4 wt% HfO_2 and 0.04 wt% CaO		*3.34*
	Mn-Zn ferrite withHfO_2 SiO_2 and CaO		*5.97*
Mixed oxides processing method	*Route 1, additives introduced after calcination*	*Mn-Zn ferrite with 0.4 wt% HfO_2 and 0.02 wt% SiO_2*	*0.18*
		Mn-Zn ferrite with 0.4 wt% HfO_2 and 0.04 wt% CaO	*0.84*
		Mn-Zn ferrite withHfO_2, SiO_2 and CaO	*0.88*
	Route 2, additives introduced before calcination	*Mn-Zn ferrite with 0.4 wt% HfO_2 and 0.02 wt% SiO_2*	*0.15*
		Mn-Zn ferrite with 0.4 wt% HfO_2 and 0.04 wt% CaO	*0.77*
		Mn-Zn ferrite with HfO_2, SiO_2 and CaO	*0.79*

Table 5.11. Electrical resistivity values of Mn-Zn ferrite with HfO_2, CaO and SiO_2 prepared by both gel and mixed oxides methods

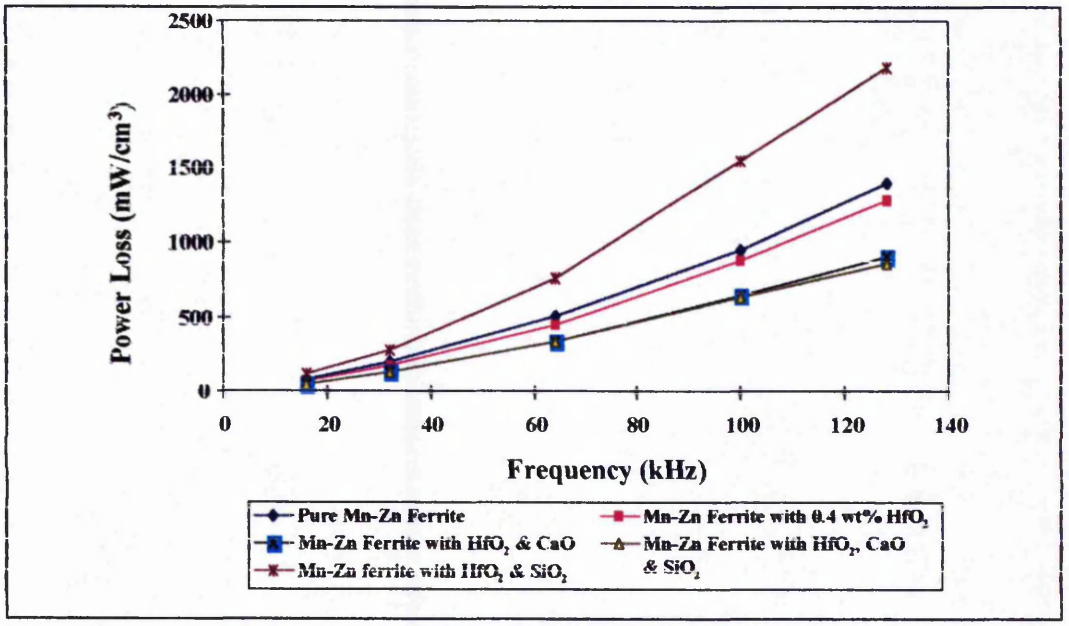

Figure 5.11. Power loss of Mn-Zn ferrite with HfO_2, CaO and SiO_2 prepared by mixed oxide method, Route 1, magnetic flux 100 mT

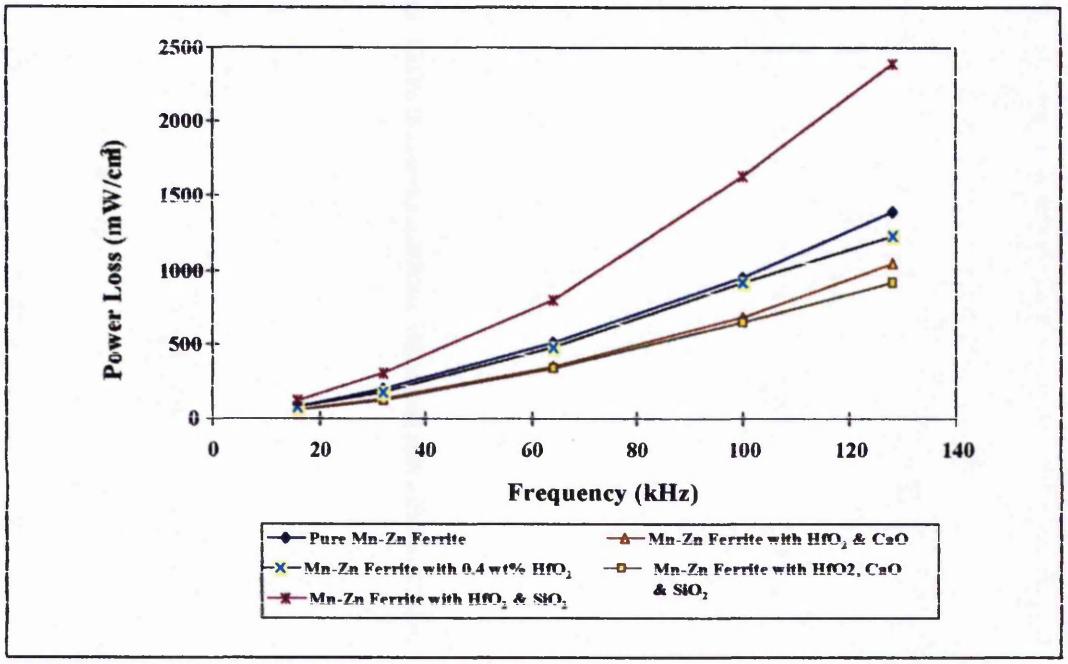

Figure 5.12. Power Loss of Mn-Zn ferrite with HfO2,CaO and/or SiO_2 prepared by oxides method, Route 2, magnetic flux 100 mT, temperature 25 ^{0}C.

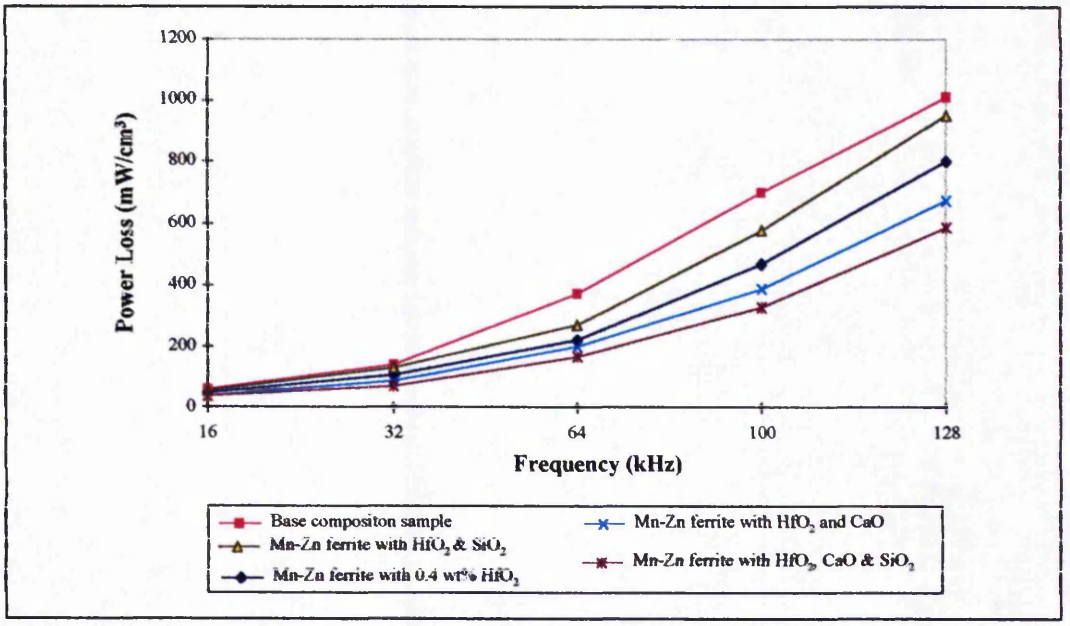

Figure 5.13. Power loss analysis of Mn-Zn ferrite with 0.4 wt% HfO_2, CaO and SiO_2 prepared by gel processing method at 100 mT, 25 ^{0}C.

The presence of a rich *HfO_2* second phase on the grain boundaries and triple points seems to have the same beneficial effect as calcia on both the resistivity and power losses. The combined addition of hafnia and 0.04 wt% *CaO* to the ferrite prepared by the mixed oxides processing method is shown to have a better effect on both power loss and resistivity than samples containing only *HfO_2* (*figures 5.11 and 5.12*). The resistivity of the gel prepared sample has increased significantly by almost 50%, while the power loss is decreased by 16% compared to sample doped with hafnia only by the addition of *CaO* (*figure 5.13*). However, this improvement in resistivity and power loss is more noticeable on comparing the *HfO_2-CaO* added sample with base composition sample. The dc resistivity has increased substantially by 3 times, while the power loss been reduced by 33%. Likewise, the resistivity values obtained from samples prepared by the mixed oxides method suggest it to have the same trend of that of samples prepared by the gel processing method. The addition of 0.04 wt% *CaO* have a very significant improvement on the resistivity values of sample prepared by both routes, thus the power loss has decreased accordingly. Once again, the dc resistivity of the sample prepared by first route (*HfO_2* and *CaO* introduced after calcination) has increased its resistivity by 2.5 times, while sample prepared by the second route (*HfO_2* and *CaO* introduced from the start) has improved its resistivity by 2.2 time compared

with the base composition. Consequently, power loss values have decreased by 27% and 18% respectively. These results again confirm a double effect that is related to the tendency of HfO_2 to make non-magnetic a *Hf-Ca-Si* containing second phase in the presence of CaO and SiO_2 on the grain boundaries that increases resistivity and thus reduces the power loss[6]. *Hendricks et. al.*[163] found that small amounts of CaO addition can significantly reduce eddy current losses by increasing the resistivity of grain boundaries. Microstructural observation of samples containing CaO along with HfO_2 show grain growth inhibition as a result of CaO addition. The reduction in grain size increases the resistivity and therefore decreases the overall power loss. *Taylor and Sale*[164] noticed that CaO addition up to 0.6 wt% inhibited grain growth. Microstructural observations carried out in this study has confirmed this finding to some extent, but it was found that the addition of 0.02 wt% silica with HfO_2 to Mn-Zn ferrite samples gives exaggerated grain growth effect as the two tends to make a *Hf-Si* containg phase on some grain boundaries which act as a liquid phase at those points and gives the exaggerated grain growth..

The effect of adding 0.02 wt% SiO_2 to a HfO_2 containing sample has been also analysed. In this case the resistivity decreased and power loss increased compared to samples containing HfO_2 only (*figures 5.11, 5.12 and 5.13*). The resistivity decreases and power loss increases are attributed to the significant grain growth which occurred. Nevertheless, if we compare the resistivity and power loss property of the SiO_2 containing sample with the base composition sample, it is obvious that, to some extend, beneficial improvements can be achieved by adding both additives to Mn-Zn ferrite. This improvement in the properties could be related to the formation of the *Hf-Si* containig second phase on the grain boundaries that been detected by TEM analysis, as discussed in *Chapter 4, section 4.4.* As indicated previously the formation of such a non-magnetic insulating layer on the grain boundaries increases the resistivity and as a result decreases the power loss[149]. However, the degradation in resistivity and power losses relative to the sample which contains CaO in addition to SiO_2 and HfO_2 is purely a microstructurally related factor as grain growth is observed on the addition of SiO_2 alongside HfO_2 to the Mn-Zn ferrite sample prepared by gel processing. Moreover, samples containing both SiO_2 and HfO_2, which were prepared by mixed oxides

processing method are the one shown to have exaggerated grain growth. For that reason the electrical resistivity reached the lowest values compared to those of other compositions. The power loss increased sharply and reached its highest values (*figures 5.11.* and *5.12*) indicating that the observed grain size is dominant parameter controlling resistivity and power loss and that intragranular porosity has a secondary effect. In this study it was found that the addition of silica to hafnia containing Mn-Zn ferrites samples was less beneficial than simultaneous additions of HfO_2, CaO and SiO_2 in an analogous manner to that observed for TiO_2.

Simultaneous 0.04 wt% CaO and 0.02 wt% SiO_2 additions along with 0.4 wt% HfO_2 proved to be of much benefit to Mn-Zn ferrite prepared by gel processing. *Table 5.11* and *figure 5.13.*, shows that the additions have made significant increases in dc resistivity and the reduction in power loss was noticeable. The resistivity has increased by almost 2.7 times compared to the 0.4 wt% HfO_2 sample. As a result, the power loss has decreased by 26% accordingly. In the case of samples prepared by mixed oxides the grain sizes reduced significantly by the addition of both impurities and become more uniform relative to that observed when both HfO_2 and SiO_2 were present. The implication of this is that the CaO, which segregates to the grain boundaries, prevents the exaggerated grain growth caused by the HfO_2 and SiO_2 by reacting to form a solid grain boundary phase. The power loss values of samples prepared by both oxide routes were very similar to those obtained when both HfO_2 and CaO present. The addition of SiO_2 and CaO has a positive effect on the resistivity as result of the uniform microstructure and the interaction at the grain boundaries. This improvement has been attributed to the formation of a rich non-magnetic *Hf-Ca-Si*-containing secondary phase on the grain boundaries and triple points of Mn-Zn ferrite[5,6]. TEM analysis in this project confirms this finding but the amount of silica present in the secondary phase is much higher than the amount of calcia, even though the amount of calcia added was twice as much as the silica addition. The proposition given by *Otsuki et. al.*[6] in which they claimed that HfO_2 tends to form a *Hf-Ca* containing secondary phase has been confirm to some extend, but TEM results obtained in this study showed indisputably that HfO_2 mostly tend to interact with SiO_2 to form a secondary phase on the grain boundaries. Although, the changes are moderate relative to the results obtained by

Otsuki et. al.[6], it must be noted that the volume of HfO_2 was 0.4 wt% in this study, while they used approximately 0.2 wt% addition. It is possible that power loss may be remarkably lowered if the HfO_2 dosage is further reduced. It should be noted that the additions of CaO and SiO_2 to the sample containing 0.4 wt% HfO_2 prepared by gel processing showed lower power losses that those of the sample containing only CaO. This could be related to the better chemical and microstructural homogeneity achieved utilising gel processing to produce the Mn-Zn ferrite powders. *Akashi*[34] concluded that the simultaneous addition of CaO and SiO_2 to Mn-Zn ferrite is effective in reducing the power loss. *Sano et. al.*[120] emphasised that in addition to the microstructural homogeneity, the grain should be coated with high resistivity $CaSi$ oxide glassy film. This film should be as thin as possible, since both CaO and SiO_2 tend to precipitate at grain boundary.

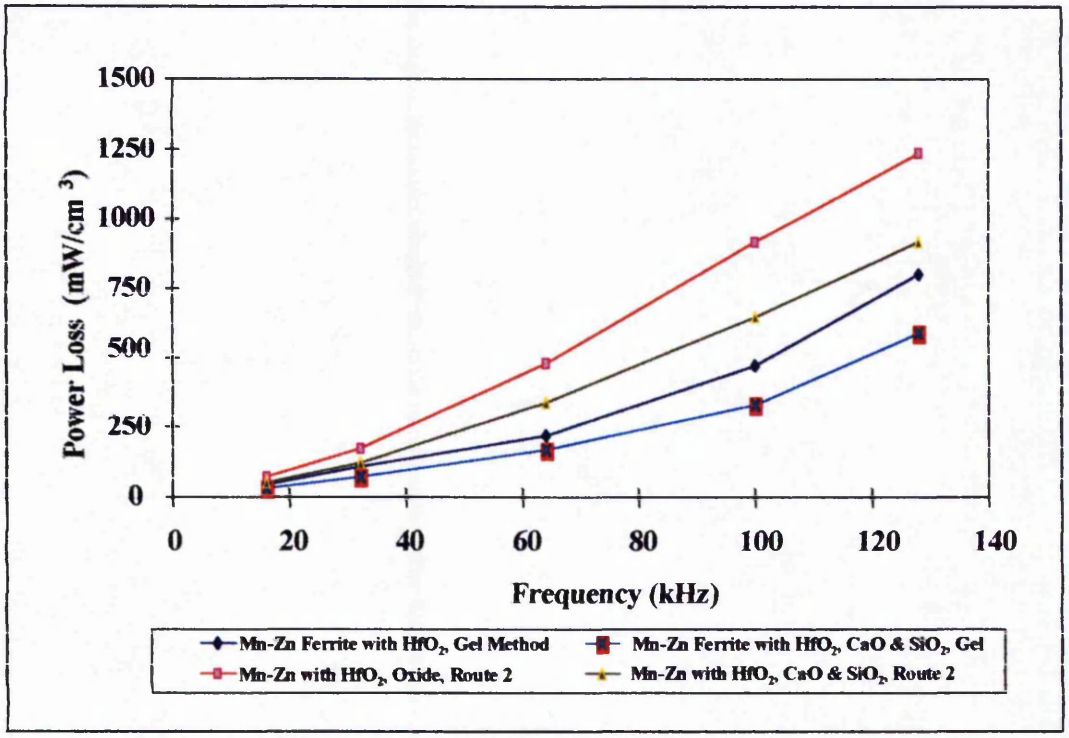

Figure 5.14. Power losses of Mn-Zn ferrite prepared by gel and oxides processing methods, magnetic flux 100 (mT)

A comparison between the power loss and resistivity values obtained using the two processing methods indicates gel processing to give better properties than mixed oxide processing, *figure 5.14*, due to the better chemical and microstructural homogeneity obtained. It was also found that the optimum stage for oxide additions was after calcination as a more uniform and better-controlled microstructure was obtained. The addition of additives to the precalcined powders during ball milling, results in a more effective distribution of additives at grain boundaries.

Chapter 6

6. Conclusions

1. Improvements in sintered density depend on sintering time and atmosphere. With controlled titanium substitutions, Mn-Zn ferrite with densities higher than 99% theoretical can be made by the gel processing method, while densities higher than 97% are achievable with controlled hafnium substitutions.

2. The introduction of a small amount of SiO_2 to the Mn-Zn ferrites enhances their sintered density, while the presence of CaO in the ferrites decreases their densities.

3. A higher sintered density is achieved for all compositions prepared by gel processing relative to the same compositions prepared by the conventional mixed oxides method.

4. The citrate gel processing always gives smaller and more homogeneous microstructures than the conventional mixed oxides method.

5. The substitution of Ti^{4+} and Hf^{4+} ions into Mn-Zn ferrites enhances the grain growth and further addition of SiO_2 promotes the grain growth further by a liquid phase mechanism, while the addition of CaO inhibits the growth due to its tendency to precipitate at the grain boundaries.

6. For samples prepared by the mixed oxide method the introduction of additives before the calcination process was shown to give larger and non-uniform grain sizes compared with those prepared by the same method but with the additives being introduced after the calcination stages. The most pronounced effect was on samples with both hafnia and silica additions

7. TEM analysis showed that TiO_2 mostly dissolves in the ferrite lattice, conversely, HfO_2 precipitates exclusively at the grain boundaries and triple points. Additionally, simultaneous CaO and SiO_2 additions with TiO_2 or HfO_2 to Mn-Zn ferrites results in secondary phases at the grain boundaries and triple points in the microstructures.

8. Ti^{4+}ion substitutions into Mn-Zn ferrites result in significant initial permeability increases, likewise HfO_2 added by gel processing gives improvements in initial permeability compared with the base composition sample. Conversely, no improvements in initial permeability occurred for Ti^{4+} substitution in samples prepared by the mixed oxide method.

9. The addition of SiO_2 increases the initial permeability of Mn-Zn ferrites, while CaO additions notably decrease the initial permeability of Mn-Zn ferrites. Moreover, combined additions of CaO and SiO_2 also decrease the permeability relative to the base Mn-Zn ferrite sample.

10. Additions of titania and hafnia into the base composition samples of Mn-Zn ferrite have been shown to give higher resistivity, with commensurate lower power losses relative to those of the base composition. The presence of CaO along with both titania and hafnia in Mn-Zn ferrites gives significant decreases in power loss and increases resistivity. Conversely, the addition of SiO_2 to samples containing titania or hafnia gives a large increase in power losses as the resistivity decreases to its lowest values.

11. In the cases where both impurities, CaO and SiO_2, were present, the power losses were further reduced as the electrical resistivity increased compared with other samples.

Chapter 7

7. Suggestions for future work

1. Additions of titania up to 0.6 wt% have been shown to have a positive effect on the magnetic, electrical and physical properties of Mn-Zn ferrite samples prepared by gel processing method. In order to complete the investigation of the true effect of titania on the ferrite, samples with titania need to be prepared by the mixed oxides processing method. It also has been shown in this study that the addition stage of the impurities have effectively influenced the final properties of the ferrite, therefore it will beneficial to study these effects during titania additions.

2. Lower addition levels than 0.4 wt% of hafnia should be utilised in both gel and mixed oxides processing methods to find out whether improvements in properties are maintained, or increased, of lower levels .

3. During this study the effect of titania and hafnia on the magnetic, electrical and physical properties of Mn-Zn ferrites have been studied. However, for certain applications it could be advantageous to investigate the effect of the additions of the two oxides on the mechanical properties.

4. The use of different levels of calcia and silica additions with both titania and hafnia in both processing methods could give a wider range of operating process parameters.

5. In order to complete the examinations of the effect of IV group on the properties of Mn-Zn ferrite samples, different levels of zirconia, calcia and/or silica should be examined.

6. Al_2O_3, Nb_2O_5 and Ta_2O_5 have been reported to have significantly improved the properties of Mn-Zn ferrites[5]. Hence, their additions to ferrites in the presence of controlled impurity levels, should be examined.

7. The introduction of combined CoO-TiO_2, HfO_2-CoO and ZrO_2-CoO in combination with calcia and silica into Mn-Zn ferrite samples prepared by both gel and mixed oxides processing methods should be also examined.

References

1. *Hadfield D., Materials & Design, Vol. X, No 5, Sep/Oct 1989, pp 222-230.*

2. *Richardson D., Modern Ceramic Engineering, Marcel Dekker, Inc, New York, 1992.*

3. *Ohiai T., In Journal De Physique IV, Eds. Cagan V. and Guyot M., ICF7, Bordeaux, 1997, pp 27-30.*

4. *Ghata B., In: Palmour H., Davies R. and Hare T. (Eds) Processing of crystalline ceramics (Materials Science Research; 11), Plenum Press, New York, 1979, pp 369-379.*

5. *Mochizuki T., In Ferrites: Proceedings of ICF6, Tokyo Japan, 1992, pp 53-58.*

6. *Otsuka T. et. al., The Japan Society of Powder and Powder Metallurgy, 1992, pp 317-320.*

7. *Baumgartner H. et. al., In Journal De Physique IV, Eds. Cagan V. and Guyot M., ICF7, Bordeaux, 1997, pp67-68.*

8. *Neamtu J. et. al., Journal of Magnetism and Magnetic Materials, 133, 1994, pp 481-483.*

9. *Stijntjes T. et. al., Philips Research Report, 25, 1970, pp 95-107.*

10. *Riches E., Ferrites, A Review of Materials and Applications, Mills & Boon Ltd., London, 1972.*

11. *Shambalev V. et. al., Journal of Magnetism and Magnetic Materials, 88, 1990.*

12. *Roess E., Phy Stat. Sol. (a), 2, 1970, K 185.*

13. *Neamtu J. et. al., In Journal De Physique IV, Eds. Cagan V. and Guyot M., ICF7, Bordeaux, 1997, pp 79-80.*

14. *Valenzuela R., Magnetic Ceramics, Cambridge University Press, 1994.*

15. *Hill R. J. et. al., Systematics of the spinel structure type, Physical Chemistry of Minerals, 4, 1979, pp 317-339.*

16. *Smit J. and Wijn H. P. J., Les Ferrites, Philips Technical Library, Paris, 1961.*

17. *Cullity B. D., Introduction to Magnetic Materials, Addison-Wesley, Massachusetts, 1972.*

18. *Michalowsky L., Baumgartner H. and Ernst W., Ceramics International, Vol. 19, 1993, pp 77-85.*

19. *Paulus M., In: Kringel W. W. and Palmour III H., (Eds.) Materials Science Research, Vol. 3, The role of grain boundaries and surfaces in ceramics, New York, 1966, pp 31-47.*

20. *Gorter E. W., Philips Research Reports, 9, 1954, pp 295-320.*

21. *Okutani et. al. ICF5,Bombay. India, 1989.*

22. *Dreikorn J. et. al., SMM 13, Grenoble, France, Sep. 1997.*

23. *Guilland C., Proc. IEEE, No. 5, 1957, p 165.*

24. *Franken P., IEEE Trans. of. Mag, 14, No. 5, 1978, pp 898-899.*

25. *Yan M. F. and Johnson D. W. Jr., J. Amer. Ceram. Soc., 60, No 7-8, 1978, pp 342-349.*

26. *Kono H., ICF1, Tokyo, Japan, 1970, pp 137-138.*

27. *Stijenjes, Broes, Knowls and Rankin, ICF1, Tokyo, Japan, 1970.*

28. *Fan J. and Sale F., In Journal De Physique IV, Eds. Cagan V. and Guyot M., ICF7, Bordeaux, 1997, pp 81-82.*

29. *Neijts R. C., Improvement of magnetic and mechanical properties in Fe deficient and Fe excess Mn-Zn ferrite, Internal Philips Report, 1988.*

30. *Chien Y-T, PhD Thesis, University of Manchester, 1993.*

31. *Nivoix V., Gillot B., Aymes D., Perriat P. and Guyot M., In Journal De Physique IV, Eds. Cagan V. and Guyot M., ICF7, Bordeaux, 1997, pp 237-238.*

32. *König U., Substitutions in manganese zinc ferrites, Appl. Phys., 4, 1974, pp 237-242.*

33. *Pashchenko V. P., Andreev A. V., Prokopenko V. K., Daroviskih E. G., Cheremenkov O. P. and Loyko A. D., ICF7, Bordeaux, France, 1996, Abstracts, 4-1 p 60.*

34. *Akashi T., Trans. Jap. Inst. Met., 2, 1961, p 171.*

35. *Pualus M. and Guillaud C., Colloque International du C. N. R. S. / Soc. Chim. Memoires, 5, 1965, pp 1175-1185.*

36. *Giles A. D. and Westendrop F. F., The effect of silica on the microstructure* ***of*** *Mn-Zn ferrites, ICF2, 1976, pp 50-51.*

37. *Toolenaar TJ. C. M., J. Mat. Sci., 23, 1988, p 3144.*

38. *Liu C. S., Wu J. M., Tsay M. J. and Chen C. J., IEEE Tran. Magn, 32, No 5, 1996, pp 4860-4862.*

39. *Nomuria T. and Mori T.,MRS Int'l. Mtg. on Adv. Mats., Vol 11, 1989 Materials Research Society, pp 233-245.*

40. *Kimura O., ICF 5, India, 1989, p 169.*

41. *Zenger M., Bogs M., Lucke R. and Schulz G., American Ceramic Society Bulletin, Vol. 74, No. 3, 1995, pp 77-81.*

42. *Bando Y., Ikeda Y., Akashi T. and Takada T., in Hauster H. H. (ed.), Modern Developments in Powder Metallurgy, Vol. 4, Plenum Press, New York, 1971, p 339.*

43. *Hamelin A. and Paulus M., ICF1, Japan, 1970*

44. *Franken P. E. C. and van Doveren H., Ber. Dt. Keram. Ges., 55, 1978, p 287.*

45. *Franken P. E. C. and Stacy W. T., J. Amer. Ceram. Soc., 63, 1980, p 315.*

46. *Ishino K. and Narumiya Y., Ceramic Bulletin, 66, 1987, pp 1469-1474.*

47. *Carpy F. M. A. and Stuijts A. L., in Popper P. (ed.), Science of Ceramics, Vol. 8, The British Ceramic Society, Stoke-on-Trent, 1976, p.23.*

48. *Roelofsma J. J. and Kools F. M., Proceeding of the 1st ECERS, Maastricht, Holland, 1989.*

49. *Yamada S. and Otsuki E., J. Appl. Phys., Vol. 81, No. 8, 1997, pp 4791-4793.*

50. *Tung et. al. , In Journal De Physique IV, Eds. Cagan V. and Guyot M., ICF7, Bordeaux, 1997, pp 71-72.*

51. *Lebourgeois R. et. al., Proc. Electroceramics IV, Vol. II, Aachen 1994, pp 1137-1142.*

52. *Žnidaršič A., Ferriti I. and Drofenik M., In Journal De Physique IV, Eds. Cagan V. and Guyot M., ICF7, Bordeaux, 1997, pp 115-116.*

53. *Slick P., In "Ferromagnetic materials", Ed. Wohlfarth H., Vol. 2, North Holland Pub. Co. 1980, p 191.*

54. *Kaczmarek W., Journal of Materials Science, 31, 1996, pp 5271-5279.*

55. *Roess E., IEEE Trans. Mag., MAG-18, 1982, p 1529.*

56. *Snelling E, Soft ferrites, 1988*

57. *Goldman A, Modern ferrite technology, Van Nostrand Reihold, New York, 1990.*

58. *Street B., Powder Metallurgy, Vol. 25, No. 3, 1982, pp 173-176.*

59. *Kimura O. and Chiba A., ICF4, Part 1, 1985, p 115.*

60. *Chien Y. T. and Ko Y. C., Journal of Materials Science, 26, 1991, p 5859.*

61. *Swallow D. and Jordan A. K., Proc. Brit. Cer. Soc., 2, 1964, p 1.*

62. *Delmon B. et. al., 2nd International Conference edited by Kuh. W. E. and Elvietsman J. (The Electrochemical Soc. New Jersey), 1974, pp 242-255.*

63. *Courty Ph. et. al., Powder Technology, 7, 1973, pp 21-38.*

64. *Mahloolojchi F and Sale F., Ceramic International, 15, 1989, p51.*

65. *Baythoun M. S. G. and Sale F. R., Journal of Materials Science, 17, 1982, pp 2757-2769.*

66. *Roberts V., Freer R. and Sale F., Proc. Brit. Ceram. Soc., 42, 1990, p 45.*

67. *Rozman M., Drofenik M. and Kolar D., in Duran P and Fernandez J. F., (ed.), Third Euro-Ceramics, Vol. 1, 1993, pp 341-346*

68. *Saimanthip P. and Amarakoon V. R. W., Annual meeting of the American Ceramics Society, Pittsburgh, Penn., 1987.*

69. *Kurukawa S., Hitachi Review, Vol. 17, Part 4, 1968, pp 122-128.*

70. *Alam I. Nair R., Ramamurti V., Effect of raw materials and process conditions on the properties of Mn-Zn ferrites, IEEE Trans. Mag., MAG-18, No.4, 1982.*

71. *Toolenaar M., Formation of Zinc ferrite, Journal of Materials Science, Vol. 24 1989, pp 1089-1094.*

72. *Nakamure T. and Okano Y., In Journal De Physique IV, Eds. Cagan V. and Guyot M., ICF7, Bordeaux, 1997, pp 91-92*

73. *Chol G. R., Damay F., Auradon J. P., and Strivens M. A., Electrical Communications, 43, 1968, p 263.*

74. *Auradon J. P., Damay F. and Chol G. R., IEEE Trans. Mag., 5, 1969, p 276.*

75. *Zaspalis V. and Mauczuk R. Boerekamp and Kolenbrander, In Journal De Physique IV, Eds. Cagan V. and Guyot M., ICF7, Bordeaux, 1997, pp 75-76*

76. *Shibuye Y, Inoue T. and Sakaguchi H., ibid, Abstracts, 5-1, p 15*

77. *Lin I. and Nadiv S., Mat. Sci. Eng., 39, 1979, p 93.*

78. *Kosmac T. and Courtny T., Journal of Mater. Res., 6, 1992, p1519.*

79. *Kaczmarek W. and Ninham B., IEEE Trans. Magn., MAG-30, 1994, p 732.*

80. *Krysicki Z. and Lubanska T., Effect of presintering process on the microstructure and initial permeability of Mn-Zn ferrite, Journal of Mag. and Magn Mat., Vol.19, 1980, pp 107-108.*

81. *Stijntjes T. G. W., Roelofsma J. J., Boostra L. H. and Dawson W. M., ICF6, Tokyo, Japan, 1992, pp 45-92.*

82. *Živič A., and Lakner V., 20th International Conference of Microelectronics, 1992, pp 425-428.*

83. *Brook R. J., Concise Encyclopaedia of Advanced Ceramic Materials. Ed. Brook R. J., Pergamon Press, Oxford, 1991.*

84. *Kuczynski G. C., ICF1, Tokyo, Japan, 1970, pp 87-95.*

85. *Wagner C., Z. Phys. Chem., (B) 34, 309, 1936; In Diffusion and High Temperature Oxidation of Metals, Atom Movements A. S. M Monograph (Cleveland 1951), p 153.*

86. *Reijnen P. J. L., In Concise Encyclopaedia of Advance Ceramic Materials, Ed. Brook R. J., Oxford, 1991, pp 445-454.*

87. *Broussaud M., Abouaf M., Perriat P. and Rolland J. L., Oxidation state/green strength relationship in Mn-Zn ferrites. ICF5, New Delhi, India, 1989, pp 75-81.*

88. *Perriat P., Gillot B. and Aymes D., In Journal De Physique IV, Eds. Cagan V. and Guyot M., ICF7, Bordeaux, 1997, pp 43-46*

89. *Kim M. G., and Yoo H. I., ICF5, New Delhi, India, 1989, pp 109-113.*

90. *Blank J. M., J. Appl. Phys., Vol. 32, No.3, 1961, pp 378S-379S.*

91. *Slick P. I., ICF1, Tokyo, Japan, 1971, pp 81-83.*

92. *Morineau R. and Paulus M., IEEE Transactions on Magnetics, Vol. Mag-11, No. 5,1975, pp 1312-1314.*

93. *Morita A. and Okamoto A., ICF3, Japan, 1980, pp 313-316.*

94. *Inaba H, J. Amer. Ceram. Soc., 78, (11), 1995, pp 2907-2912.*

95. *Reijnen P. J. L., In Sci. Ceramics, Edited by Stewart G. H., Vol. 4, 1968, pp 169-188.*

96. *Brook R. J., Journal of American Ceramic Society, Vol. 52, No. 1, 1969, pp 56-57.*

97. *Carpy F. M. A., Ceramic Microstructures, 76, Fulrath R. M., and Pash A. Editors, Colorado, 1977, pp 261-275.*

98. *Žnidaršič A. and Drofenik M., Journal of American Ceramic Society, Vol. 32, No. 3, 1996, pp 1941-1945.*

99. *Han Y. H., Suh J. J., Shin M. S. and Han S. K., In Journal De Physique IV, Eds. Cagan V. and Guyot M., ICF7, Bordeaux, 1997, pp 111-112*

100. *Dawson W.M., In Journal De Physique IV, Eds. Cagan V. and Guyot M., ICF7, Bordeaux, 1997, pp 61-62*

101. *Beer A. and Schwartz T., IEEE Trans. Mag, 2, 1966, p 470.*

102. *Drofnik M., Besenicar S. and Limpel M., Advances in Ceramics, 16, 1985, p 229.*

103. *Chen S. H. et. al., IEEE Transactions on Magnetics, Vol. 32, No. 5, 1996, pp 4857-4861.*

104. *Okazaki Y, Kitano Y. and Narutani T., ICF6, Japan, 1992, pp 313-316.*

105. *Tasaki J. and Ito T., ICF1, Japan, 1970, pp 84-86.*

106. *Tsay M. J., Tung M. J., Chen C. J. and Liu T. Y., In Journal De Physique IV, Eds. Cagan V. and Guyot M., ICF7, Bordeaux, 1997, pp 71-72*

107. *Ochia T. and Okutani K., Proceeding of the 4th International Conference on Ferrites, 1984, p 447.*

108. *Nomura T., Okutani K. and Ochiai T., Fine Ceramics, Editor Saito S., Tokoyo, 1987, p 254.*

109. *Okamoto S., Nomura T. and OchiaiT., Elekutoronikuseramikusu, 16, 73, 1985, p 41.*

110. *Roess E., Electronic Component Bul., No. 1, 1966, p. 138.*

111. *Perduijn R. and Peloschek A., Proceeding of British Ceramic Society, 10, 1968, pp 263-273.*

112. *Kingery W. D., Bowen H. K., and Ulmann D. R., Introduction to Ceramics, 2nd Ed., John Wiley & Sons Inc., New York, 1975.*

113. *Chiang Y-M., Birnie III. D. and Kingery W. D., Physical Ceramics, Principles for Ceramic Science and Engineering, 1st Ed., John Wiley & Sons, Inc., New York, 1997.*

114. *Van der Zaag P. J., Johnson M. T., Ruigrok J. J. M., Bordel C. and de Wit H. J., J. Mag. and Mag. Mat., 129, 1994, pp 1137-1140.*

115. *Fan J. and Sale F.R., IEEE Transactions on magnetics, Vol. 32, No. 5, 1996, pp 4854-4856.*

116. *Bogs M. and Holubarsch W, In Journal De Physique IV, Eds. Cagan V. and Guyot M., ICF7, Bordeaux, 1997, pp 117-118*

117. *Snelling E. C. and Giles A. D., Ferrites for inductors and transformers, Philips Research Laboratories, Redhill, Surry England, 1983, p 54.*

118. *Visser E. G., in Steel B. C. H. (Ed), Electronic Ceramics, Elsevier, England, 1991, p 148.*

119. *Visser E. G., Roelofsma J. J. and Aaftink G. J. M., ICF 5, India, 1989, p 605.*

120. *Sano T., Morita A. and Matsukawa A., 5th ICF, New Delhi, 1989, pp 595-603.*

121. *Ohta K., J. Phys. Soc., Japan, 18, 1963, p 685.*

122. *Stoppels D., J. Appl. Phys., 51, 1980, p 2789.*

123. *Berger M. H., Laval J. Y., Kools F. and Roelofsma J. J., ICF 5, India, 1989, p 619.*

124. *Roshen W., IEEE Trans. On Magn., Magn 27, No. 6, 1991, p 4407.*

125. *Otsuki E., Yamada S., Otsuka T., Shoji K. and Sate T., J. Appl. Phys., 69, 1991, p 5942.*

126. *Inaba H., Abe T., Kitano Y. and Shimomura J., J. Mag. Magn. Mater, 133, 1994, p 487.*

127. *Inoue O., Matsutani N. and Kugimiya K, ICF 6, Tokyo, Japan, 1992, p 1155.*

128. *Stijntjes T. G. W., ICF 5, India, 1989, p 587.*

129. *Ohta J., et. al., Proceeding of European Power Conference, PC79-1.2, 1, 1979.*

130. *Wu J-M and Wang H-W, J. Am. Ceram. Soc., Vol. 71, No. 10, 1988, pp 869-875.*

131. *Wang H-W, Hall D and Sale F, J. Am. Ceram. Soc., Vol. 75, No. 1, 1992, pp 124-130.*

132. *Hung Y. H. and Ko Y. C., J. Materials Science, L12, 1993,pp 1900-1901.*

133. *Gholinia A., PhD Theses, University of Manchester, 1994.*

134. *Ramesh M, Crowell R. W. and Dey S., IEEE Trans. on Magn., Vol. 30, No. 6, 1994, pp 4872-4874.*

135. *Rozman M and Drofenik M., J. Am. Ceram. Soc., Vol. 78, No. 9, 1995, pp 2449-2455.*

136. *Sisk M., Kilbridge I. and Barker A. J., J. Mat. Sci. Letters, 14, 1995, pp 153-154.*

137. *Stuijts A. L., ICF1, Tokyo, 1970, pp 108-113.*

138. *Sale R. F., J. Fan and ChienY-T., The Second European Ceramic Society Conference, Augosburg, 1991.*

139. *Miyoshi Y., Okamoto N. and Kageyama K., ICF6, Tokyo, Japan, 1992, pp 325-328*

140. *Hon Y. S. and Ko Y. C., ICF6, Tokyo, Japan, 1992, pp 305-308.*

141. *Rosales M. I., Plata A. M, Nicho M. E., Brito A., Ponce M. A. and Catano V. A., J. of Mat. Sci., 30, 1995, pp 4446-4450.*

142. *Drofenik and Rozman, In magnetic Ceramics, Ed. Ghata B. and Simmins J., Ceramic Transitions, Vol. 47, The American Ceramic Society, 1995, pp 287-294.*

143. *Tasako J. and Ito T., ICF 1, Tokyo, Japan, 1970, pp. 84-86.*

144. *Mullin J. T. and Willey R. J., In Advances in Ceramics, ICF 4, Vol. 15, Part I, 1984, pp 187-191.*

145. *McColm I. J. and Clark N. J., Forming, shaping and working of high performance ceramics, 1988,Blackie, Glasgow, pp 1-338.*

146. *Lin S. T. and German R. M., Compressive stress for large-pore removal in sintering, Journal of American Ceramic Society, 71, C-432-3, 1988.*

147. *Reijnen P., Reactivity of Solid, Ed. Mitchel W. J., et. al., 1969, pp 99-114.*

148. *Johnson D. W. Jr., Vogle E. M. and Ghata B. B., ICF 3, 1980, pp 285-291.*

149. *Jain G. C., Das B. K. and Kumari S., J. Appl. Phys., 49, 1978, p 2894.*

150. *Maun A. and Osborn E. F., "Phase equilibria among oxides in steelmaking", Addison-Wesley, Reading MA, 1965, p114.*

151. *Hung Y-H., Chien Y-T. and Ko Y-C., J. Mat. Sci. Letters, 13, 1994, pp 1416-1418.*

152. *Drofenik M., Besenicar S, Limpel M. and Gradasevic V., ICF 4, In Advances in Ceramics, Part 1, Vol. 15,1994, pp 229-236.*

153. *Rikukawa H. and Sasaki I., ibid, pp 215-219.*

154. *Ochiaki T. and Okutani K., ibid, pp 447-456.*

155. *Sainamthip P. and Amarakoon V. R. W., J. Amer. Ceram. Soc., 71, 1988, pp 644-648.*

156. *Mishra R., ibid, 64, 1981, p 520.*

157. *Stoppels D., J. Mag. and Magnetic Mat., 160, 1996, pp. 323-328.*

158. *Sakaki Y. and Matsuok T., IEEE Trans. of Mag., Vol. Mag-22, 5, 1986, p. 623.*

159. *Van Utiert L. G., J. Chem. Phys., 24, 1956, p 306.*

160. *Johnson M. T., Noordemeer A., Severin M. M. E. and Meeuwissen W. A. M., J. Mag. and Magn. Mat., 116, 1992, pp. 169-176.*

161. *Tsunekawa H., Nakata A, Kamijo T., Okutani K., Mishra R. K. and Thomas G., IEEE Trans. on Mag., Mag-15, 1979, p 1855.*

162. *Otsuki E., ICF 6, Tokyo, Japan, 1992, pp. 59-64.*

163. *Hendricks C. R., Amarakoon V. W. R. and Sullivan D., Amer. Ceram. Soc. Bull., 70, 1991, p. 817.*

164. *Taylor S. M. O. and Sale F. R., In 3rd Euro. Ceramics, Spain, Vol. 2, 1993, p 431.*